8-25-2015 12:00 AM

Resting and Functional Magnetic Resonance Spectroscopy of Glutamate in Schizophrenia at 7 Tesla

Reggie E. Taylor, *The University of Western Ontario*

Supervisor: Dr. Jean Théberge, *The University of Western Ontario*
Joint Supervisor: Dr. Peter Williamson, *The University of Western Ontario*
A thesis submitted in partial fulfillment of the requirements for the Doctor of Philosophy degree in Medical Biophysics

RESTING AND FUNCTIONAL MAGNETIC RESONANCE SPECTROSCOPY OF GLUTAMATE IN SCHIZOPHRENIA AT 7 TESLA

(Thesis format: Integrated Article)

by

Reggie Taylor

Graduate Program in Medical Biophysics

A thesis submitted in partial fulfillment
of the requirements for the degree of
The Doctorate of Philosophy in Medical Biophysics

The School of Graduate and Postdoctoral Studies
The University of Western Ontario
London, Ontario, Canada

Abstract

Schizophrenia is a debilitating disease that affects about 1% of the population. Current therapeutic interventions mostly target dopaminergic neurotransmission but are not effective in treating all symptoms. There is growing evidence to support involvement of glutamatergic neurotransmission, which may better account for the symptomatology of schizophrenia.

Glutamate concentrations can be measured *in vivo* using magnetic resonance spectroscopy (MRS). Stronger magnetic field strengths provide benefits for MRS, but they also present challenges. Simulations were designed to examine how MRI field strength influences metabolite quantification. Glutamate and its metabolic precursor, glutamine, were more reliably and independently quantified with higher MRI field strengths, showing a clear benefit for MRS.

Using a 7 T MRI, voxels were placed within the dorsal anterior cingulate cortex (dACC) and thalamus of volunteers with schizophrenia, a psychiatric control group of volunteers with major depressive disorder (MDD), and healthy controls. Glutamine and glycine, both involved in glutamate neurotransmission, were lower in the thalamus in schizophrenia relative to healthy controls, whereas dACC glutamate concentrations were higher, demonstrating glutamatergic abnormalities in schizophrenia at rest.

Prior MRS studies of schizophrenia have been in resting conditions. In a proof of concept study with healthy controls, it was shown that the Stroop Task was able elicit a significant glutamate increase in the dACC when in a functional state (glutamate fMRS) relative to resting conditions using the 7 T MRI. This was then explored in the same schizophrenic and MDD subjects as the resting MRS study. Glutamate significantly increased in the healthy controls, but not in the schizophrenic and MDD groups. The schizophrenic group had a slower glutamatergic response followed by a slower recovery, and, was the only group to demonstrate significant glutamine increases when activated, indicating potential abnormalities in glutamate dynamics.

Using a 7 T MRI, glutamate was explored in resting and activated conditions in schizophrenia. Glycine was demonstrated to be lower in schizophrenia using MRS for the first time, and the first functional MRS study was performed in a psychiatric population. The

studies were made stronger by inclusion of a psychiatric control group. Future studies of schizophrenia with glutamate fMRS should focus on the delayed glutamatergic response to functional activation and abnormal recovery.

Keywords

Schizophrenia, major depressive disorder, glutamate, glutamine, glycine, 7 T, fMRS, MRS, simulations, metabolite quantification, Stroop task, anterior cingulate cortex (ACC), thalamus.

Co-Authorship Statement

This thesis contains material from one manuscript that has been published in NeuroReport (chapter 4), one manuscript that is currently in press in npj Schizophrenia (chapter 5), one manuscript that has been submitted to Magnetic Resonance in Medicine and is currently being edited for resubmission (chapter 2), and one manuscript in preparation to be submitted to the British Journal of Psychiatry (chapter 3). Each of these manuscripts have had contributions from multiple authors, which are listed for each chapter.

Chapter 2 – This manuscript has been submitted to Magnetic Resonance in Medicine and is currently being edited for resubmission. The manuscript and the batch program for all the simulations (creation, fitting, and analysis) were all written by Reggie Taylor. Dr. Jean Théberge and Dr. Peter C. Williamson helped with the design of the study and the interpretation of the results. Both have also reviewed the manuscript and made edits

Chapter 3 – This manuscript is currently in preparation to be submitted to the British Journal of Psychiatry. All of the pulse sequence and protocol development, data acquisition, post-processing, statistical analysis, and manuscript writing was done by Reggie Taylor. Subject recruitment was performed Betsy Schaefer and Dr. Elizabeth A .Osuch. The Structured Clinical Interview for DSM-IV (SCID) was performed on all subjects by Betsy Schaefer and Dr. Peter C. Williamson. Anatomical landmarks for the voxel position were chosen by Dr. Nagalingam Rajakumar. All statistical analyses were processed after consultation with Dr. Richard W.J. Neufeld. Dr. Jean Théberge and Dr. Peter C. Williamson helped with the design of the study and the interpretation of the results.

Chapter 4 – This manuscript has been published in NeuroReport (2015; 26:107-112) in open access and requires no written permission letter to be reused in this dissertation. All of the pulse sequence and protocol development, data acquisition, post-processing, statistical analysis, and manuscript writing was done by Reggie Taylor. Subject recruitment was performed by Betsy Schaefer. Maria Densmore helped with the voxel segmentations into grey matter, white matter, and CSF. Dr. Richard W.J. Neufeld guided all statistical analyses and contributed to the design of the Stoop protocol. Anatomical landmarks for the voxel

position were chosen by Dr. Nagalingam Rajakumar. Dr. Jean Théberge and Dr. Peter C. Williamson helped with the design of the study and the interpretation of the results.

Chapter 5 – This manuscript has been accepted and is currently in press at npj Schizophrenia (NPJSCHZ#00068) for open access publication and requires no written permission letter to be reused in this dissertation. All of the pulse sequence and protocol development, data acquisition, post-processing, statistical analysis, and manuscript writing was done by Reggie Taylor. Subject recruitment was performed Betsy Schaefer and Dr. Elizabeth A. Osuch. The Structured Clinical Interview for DSM-IV (SCID) was performed on all subjects by Betsy Schaefer and Dr. Peter C. Williamson. Anatomical landmarks for the voxel position were guided by Dr. Nagalingam Rajakumar. Dr. Richard W.J. Neufeld guided all statistical analyses and contributed to the design of the Stoop protocol. Dr. Jean Théberge and Dr. Peter C. Williamson helped with the design of the study and the interpretation of the results.

Acknowledgments

The work presented in this thesis would not have been possible without the contributions and support of the many people who have assisted me and been there for me throughout the years. One of the biggest lessons I have learned in grad school is that sometimes you need to ask others for help, and there's nothing wrong with that. Below I have listed some of the main people that need to be thanked, but the list is certainly not exhaustive.

First of all, my supervisors, Jean Théberge and Peter Williamson, have both guided me with plenty of patience throughout this project and have been excellent mentors. My transition from a naïve graduate student to a Ph.D. Candidate has largely been due to their support and I can't thank them enough for believing in me over the years.

The rest of my advisory committee, Jim Neufeld and Rob Bartha, have both provided excellent insight and feedback into the design of these studies. Jim has been especially influential in the development of the fMRI/fMRS protocol, and has been a very helpful resource for any statistical questions that I've had.

To my former lab mate, Linden Barton, thanks for always being willing to be my human guinea pig for protocol development with the 7 T (in exchange for my own services as a guinea pig, of course). You've been a good friend and I look forward to many more good times.

There was always an open door just down the hallway from my office where I could take a break and have a talk with Maria Densmore. She has often been a voice of reason and has often provided some very helpful advice. Thanks for always making time for me.

The many hours spent acquiring data on the scanners would not have been the same without the upbeat presence of Betsy Schaefer to make the time go by. This thesis could not have come to fruition without the hard work that Betsy put in to recruit and schedule so many subjects. Thanks for everything.

Prior to scanning subjects, countless hours were spent taming the beast that was the 7 T. Thanks to Joe Gati, Martyn Klassen, Ravi Menon, David Rudko, Andrew Curtis, Kyle Gilbert, Igor Solovey and the rest of the CFMM for all the technical support provided. In

addition, I would like to thank Jacob Penner, Jean-Guy Belliveau, Kathryn Manning, Kim Krueger, Izabela Aleksanderek, Oksana Opalevych, John Drozd, and Trevor Szekeres for discussions and support at the scanners as well.

There are many people that I have met at Lawson and Robarts that have grown to become my friends, including many great officemates. Fang Liu, Udunna Anazodo, Harini Suraweera, Karina Quiaoit, Anindita Sengupta, Andrea Mitchell, and all the others that had a brief stint in that office, thanks for being so great. I really do hope that we'll be able to keep in touch going forward. I would also like to quickly thank all the administrative staff I have worked with including Shelagh Ross, Michele Avon, and Brenda Dubois at Lawson, Wendy Hough in the biophysics office on campus, and Sheri-Lee Bradshaw at University Hospital. Thanks for all your hard work.

Throughout my time in London at Western, I have had many friends come and go. Although it can be hard having friends move away to continue on with their lives, I'm thankful to all of them for the memories we've made and the time that we've spent together. Matt Garton, Frasor Pollard, Mike Besser, Mevan Perrera, Jesse Melo, Jacqui Hayworth, Aaron Parsons, James Dusten and Yashaan Malvalvala have all been housemates in the past and have been great friends. I specifically need to acknowledge Jesse Melo for much of his help with introducing me to some of the more advanced aspects of computer programming, which really improved my programming abilities for this thesis.

I've been involved with many sports teams to which I've enjoyed the company of my teammates, including my hardball team (London Area Angels, formerly Forest City Barons), my softball team (LAFS), and my old intramural Frisbee team. It was always nice to take my mind off of school work and spend some time with friends having fun and getting exercise.

The Western Outdoors Club have been a huge component of my life away from school work for about eight years now. This is where I have met some of my closest friends. When the stress of school was becoming so great, the best remedy was a couple nights camping in the middle of nowhere with some good friends and some new friends. Although it was hard to see so many people come and go as they started and then finished school, I still cherish all of their friendships. Thank you to everyone involved.

Finally, my family, especially my mom and dad, deserve the biggest thanks, as they have been so supportive the entire time. Always optimistic and ever encouraging, their support has really made a big difference.

As I mentioned before, this list is far from exhaustive, and there are many more whom have helped me get through this degree. To all of you, thanks.

Table of Contents

List of Tables

List of Figures

List of Abbreviations and Symbols

ω	frequency (rad/s)
γ	gyromagnetic ratio
ϕ	phase
σ	shielding constant
δ	ppm value
^{1}H	Hydrogen nuclei, proton
^{1}H-fMRS	proton functional magnetic resonance spectroscopy
^{1}H-MRS	proton magnetic resonance spectroscopy
ACC	anterior cingulate cortex
Ala	alanine
Asp	aspartate
ATP	adenosine triphosphate
BGTHC	basal Ganglia thalamocortical
B_0	external magnetic field
B_1	applied magnetic field
Ca^{2+}	calcium
CB	cerebellum
CHESS	chemical shift selective
Cho	choline
$COV_{(metA,metB)}$	covariance between metabolite A and B
Cr	creatine
CRLB	Cramer-Rao Lower Bounds
CO^2	cardon dioxide
CSI	chemical shift imaging
CV	coefficient of variation
d	delay time
EAAT	excitatory amino acid transporter
FGA	first-generation antipsychotic
FID	free-induction decay
fMRI	functional magnetic resonance imaging
FOV	field of view
FWE	Family-Wise Error
GABA	gamma-aminobutyric acid

Glc	glucose
GLN	glutamine
GLU	glutamate
GLX	glutamate+glutamine
GLY	glycine
GLYt1/2	glycine transport inhibitors
GPCho	glycerophosphorylcholine
GS	glutamine synthetase
GSH	glutathione
$G_{(x,y,z)}$	gradient in direction x, y, or z
HIP	hippocampus
HLSVD	Hankel-lanczos singular value decomposition
IE1/2	Inexact seeding type 1 or 2
Lac	lactose
LW	linewidth
MDD	major depressive disorder
$mGluR_{(1-8)}$	metabolic glutamate receptors
MM	macromolecules
M0	resting magnetization
MRI	Magnetic Resonance Imaging
MYO	myo-inositol
NA	nucelus accumbens
NAA	N-acetylaspartate
NAAG	N-acetylaspartyl-glutamate
NAVG	number of averages
NADH	nicotinamide adenine dinucleotide
NMDA	N-methyl-D-aspartate
NMR	nuclear magnetic resonance
nt	number of transients
OVS	outer volume suppression
PAG	phosphate-activated glutaminase
PCho	phosphorylcholine
PCP	phencyclidine
PCr	phosphocreatine
PE	phosphorylethanolamine
PFC	prefrontal Cortex
PRESS	point resolved spectroscopy

QUECC	quality eddy current correction
RF	radiofrequency
$R_{(metA,metB)}$	correlation between metabolite A and B
SAR	specific absorption rate
Scy	scyllo-inositol
Ser	serine
SGA	second-generation antipsychotic
SNR	signal to noise ratio
STEAM	stimulated echo acquisition mode
SZ	schizophrenia
T	Tesla
T_1	spin-lattice relaxation
T_2	spin-spin relaxation
Tau	taurine
TE	echo time
TH	thalamus
TM	mixing time
TMS	tetra-methylsilane
TORO	transmit-only receive-only
TR	repetition time
VAPOR	variable power and optimized relaxation delays
VTA	ventral tegmental area

List of Appendices

Chapter 1

1 Introduction

The ultimate objective of this thesis is to gain insight into the state of glutamate and its metabolic affiliates in the brains of individuals with schizophrenia using advanced MRI hardware and methodology. This is, of course, a very general statement, as a brief overview of schizophrenia and MRI physics is necessary to fully appreciate the specific intentions and methods of the works in this thesis. This chapter will serve as a thorough tutorial towards the development of specific hypotheses outlined in this work, and will provide additional background information for the otherwise self-contained chapters 2, 3, 4 and 5.

1.1 Schizophrenia; background and physiology

1.1.1 From *dementia praecox* to schizophrenia

Schizophrenia (SZ) was first separated from other psychoses by Emil Kraeplin in 1899, who at the time called the disorder "*dementia praecox"*[1]. Krapelin's descriptions of *dementia praecox* were very similar to the modern classification of SZ in the *Diagnostic and Statistical Manual of Mental Disorders, Fourth Edition, Text Revision* (DSM-IV-TR)[1]. The term "*dementia praecox*" was eventually replaced by SZ in 1911[2]. Although the classification of SZ is relatively recent, the disease is believed to have been with humans throughout civilization, given early descriptions of similar illnesses in historical texts[1,3,4].

The prevalence of SZ in the population is approximately 1%, with a similar incidence among men and women[5,6]. The typical age of onset is in the adolescent phase of a person's life (usually early twenties), with the onset being 3-4 years earlier in men than in women[5]. Although onset typically occurs beyond puberty, subtle symptoms have been identified retrospectively in childhood prior to disease diagnosis[7]. The cause of SZ is still

unknown, although there are convincing arguments pointing towards the idea that there is both a genetic and an environmental component. One meta-analysis of 12 studies of twins (both monozygotic and dizygotic) found an 81% heritability component due to genetics and an 11% heritability component due to the environment, such as exposure to infectious agents, dietary characteristics, etc[8]. It is probable that there are in fact multiple factors that can lead to the final common pathway of SZ[2,9]. What is clear is that, at the point when a diagnosis of SZ would be made, there is a substantial contribution of neurotransmitter anomalies influencing the symptoms of SZ.

1.1.2 Neural physiology of schizophrenia

The symptoms of SZ are variable in each individual, but generally can be subdivided as either positive (i.e. auditory hallucinations and delusions), negative (i.e. asociality, avolition, anhedonia, affective flattening, and alogia) or cognitive (i.e. attention and working memory deficits, visual and verbal learning memory, reasoning and problem solving)[7,10,11]. Most current antipsychotics offer effective relief from positive symptoms by targeting dopaminergic neurotransmission but most do little to offer relief from the negative and cognitive symptoms[7,12–14] and can actually worsen cognitive symptoms[15]. The negative and cognitive symptoms are present in 40-80% of people with SZ[10] and are better indicators of functional outcome[7,9,10,13,14]. There are currently no approved treatments that target negative and cognitive symptoms specifically. The drugs that can treat both positive and negative symptoms typically come with heavy undesirable side effects (e.g. clozapine increases risk for agranulocytosis and requires regular blood tests)[12,16], which can influence patient compliance with regularly taking their prescribed medication. These poorly treated negative and cognitive symptoms lead to progressive deterioration in functioning throughout their lives[10,15].

Differences in the effectiveness of drug interventions are likely due to the underlying differences in brain physiology between positive, negative, and cognitive symptoms. Positive symptoms have been connected to dopaminergic pathways originating in the ventral tegmental area and projecting to the nucleus accumbens[2], and, as such, the current

antipsychotics generally target the D2 dopamine receptors in this area[15]. It is believed that different brain pathophysiology is implicated in the negative and cognitive symptoms[7], and it is likely that the physiology of positive, negative, and cognitive symptoms are connected through neural circuits, known as the basal ganglia thalamo-cortical circuits (BGTHC)[2,12] (Fig 1-1).

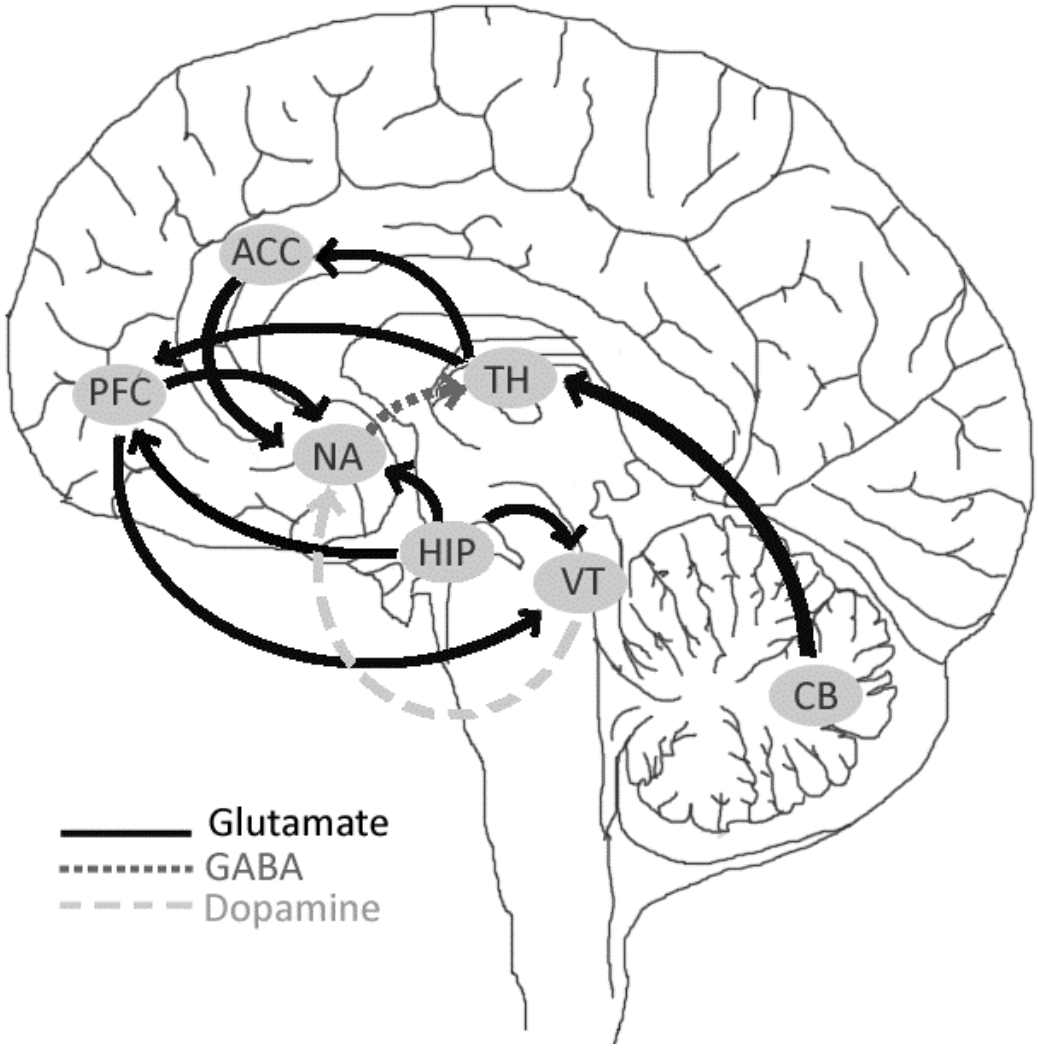

Figure 1-1. A few neurotransmitter pathways within the limbic basal ganglia thalamocortical circuits.

ACC=anterior cingulate cortex; PFC=prefrontal cortex; NA=nucleus accumbens; HIP=hippocampus; VT=ventral tegmental area; TH=thalamus; CB=cerebellum.

The BGTHC are essential links between motivation and action in the brain, and are important when learning new behaviours[2]. As the name implies, these are circuits that cycle from the cortex, to the basal ganglia, through to the thalamus, and then back out to the cortex, creating a flow of cyclical communication through these brain areas[2,17]. The communication throughout each circuit is largely mediated by the main excitatory neurotransmitter, glutamate (GLU; Fig 1-2A), with contributions from both dopamine and the inhibitory neurotransmitter, gamma-aminobutyric acid (GABA). One BGTHC of particular interest in the pathophysiology of SZ, the limbic BGTHC, completes a circuit through the dopaminergic pathway from the ventral tegmental area (VTA) to the nucleus accumbens, a pathway central to explaining the positive symptoms of SZ. The anterior cingulate cortex (ACC)[2,13,18–25], and the thalamus[2,22,24–30] are key nodes within circuits that are repeatedly implicated through the negative symptoms of SZ. The thalamus, being a central hub of each BGTHC, is an area of interest in studies of SZ that have demonstrated structural abnormalities[26,27], abnormal functional connectivity[27,28] and metabolic abnormalities[22,24–26,31,32]. The dorsal component of the ACC, believed to be involved in selective encoding of stimulus properties[33], attention[34] , and organization of conflicting stimuli[35,36], is associated with negative and cognitive symptoms in SZ[7,13] and is another important structure within the limbic BGTHC. Functional MRI (fMRI) studies have demonstrated hypofunction in the ACC upon completion of complex tasks such as a word-fluency task[20] and the color-word Stroop task[19] in people with SZ compared to

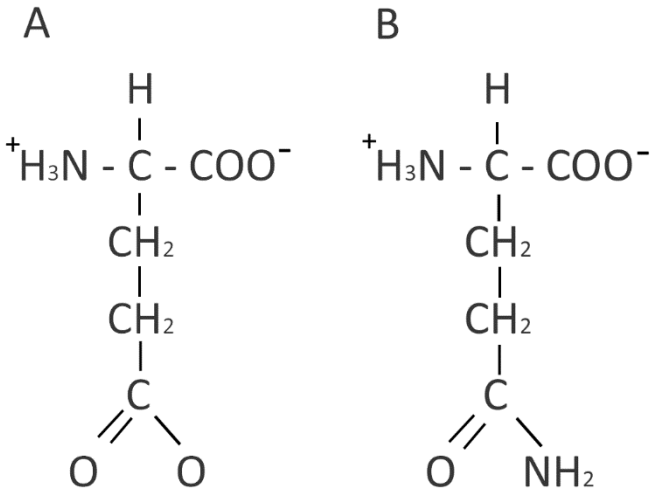

Figure 1-2. The chemical structure of (A) glutamate and (B) glutamine

healthy controls. The ACC is an area that is heavily innervated with GLU neurons that mediate the communication with functionally connected brain regions. Therefore, it is possible that the positive, negative, and cognitive symptoms of SZ are due to the actions of impaired GLU neurotransmission within areas of the BGTHC, with the dopamine levels causing the positive symptoms as a downstream effect. Much of the current understanding of the neural physiology of SZ actually comes from studies involving drugs that act on GLU receptors, such phencyclidine (PCP) and ketamine[37–39]. These drugs are antagonist of the N-methyl-D-aspartate (NMDA) ionotropic GLU receptor[37–40]. They have been shown to induce both positive and negative symptoms when administered to healthy controls, but will exacerbate existing symptoms in people with SZ[41,42]. The prevalent stance in the GLU theory of SZ postulates that the presence of localized NMDA receptor hypofunction as a likely cause of reduced efficiency or function of GLU neurotransmission in connected regions[12,43]. There is also some evidence pointing towards the presence of glutamate excitotoxicity in SZ in a small number of studies (n=7)[44]. The exact biochemical mechanism of GLU neurotransmission deficiency in SZ is still unknown but it is likely located somewhere within the glutamate-glutamine (GLU-GLN) cycle.

1.1.3 The glutamate-glutamine cycle in a healthy state

The efficient recycling of GLU is an essential component to neural function. It is estimated that 60-80% of neuronal glucose consumption directly supports the GLU-GLN cycle[45] (Fig. 1-3). Neuronal GLU is first created when glucose enters the Kreb's cycle (Tricarboxylic acid cycle) in the neuronal mitochondria. After citrate reacts with NAD+ to form alpha-ketoglutarate, CO_2, NADH+ and H^+, the alpha-ketoglutarate exits the Kreb's cycle and binds with an alpha-amino acid using aminotransferase to facilitate the reaction[46–48]. This creates the amino acid GLU. Approximately 4000 GLU molecules are then packaged into a vesicle for exocytosis into the synapse at a rate of 1.2 vesicles per second, or 4800 GLU molecules per second[49]. After release into the synapse, GLU binds with ionotropic receptors (NMDA, kainate, AMPA) or metabotropic receptors ($mGluR_{1-}$

$_8$) on the post-synaptic membrane, an event modulated by certain agonists[7,40,48,49]. For example, there is a glycine (GLY)/D-serine site on the NMDA receptor that needs to be filled for GLU neurotransmission to be possible on that receptor[50]. With both GLU and GLY sites bound, the NMDA channel opens and results in a Ca^{2+} influx into postsynaptic neuron. The GLU molecule is eventually released from the receptor. A small percentage will be reabsorbed into the presynaptic neuron, but the majority will be rapidly taken up into the adjacent glial cell (astrocyte) by excitatory amino acid transporters (EAAT), primarily EAAT2, to avoid excitotoxicity[49,51]. Each EAAT2 can transport a GLU molecule once every 70 ms, so hundreds of them need to be present[49]. This is an active transport of GLU which requires ATP[45]. In the glial cell, GLU can either be oxidized or can undergo an amination reaction via glutamine synthetase (GS), an enzyme located exclusively in the glial cell[46,47,52], that will convert the GLU to glutamine (GLN; Fig 1-2B)[45–47,49,53]. The GLN can then be passively transported back into the neuron where the phosphate activated enzyme glutaminase (PAG) can convert it to GLU through hydrolysis for re-use in neurotransmission[46,47]. Approximately ¾ of the GLU will undergo the amination reaction to GLN in the glial cell, and the remaining ¼ will be oxidized using glutamate dehydrogenase[46,47] to convert it to alpha-ketoglutarate[54], which can be fully degraded to CO_2 and water within the glial cell for energy purposes[55]. Therefore, each GLU molecule is only used a few times before it is ultimately oxidized for energy[46,47,49]. This process of recycling GLU after it has been used for neurotransmission is the GLU-GLN cycle, a process that is tightly coupled to neuronal energy consumption from glucose[45]. Without glucose to resupply the loss of GLU through oxidation, the GLU supply will be depleted in approximately 1 minute[49]. There are, therefore, many metabolic processes within the GLU-GLN cycle that could ultimately lead to hypofunction of GLU neurotransmission if they are not operating efficiently (e.g. reduction in enzymatic levels, reduction in transporters, reduction in number of receptors, dysfunctional receptors, etc). If there is a dysfunction somewhere in the GLU-GLN cycle, one would expect an offset in the equilibrium concentration of GLU and/or GLN. SZ does not spontaneously occur in animals other than humans and laboratory animal models of SZ tend to only mimic a very specific feature of SZ (i.e.

dopamine hyperresponsivity). Fortunately, there are methods by which GLU and GLN can be measured non-invasively in human brains affected by SZ.

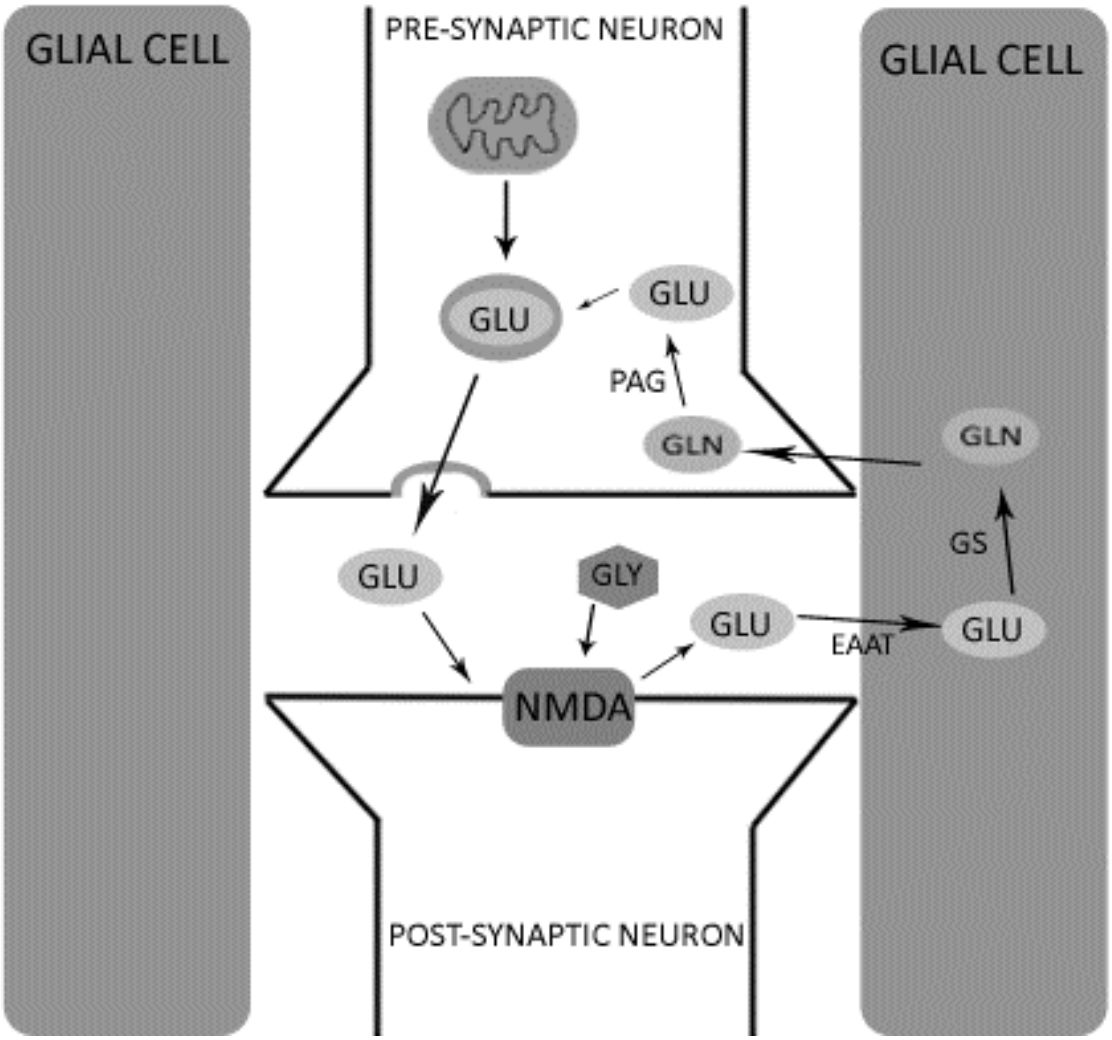

Figure 1-3. A simplified diagram of the GLU-GLN cycle in a healthy state. GLU is created in the mitochondria, packaged into vesicles to be released in the synaptic cleft where it binds with receptors on the post-synaptic membrane. This reaction is mediated by local GLY. GLU is then actively transported into the adjacent glial cell (via EAAT), where it is converted to GLN via GS. GLN is then passively transported back into the neuron, where it can be converted back into GLU via PAG. GLU = glutamate; GLN = glutamine; GLY = glycine; NMDA = N-methyl-d-Aspartate; EAAT = excitatory amino acid transporters; GS = glutamine synthetase; PAG = phosphate-activated glutaminase

1.1.4 Measuring components of the GLU-GLN cycle in SZ

1.1.4.1 Glutamate/Glutamine

Since the first lines of evidence for the GLU theory of SZ emerged, there have been many studies examining GLU and GLN in SZ. Although the GLU theory has evolved throughout the years[56], there has been relatively little progression given the number of studies and the massive efforts put forth by researchers, demonstrating that it is a complex disorder and there are still many obstacles to overcome. There have been useful post-mortem studies of brain tissues from people with SZ that have found abnormalities in the expression of proteins related to synaptic activity and GLU neurotransmission[32,51,57,58]. However, post-mortem studies have limited results because the tissues are typically from people with chronic SZ who have been heavily medicated throughout the duration of their illness. This is a problem because there has been substantial evidence showing that the GLU and GLN concentrations likely change throughout the course of the disorder[18,25] and that medications can influence their concentrations in the human brain[59,60]. Another challenge of GLU and GLN studies in SZ is that it appears to be a uniquely human disorder[2] and although symptom analogs have been well documented and studied in animal models (i.e. ketamine administrations[61]), this fact still limits the translational potential of animal studies. Genetic studies have identified some gene variants that affect the NMDA pathway and the susceptibility for SZ[7] but, so far, there has not been a "schizophrenia gene" identified. Therefore, it is desirable to be able to non-invasively detect GLU and GLN concentrations in the brains of humans with SZ *in vivo*. One method that has been extensively used for this is proton magnetic resonance spectroscopy (^{1}H-MRS).

There have been many ^{1}H-MRS studies of SZ to date in various areas of the brain[12,18,62,63]. Unfortunately, many of the studies are difficult to compare considering all the possible factors that influence the results. As mentioned already, whether the SZ subjects are first-episode, anti-psychotic naïve or chronic patients will influence the results[18,25,59,60]. Studies are performed on different magnetic field strength scanners (1.5 T -7 T), using different ^{1}H-MRS acquisition pulse sequences and parameters, with different

post-processing methods and different fitting algorithms[63]. Some studies use water to determine the metabolite concentration (explained below) and others simply examine ratios of metabolites to creatine, another metabolite detectable with ^{1}H-MRS. Different voxel sizes are used, and the placement of a voxel can be very different from one study to the next. For example, the ACC is a structure that is much larger than a typical ^{1}H-MRS voxel size ($1.5cm^3 – 8cm^3$) with very different functions from one location to another[2]. Not all studies specify all the metabolites that they fit, and, specifically, many studies do not explain what metabolites are included in their GLU definition. At lower magnetic field strengths, it can be necessary to combine GLU and GLN into one unitary concentration, as the metabolites cannot be reliably separated for quantification. It is then common to define "GLX" as GLU+GLN, but this is not always made clear, leading one to assume that GLX could actually be a combination of GLU, GLN, and any other metabolites (GABA, glutathione) or macromolecules that overlap their spectra. Even with all these limitations in comparing studies, GLU, GLN, or GLX concentrations are consistently implicated in voxels throughout the brain in SZ.

A recent meta-analysis was completed of 28 ^{1}H-MRS studies with 647 subjects with SZ and 608 healthy controls at various voxel sizes and field strengths[18], of which 9 studies were completed in the medial frontal lobe (including the ACC and medial prefrontal cortex)[22,24,64–71]. The study determined that GLU concentrations are typically lower than controls at the onset of the disease, whereas GLN is typically higher than controls. Both GLU and GLN decreased in concentration faster as the SZ subjects aged than in the healthy controls. The same meta-analysis has examined GLU concentrations in 3 studies in the thalamus, but determined no significant difference in SZ from healthy controls. There were not enough studies in the meta-analysis to determine an effect of GLN in the thalamus, but it has previously been demonstrated that there is increased GLN in first-episode, antipsychotic naïve subjects with SZ[22] and chronic SZ[24] relative to controls, with the GLN concentration decreasing after 30 months of antipsychotic treatment[25].

One particularly interesting ^{1}H-MRS study of the ACC involved healthy controls being challenged with a sub-anesthetic dose of the NMDA antagonist ketamine[72]. This study observed an increase in ACC GLN after the healthy controls had been exposed to

ketamine, which returned to normal ten minutes later. This observation is consistent with the GLU theory of NMDA hypofunction in SZ, as it has been observed that when the NMDA receptor is in a condition of hypofunction there is an increase in the activity of GLN synthetase leading to higher GLN concentrations synthesized[73]. Therefore, increased GLN observed in people with SZ provides strong support for the GLU theory of SZ.

1.1.4.2 Dynamic measurements of GLU and GLN

Static measurements of ^{1}H-MRS have been paramount in moving research forward into the possibility of GLU dysfunction in SZ, but a limitation of these studies is that all were acquired in a resting condition, at only one time point. This is based on the assumptions that the metabolite concentrations are not dynamic, and that the brain at rest is truly at rest. It has since been demonstrated that the concentrations of some metabolites will change when the tissue within the voxel is stimulated[74–85]. This technique is called functional ^{1}H-MRS (^{1}H-fMRS). The first ^{1}H-fMRS studies were largely looking at lactate concentrations in the occipital lobe after visual stimulation in dyslexic children[84], and in subjects with migraines[83]. Since then, there have been reports that show that local GLU (or GLX) concentrations will increase when an area of the brain is stimulated using a visual task in the occipital lobe[75–77,81], a finger tapping paradigm in the motor cortex[80], pain paradigms in the ACC[78] and inferior parietal cortex[79], and a sexual arousal task in the ACC[82]. It is likely that the GLU increase is related to the creation of new GLU for neurotransmission *de novo* from glucose, while the remaining GLU undergoes recycling via the GLU-GLN cycle. In a dynamic state while the GLU-GLN cycle is being challenged, it is possible that a dysfunction somewhere in the GLU-GLN cycle would manifest itself as a significantly different response of GLU than in healthy controls, or possibly even a change in GLN.

The previously mentioned ^{1}H-fMRS studies of the brain have been pivotal in demonstrating that metabolic changes can be observed as a result of functional activation. A limitation of past studies is that no study has yet demonstrated that GLU increases can

be seen using a cognitive behavioural task or in a psychiatric disorder. A behavioural task is desirable if the technique is going to be extended to the study of psychiatric disorders featuring impaired cognitive processing, such as SZ.

There are many possible cognitive tasks that could be chosen as the functional paradigm for ^{1}H-fMRS but there are also multiple considerations. First, the task needs to stimulate a specific area of the brain, much like the visual tasks stimulate the occipital lobe[75–77,81] and the motor tasks stimulate the motor cortex[80]. The first decision, then, needs to be in what area of the brain is the voxel going to be placed. For a ^{1}H-fMRS study of SZ, it would be interesting to observe metabolic changes in an area implicated through the negative symptoms. The task must also be able to actively engage the participant for an extended period of time. If the participant loses interest or is not finding the task particularly challenging anymore it is likely that the area of interest will also not be stimulated as strongly, potentially biasing the results to any attentional impairment. This is an important aspect to consider given that behavioural tasks already do not illicit as strong of a neural response (according to measurements of the blood-oxygen level dependent (BOLD) effect) as the visual and motor tasks[86]. It has been postulated that the deficiencies in SZ may arise from an increased number of subprocesses that are involved in the encoding of cognitive stimuli into task facilitative formats[33,87]. The color-word Stroop Task[88–92] is one such cognitive task that requires encoding operations in the presence of interfering information that activates the ACC[19,35,36,93–95].

The color-word Stroop Task is a common psychiatric battery that people in SZ find more challenging (lower time efficiency) than healthy controls, although with a similar rate of correct answers[19,67,96]. It involves the presentation of a color-word written in a certain color of ink in a congruent condition (i.e. the word “red” written in red ink), incongruent condition (i.e. the word “green” written in red ink), color-only condition (i.e. letters (“XXXX”), or a nonsense word written in red ink) or word-only condition (the word “red” written in white ink). The color of the ink is the expected correct response in all but the word-only condition, where the word is the expected correct response (i.e. “Red” would be the correct response in each of the previous examples). The organization of conflicting or complex stimuli is often attributed to activity in the dorsal ACC[20,35,36],

which the color-word Stroop Task robustly and reproducibly activates[19,35,93,95,97]. Therefore, due to the implication of ACC in negative and cognitive symptoms, the Stroop Task appears to be a good cognitive paradigm for a ^{1}H-fMRS study of SZ.

In a neuropsychiatric disorder like SZ, where one of the leading hypotheses is related to hypofunction of the GLU-GLN cycle, ^{1}H-fMRS has the potential to utilize the added dimension of time to identify possible metabolic steps within the GLU-GLN cycle that are functionally deficient, based on GLU or GLN accumulations (or lack thereof). While ^{1}H-fMRS in SZ should provide valuable information on the glutamatergic system, there is certainly still a role for static ^{1}H-MRS measurements of brain tissue in a controlled resting state. As technology has improved, so has the quality of ^{1}H-MRS spectra. This can translate to improved measurements of metabolites that are of low concentration and have been traditionally difficult to quantify. One such metabolite that plays a pivotal role in GLU neurotransmission is GLY.

1.1.4.3 Glycine

One of the growing ideas for potential pharmaceutical interventions of the NMDA hypofunction is to try to increase GLY concentrations in glutamatergic neurons. There is a GLU site and a GLY/D-serine site on the NMDA receptor (the NR2 and NR1 subunits, respectively) that needs to be filled for successful GLU neurotransmission[7,12,40,50,98]. Without an adequate supply of GLY (or D-serine) present in the synaptic cleft the NMDA receptor will not operate optimally. This could be a target for pharmacological intervention to increase the local concentrations. However, there are some obstacles to overcome. First, GLY is also an inhibitory neurotransmitter, so increasing the concentration throughout the brain may have some adverse effects. Another issue is that GLY crosses the blood brain barrier very poorly[99] so to increase concentrations in the synaptic cleft just from the diet, there needs to be a large dose of GLY ingested, although one study has demonstrated that increased GLY concentrations can be detected in the brain using ^{1}H-MRS after 2 weeks of ingesting it[100]. A molecule that is similar to GLY but can cross the blood-brain barrier could be ingested, but GLY has such a small

chemical structure that there is really not much leeway in creating a similar molecule[50]. Alternatively, there could be a way to redirect more GLY into the synaptic cleft. One such method lies in targeting GLY transport inhibitors.

There are two GLY transport inhibitors in the brain, GLYt1 and GLYt2, and they both have very different functional mechanisms[50]. GLYt2 is located at the GLY inhibitory neurons, and GLYt1 is located on glial and neuronal membranes and controls the GLY concentration within the synaptic cleft[50]. It is possible to selectively target the GLYt1 receptor with 99% specificity over the GLYt2[50]. Therefore, GLY and its transport inhibitors are an exciting possibility for future drug interventions to improve NMDA efficiency, but so far there has only been limited success[40,50,98,101].

To date, there have only been limited studies of GLY in SZ. One study examined the serum of people with SZ receiving either first-generation antipsychotics (FGA), second generation antipsychotics (SGA), or the atypical antipsychotic clozapine[102] and found the patients receiving clozapine had lower serum GLY levels than patients taking FGA or SGA. This is interesting because clozapine is one of the few currently approved antipsychotics that has some effectiveness in treating negative symptoms[2]. Another study examined GLY levels in the plasma of people with treatment-resistant SZ before and after clozapine treatment[103]. This study found significantly increased plasma GLY levels after clozapine treatment in the SZ group, which was also significantly higher after treatment when compared to controls. Although the results of this study are somewhat contradictory, they do both implicate GLY in the pathophysiology of SZ. It is also important to note that treatment-resistant SZ may operate under different mechanisms than SZ that can be successfully treated with FGA or SGA, going back to the notion that SZ may be a final common pathway of multiple sub-disorders. However, a number of other plasma/serum studies of GLY have shown increased, neutral, or decreased levels of GLY, meaning that the results have been fairly inconsistent[103]. One of the limitations of plasma/serum studies is that it is not necessarily an indication of tissue GLY levels, and the results are not specific to one area of the brain. It would be ideal if GLY could be measured accurately *in vivo* in a localized area of the brain. One possible technique to do this would be ^{1}H-MRS.

The spectral signature of GLY consists of a single resonance at 3.548 ppm[104]. It is a challenging metabolite to quantify reliably with ^{1}H-MRS due to its low concentration and the proximity of its spectral peak with the spectral signature of *myo*-inositol (MYO), a high concentration metabolite with a complicated spectral signature (strong J-coupling). Two studies have been able to detect GLY reliably on 4 T MRI scanners by using a special pulse sequence called echo-time averaging sequence[100,105]. One of these studies examined GLY concentrations in the occipital cortex before and after a 2 week period of oral GLY supplementation and found that they were able to detect a significant increase in GLY concentration after the 2 week period[100]. Another study used a 7 T MRI to detect GLY reliably, again in the occipital lobe[106]. All these ^{1}H-MRS studies have been in healthy controls, and, to date, there have been no published studies on GLY measurements *in vivo* in SZ using ^{1}H-MRS[63].

1.1.5 Summary of ^{1}H-MRS in SZ

As technology has improved, so has the potential to achieve higher quality ^{1}H-MRS spectra. To advance the understanding of SZ it is necessary to utilize these advances and push the limits of what can be achieved. Reliable measurements of GLY concentrations along with static and dynamic measurements of GLU and GLN in SZ in implicated areas within the brain would provide some critical information concerning the health of GLU neurotransmission in SZ. Optimizing ^{1}H-MRS spectra is critical to be able to reliably make these measurements. This will require basic understandings of MRI and ^{1}H-MRS principles.

1.2 Magnetic Resonance Spectroscopy

This will be a brief introduction to concepts and processes involved in acquiring, processing and quantifying ^{1}H-MRS data. For a more thorough review of these topics, please see references[107–113].

1.2.1 Origin of the signal

To understand the mechanisms of ^{1}H-MRS and ^{1}H-fMRS, it is important to first understand some basic principles of nuclear magnetic resonance (NMR). The first requirement for any signal in NMR is a nucleus with a magnetic moment. The magnetic moment comes from a particle's spin, which is a basic property of any nucleus, along with mass, magnetism, and electric charge. Generally, all nuclei with an even mass are bosons and will have full integer spin (i.e. -1, 0, 1), and all nuclei with an odd mass are fermions and will have a half-integer spin (i.e. -½, ½). For any nucleus, there are |2*Spin| + 1 stable spin states. In the absence of an external magnetic field (B_0), every one of these stable rotational states are considered degenerate, meaning they will have the same potential energy. When a B_0 is applied, the degeneracy is removed and there will be an energy separation between the quantum rotational states. This is called the Zeeman effect, or Zeeman splitting, which underlies every observation in NMR spectroscopy.

A ^{1}H nucleus has a ½ spin. It, therefore, has |2*(½)| + 1 = 2 stable spin states. When a B_0 is applied, the magnetic moment of the ^{1}H will precess about the B_0 in one of its two stable energy states, which is either parallel or anti-parallel to the B_0 (Fig 1-4). The parallel alignment is the lower energy state, so, at body temperatures, there will be a small excess of nuclei in the parallel state relative to the anti-parallel. The interaction of B_0 with the particle's magnetic moment results in a torque that will cause the precession of the nuclei about the B_0, and the speed of this precession is proportional to the strength of the B_0. This relationship between the precession frequency (ω) and the B_0 is the Larmor equation:

$$\omega_0 = \gamma * B_0 \qquad 1.1$$

where γ is the gyromagnetic ratio, a nucleus specific value for the ratio between the magnetic moment and the spin angular momentum. In a ^{1}H nucleus, γ is equal to $267.52*10^{6}$ rad/(s*T). Due to the excess number of ^{1}H nuclei in the parallel orientation, there is an accumulation of magnetic moments that leads to a bulk magnetization (M_{0z}) in the longitudinal axis (z-axis). By applying an additional magnetic field (B_1) perpendicularly to B_0 and at the resonant frequency ω_0 it is possible to tip M_0 out of

alignment with B_0 and into the transverse (xy) plane (M_{0xy}) (Fig. 1-5). Figure 1.5 assumes that the axes are precessing about B_0 at ω_0. This is called the rotating frame of reference. By choosing to view the magnetization with this rotating frame of reference, it is easy to visualize the magnetization being tipped by the B_1 pulse:

$$\theta = \omega_1 * T \quad (1.2)$$

where θ is the nutation angle, T is the pulse duration, and ω_1 is the frequency in the rotating frame:

$$\omega_1 = \gamma * B_1 \quad (1.3)$$

The transfer of M_{0z} to M_{0xy} is known as an "excitation pulse", and it enables the detection of the precessing magnetization via an electromotive force induced into a nearby radiofrequency (RF) coil. The electromotive force can be measured as a voltage using a digital voltmeter with a high sampling rate (~1GHz). This voltage is what is typically known as the NMR signal.

1.2.2 Relaxation

After M_z has been transferred to M_{xy}, the magnetization will gradually return back to M_z. This process is called spin-lattice relaxation, or T_1 relaxation:

$$M_z(t) = M_0 * (1 - e^{-\frac{t}{T_1}}) \quad (1.4)$$

where $M_z(t)$ is M_z with respect to time, M_0 is the magnitude of the equilibrium magnetization vector, t is time, and T_1 is the time required for the signal to recover ($1-e^{-1}$) of M_z. The greatest amount of signal is induced into the RF coils when $M_z = 0$, and all the magnetization is in the M_{xy} plane ($M_{xy}=M_0$). In this case, the excitation pulse is known as a 90° flip angle. The T_1 relaxation is an important factor in determining the time between successive excitations. If M_z has not recovered sufficiently there will be less magnetization transferred into M_{xy} in the following acquisition. The most basic NMR

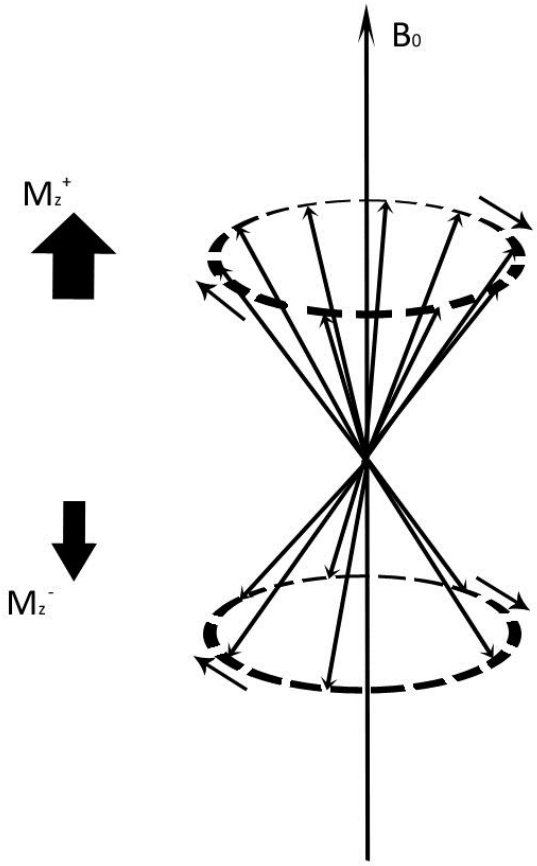

Figure 1-4. The precession of spin-1/2 nuclei in the presence of a magnetic field (B_0) will preferentially orient parallel to the applied field

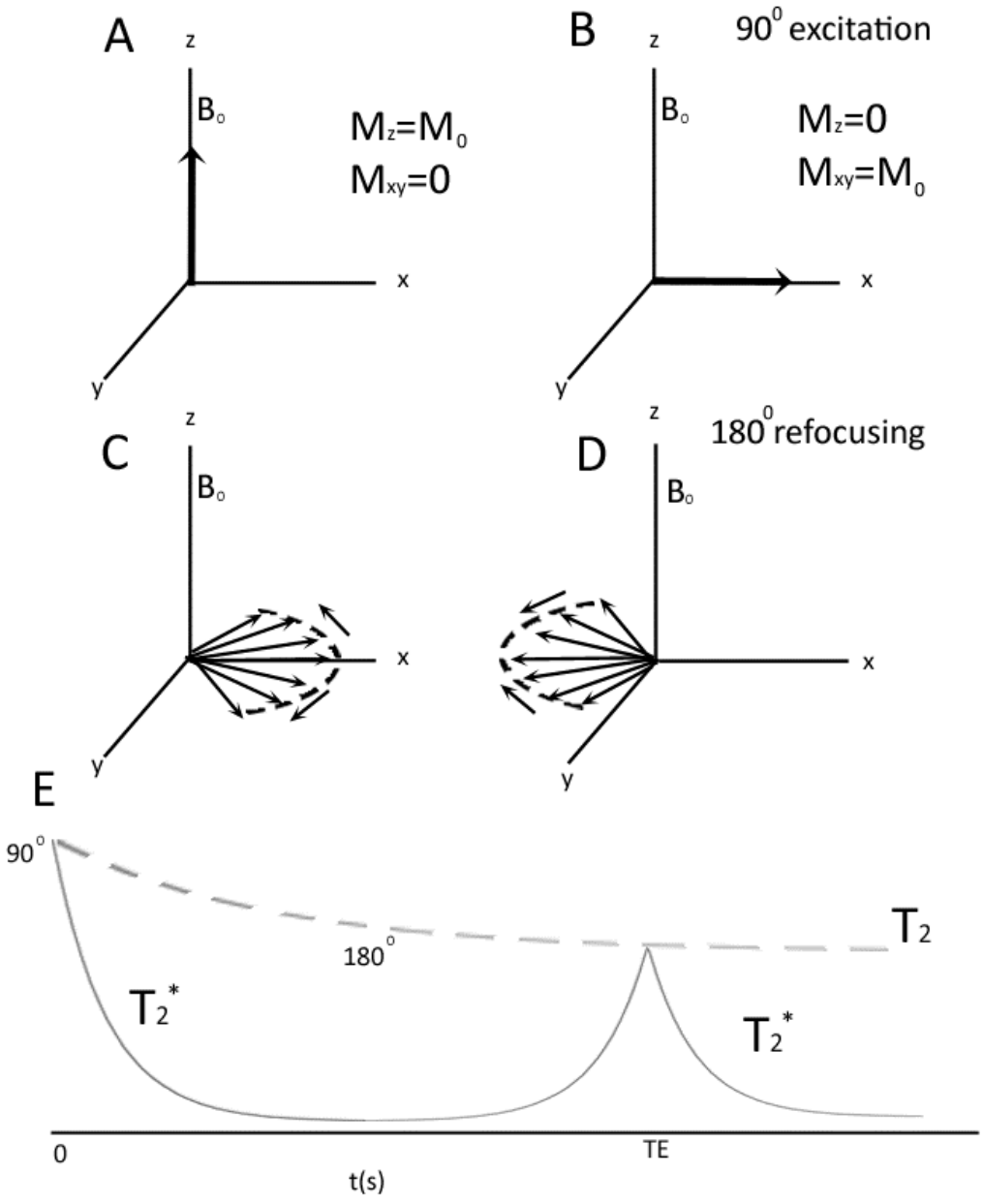

Figure 1-5. Excitation and refocusing of the magnetization in a spin-echo sequence (A) In the presence of an external magnetic field, B_0, the magnetization in the z-axis, M_z, is initially equivalent to the resting magnetization, M_0. (B) After a 90° excitation, the M_z component is fully transferred to the transverse magnetization, M_{xy} and (C) will immediately begin to dephase. (D) After applying a 180° pulse, the M_{xy} is flipped and begins to rephase. (E) This can be visualized by examining the signal in the time domain.

pulse sequence, the "pulse-acquire" sequence, consists of one 90° excitation RF pulse tipping M_z into M_{xy} immediately followed by a signal recording the induced electromotive force into the RF coil. This signal is recorded as a free-induction decay (FID), which is heavily influenced by another form of relaxation called spin-spin relaxation or T_2 relaxation.

To reiterate, the ω_0 is determined by the γ and the B_0. Although efforts are made to make the local magnetic field over the volume of interest as homogenous as possible, the B_0 produced by the MRI and the magnetic characteristics of local environments at the microscopic scale (i.e. local sources of magnetic field distortions, such as blood vessels and interaction between intra- and extra-molecular spins) are still going to be heterogeneous (static dephasing) and fluctuate randomly in time (dynamic dephasing). The relaxation of the M_{xy} in the xy-plane due to the presence of fluctuations in the local magnetic environments of individual spins at the microscopic level is the cause of T_2 relaxation. The M_{xy} will eventually decay to 0 due to this relaxation. The overall effective decay rate observed during as FID, T_2^*, has two components:

$$\frac{1}{T2^*} = \frac{1}{T2} + \frac{1}{T2'} \qquad 1.5$$

where T_2 represents the irreversible decay, T_2' represents a reversible component. The M_{xy} decay is an exponential decay:

$$M_{xy}(t) = M_0 * e^{-\frac{t}{T2^*}} \qquad 1.6$$

where $M_{xy}(t)$ is the magnitude of the transverse magnetization changing in time, and T_2^* is the observed time for M_{xy} to decay to e^{-1} of its original value. T_2 relaxation is specific to the transverse magnetization, while T_1 relaxation is specific to the longitudinal magnetization. During T_2 decay, the bulk magnetization is still in M_{xy}, it is just out of phase. Within a voxel, there are many pockets of spins that experience the same local and relatively unchanging magnetic field called isochromats. These isochromats will accrue phase differences relative to each other. By applying a 180° pulse, the M_{xy} will flip and the isochromats will rephase forming an "echo" (Fig 1-5). Most ^{1}H-MRS pulse sequences

utilize some echo formation method to refocus some of the reversible decay. As the rate of T_2 decay is slower than the rate of T_2^*, echo formation allows for a significant delay between the excitation pulse and the sampling of the signal. This delay is required to implement the essential step of spatial encoding of the MR signal allowing the selection of signals from a given volume of interest rather than from the entire sample.

1.2.3 Electron shielding and chemical shift

If all ^{1}H nuclei experienced the same magnetic field, they would all resonate at the same ω_0. Fortunately for ^{1}H-MRS, the local magnetic field differs from B_0 due to the weakening of B_0 from the electron spins surrounding adjacent nuclei within the chemical structure of a molecule. This phenomenon is called electron shielding. ^{1}H-MRS would not yield useful information without the frequency difference that results from electron shielding as each ^{1}H will resonate at a specific frequency determined by both B_0 and its local magnetic environment. The contributions to the local magnetic environment from surrounding nuclei is much smaller than the contribution of the B_0. It translates to a difference in frequency on the order of Hz, which is considerably smaller than frequencies in the MHz range from the main B_0. This shift in frequency is called the chemical shift:

$$\omega_{shield} = \gamma * B_0(1 - \sigma) \quad 1.7$$

where ω_{shield} is the resonant frequency of the shielded resonance, and σ is the shielding constant. It is common to refer to the chemical shift in a parts per million (ppm) scale:

$$\delta = \frac{\omega_0 - \omega_{shield}}{\omega_0} \, x \, 10^6 \quad 1.8$$

with δ as the resonance frequency in ppm and ω_0 as the frequency of a resonance at B_0. In ^{1}H NMR, 0 ppm is represented by tetramethylsilane (TMS). TMS contains 4 CH_3 groups attached to one Si. Each of the ^{1}H nuclei are maximally shielded by surrounding electrons. As shielding decreases, the ppm value increases. The ppm scale is convenient because there are multiple common B_0 utilized in MRI studies and the δ of each ^{1}H nuclei

does not change with B_0. For example, creatine resonates at 191.6 Hz relative to TMS at 1.5 T, 383.2 Hz on a 3 T and 894.1 Hz on a 7 T. Using ppm values, creatine resonates at 3.02 ppm relative to TMS at all fields. Electron shielding determines the ω, but the shapes of spectra originating from molecules with more than one proton are complicated by the intra-molecular interaction of spins (via their electron spin), an effect known as J-coupling.

1.2.4 J-coupling

Also known as peak-splitting, J-coupling refers to the possibility that multiple local magnetic field environments are possible within a molecule, which can reduce one strong singlet peak into multiple smaller peaks (Fig 1-6). This can best be understood with an example. The molecular structure of GLU is shown in Figure 1-2A, featuring five protons (hydrogen nuclei). Each ^{1}H nuclei attached to the C4 (carbon atom number 4) can align itself with or against B_0. They both can be up, they both can be down, or one can be up and one can be down with the latter option having twice the probability. This means there are three different local magnetic fields possible that the ^{1}H nuclei on the C3 can experience due to the ^{1}H nuclei on the C4, splitting a singlet from a ^{1}H on the C3 into a triplet. The triplet is then further split into a complicated multiplet due to significant interaction with the ^{1}H nuclei on the C2, which can also align themselves with or against the magnetic field. Peak splitting reduces the amplitude of the signal from resonances closer to the level of noise, and widens the spectral signature for a given metabolite, further complicating quantification.

Spin pairs can be strongly coupled (AB) or weakly coupled (AX). J-coupling leads to phase cancellation within a multiplet, called J-dephasing. Stronger coupling accentuates these effects and further complicates the relative amplitudes of the peaks that are being split. Weak coupling will perform in very predictable ratios according to Pascal's triangle, while strong coupling will skew the proportions based on how strongly they are coupled (Fig. 1-6). The coupling strength is determined by the relative magnitude of the J-coupling constant to the differences in resonance frequency. For example, heteronuclear

coupling (i.e. between a ^{1}H spin and a ^{13}C spin) would be very weakly coupled due to the large differences in their resonant frequencies (i.e. MHz). GLU and GLN are examples of two metabolites that experience strong J-coupling resulting in broader spectral patterns. Due to the similar chemical structures between GLU and GLN, this broadening of the spectral patterns leads to much overlap and can make them very hard to differentiate in ^{1}H-MRS. Fortunately, it is possible to reduce the influence of J-dephasing. The local

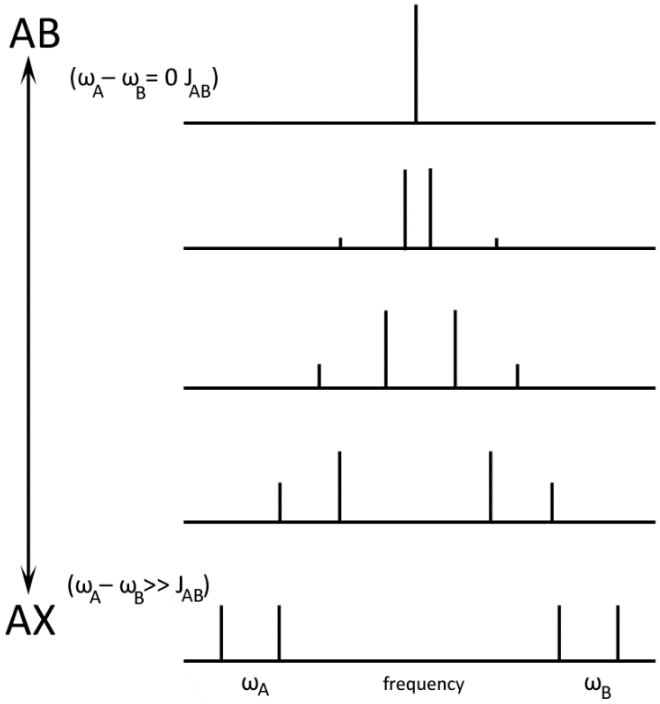

Figure 1-6. The splitting of peaks in coupled spin systems.
When the J-constant between two resonances, J_{AB}, is comparable to the relative difference between the centers of the two resonant frequencies, ω_A and ω_B, the pair is deemed to be strongly coupled (i.e. AB). When J_{AB} is not comparable to the difference between ω_A and ω_B, as in heteronuclear systems, for example, the pair is considered to be weakly coupled (i.e. AX).

magnetic field differences due to the multiple possible spin orientations that cause J-coupling are not influenced by B_0. Therefore, on a ppm scale, as B_0 increases, the shape of the multiplets slowly begin to converge towards being a single peak (unresolved multiplet). This increases the peaks' signal above the noise, and reduces the peaks' overlap with other spectral signatures. This effect will be described in greater detail in chapter 2.

1.2.5 Ultra-High Field (≥ 7 T) Spectroscopy

One of the biggest determinants of spectral quality is the B_0 strength of the MRI. Although stronger B_0 MRI scanners can be expensive, there are many potential benefits. As mentioned in the above section, strong B_0 reduces the influence of strong J-coupling on the spectral lineshape on a ppm scale. By a similar argument, the spectral dispersion of the spectra also improves. That is, the ratio of the distance between peaks of two different ^{1}H nuclei and their Lorentzian linewidths is increased, which results in sharper peaks and less spectral overlap between metabolites. Some of the improvements in spectral dispersion are countered by increased Lorentzian linewidths (decreased T_2*) at stronger B_0 that increase *in vivo* at a rate of 1.35 Hz/T[114]. The linewidths are a measure of the exponential T_2* decay of the signal, such that slowly decaying signals (i.e. long T_2*) will have sharper spectral peaks than fast decaying signals (i.e. short T_2*). Even with this broadening of the resonance, there is still a net reduction in spectral overlap when B_0 increases (assuming similar conditions).

A stronger B_0 causes more ^{1}H nuclei to align themselves parallel to the field. It also induces more torque on the spin, leading to a faster ω (in accordance with the Larmor frequency, Eq 1.1). All together, the SNR improves as B_0 strengthens with an approximately linear relationship when scanning humans[115]. ^{1}H-MRS is a traditionally low SNR technique and requires many signal averages (addition of repeated measurements). In NMR, SNR is essentially a currency that can be traded for smaller voxels to reduce partial volume effect on small brain structures, faster scan times (by reducing averages) to reduce patient motion during the scan (and perhaps scan more

voxels), or it can simply be used for improved quantification of the data. Therefore, there are huge potential improvements that can be realized using ultra-high field B_0, but there are also challenges to overcome.

As the main B_0 increases, so do the technical limitations. For example, the wavelength of a B_1 pulse in human brain tissue at 3 T is approximately 30cm. At 7 T, this wavelength is approximately 13cm, which is also approximately the width of the human head. This is a problem in imaging because there will be bright and dark spots throughout the volume due to the nodes of the electromagnetic B_1 pulse. Fortunately for spectroscopy, the phase of the B_1 pulse does not change substantially over a typically sized voxel. This problem can effectively be mitigated in ^{1}H-MRS by using an increased number of transmitters and B_1 shimming[116].

A limitation of ultra-high field B_0 ^{1}H-MRS is that the power required for a B_1 pulse to achieve a given ω_1 increases with B_0[117]. Although B_1 shimming can help this issue, hardware limitations and increased thermal energy deposition, or specific absorption rate (SAR), are real problems at high B_0. This needs to be considered during sequence development.

1.2.6 Voxel localization

In vivo ^{1}H-MRS is generally divided into single-voxel ^{1}H-MRS (SVS) techniques and chemical shift imaging (CSI) techniques. CSI outputs spectra from a slab or volume of voxels, while SVS generally only outputs a spectrum from one or two voxels. There are advantages and disadvantages to both techniques. With CSI it is obviously a benefit to have multiple spectra from throughout the volume. This is especially good for observing the three strongest singlet signals in ^{1}H-MRS, namely N-acetylaspartate (NAA), creatine (Cr), and choline (Cho). The disadvantages to CSI include the potentially very long acquisition times, the contamination of the spectra from signals outside each voxel (point spread function), and the increased linewidths from poorer B_0 shims throughout the brain that lead to reduced spectral quality[111]. SVS has superior spectral quality to CSI. It is

much easier to shim over one localized voxel than it is to shim over the entire brain, the SVS spectra can be acquired individually then easily frequency and phase corrected, signals from outside the voxel can be suppressed using outer volume suppression (OVS) techniques and there is usually sufficient time to acquire a water unsuppressed spectrum and a metabolite suppressed spectrum (discussed below) to strongly improve overall quantification of metabolites. Only SVS spectra were acquired for this thesis due to the superior spectral quality required for quantification of glutamate and glutamine. For the remainder of the thesis, ^{1}H-MRS will refer to SVS.

As previously mentioned, most ^{1}H-MRS pulse sequences utilize some method to refocus M_{xy}. This is more of a necessity because ^{1}H-MRS pulse sequences require voxel localization. Voxel localization is the process by which the tissue within a specific volume becomes excited while leaving the area around it in a relaxed or un-refocused state. This is typically done using three slice-selective B_1 pulses and orthogonal magnetic field gradients. Magnetic field gradient pulses create magnetic field intensity distributions throughout the volume that vary linearly along a selected direction. A slice-selective RF pulse with a specific carrier frequency, excitation bandwidth, and gradient amplitude alters B_0 (and, therefore, ω_0) along the axis of the gradient pulse and will excite a specific slab within the volume (Fig 1-7). If this is done along all three axes then there will be a rectangular volume at the intersection of all three slabs, the ^{1}H-MRS voxel, from which ^{1}H-MRS signal will be refocused (generation of an echo signal). This process allows selection of voxel position, shape, and volume. The two most common ^{1}H-MRS techniques for voxel localization are Stimulated Echo Acquisition Mode (STEAM)[118] and Point-Resolved Spectroscopy (PRESS)[119], both of which have their advantages and disadvantages[120].

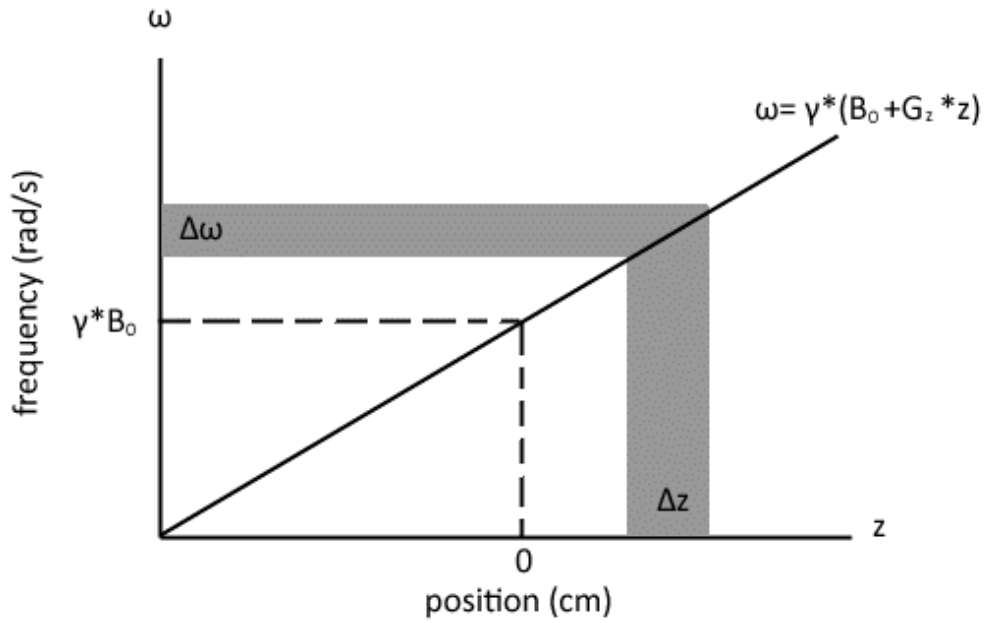

Figure 1-7. Slice-selection frequency bandwidth for a slice thickness and position. A slice-select gradient, given by the equation $\omega = \gamma * (B_0 + G_z * z)$, can create a difference in the local magnetic field in one direction across a volume. Therefore, a specific excitation bandwidth, $\Delta\omega$, can be used to excite a specific slice, Δz, while leaving the remaining volume unexcited.

PRESS is a powerful technique that utilizes a slice-selective 90° pulse followed by two slice selective 180° pulses. The initial 90° pulse will excite a slab by flipping the signal from the longitudinal axis into the transverse axis (M_z to M_{xy}). The first 180° pulse will excite another slab along a different axis, which will effectively flip the M_{xy} magnetization about the z-axis in the voxel of interest. The final 180° pulse excites the final slab that flips the magnetization within the voxel one more time about the z-axis and leads to a spin echo from the voxel at a certain echo time (TE).

STEAM (Fig 1-8) utilizes three 90° pulses instead of the 90°, 180°, 180° combination for PRESS. The first 90° pulse excites a slab similar to the first pulse in PRESS. The

second 90° pulse then flips the signal from the voxel into the longitudinal axis for a duration known as the mixing time (TM), before the final 90° pulse flips the signal back into the transverse plane to form a stimulated echo. The 90° pulses require less power and deposit less thermal energy, or SAR, into the volume. At high B_0, power and SAR become serious limitations during sequence development. The 90° pulses also have better slice profiles, which means that the spectra will have less contributions from signals outside the nominal voxel volume (the theoretical rectangular prism defining the desired voxel boundaries). The TM can be much longer than the TE, which means that additional saturation pulses and crusher gradients can be played out during this time without reducing the signal (with the exception of some T_1 relaxation). In addition, due to the temporary storage of the magnetization into the longitudinal axis during the TM, the sequence can have a shorter TE than a PRESS sequence. Lower TE reduce the amount of signal decay from T_2 relaxation and reduce the signal lost to J-dephasing in J-coupled metabolites. Due to the strong coupling of GLU and GLN signals, lower TE are desirable. A downside to the STEAM sequence is that only half of the magnetization gets restored into the transverse plane, leading to half of the measured signal from the voxel and reduces the SNR. However, this is partially compensated by the reduced achievable TE. There are many benefits to STEAM at high B_0, so it will be used for all ^{1}H-MRS measurements in this thesis and has been used by our lab previously[22,24]

1.2.7 Water Saturation

One of the obstacles to overcome with ^{1}H-MRS is the overwhelming signal from the two ^{1}H nuclei in water molecules. In the human brain, the concentration of water is approximately 37 mol/L[121]. This is huge in comparison to the concentrations of metabolites of interest that are generally in the 1-10mmol/L range, approximately four orders of magnitude smaller. It would not be possible to reliably measure metabolites *in vivo* ^{1}H-MRS without an effective means to remove the water signal peak located at 4.7 ppm. The typical method to do this involves a hard narrowband B_1 pulse centered on 4.7

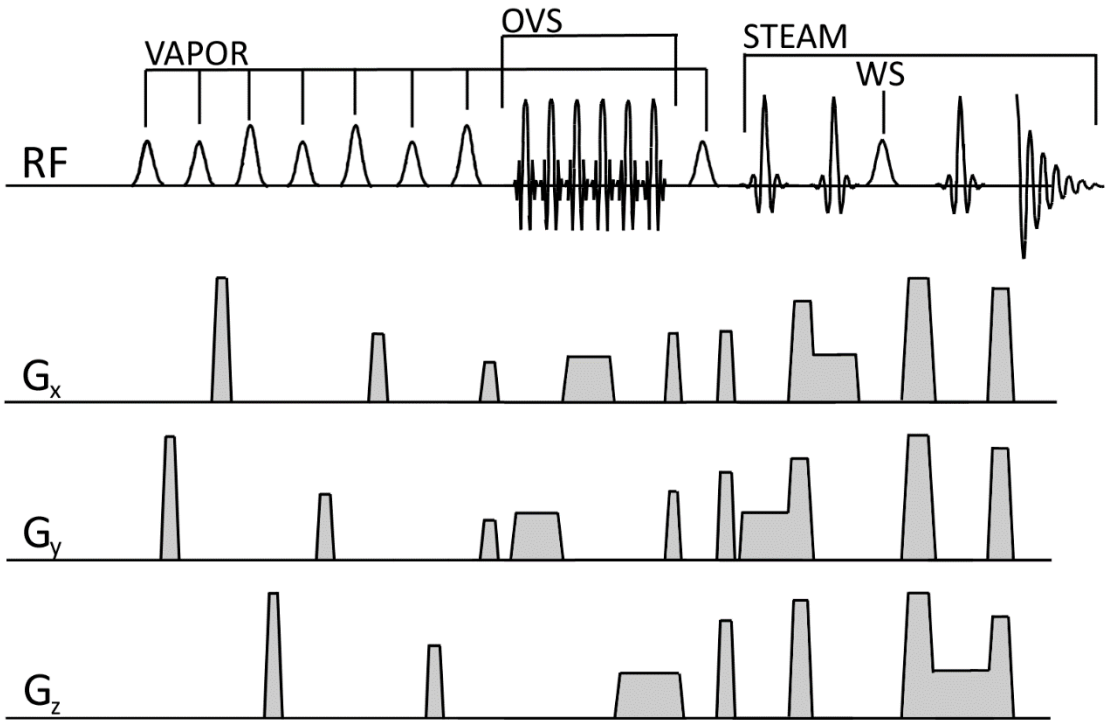

Figure 1-8. The ^{1}H-MRS STEAM pulse sequence with VAPOR water suppression. The sequence begins with VAPOR water suppression, which has 8 radiofrequency (RF) pulses that are chemical shift selective (CHESS) and 1 block of outer volume suppression (OVS) interleaved between the 7 T^{h} and 8^{th} pulses. Voxel selection is then performed by a STEAM sequence that has three slice-selective pulses one in each axis. An additional water suppression pulse has been added in-between the 2^{nd} and 3^{rd} slice-selective pulses. G_x, G_y and G_z represent gradients that are played out in each of the x, y, and z axis, respectively.

ppm that selectively excites the water signal into M_{xy} prior to the start of the voxel localization sequence. The water signal is then sufficiently crushed using magnetic field gradients, eliminating the detectable component of the water signal. It is common practice to use multiple B_1 pulses to provide more efficient suppression. One such sequence, Variable Power and Optimized Relaxation Delays (VAPOR)[122], involves eight B_1 pulses separated by crusher gradients and timing intervals is particularly insensitive to small variations in B_1 pulse power, which typically needs to be optimized at the start of each acquisition. An example of a VAPOR water suppression sequence that could be played out prior to a STEAM sequence is in Fig. 1-8.

1.2.8 Post-processing

After the FID for the spectra have been recorded there are multiple processing steps necessary before the data is ready to be quantified.

1.2.8.1 Receiver combination

Most head coils have a multiple-receiver setup, especially if the brain area of interest is not located on the periphery. Each coil will record a FID for every ^{1}H-MRS acquisition. Some of these coils will be close to the signal source, while others may be far away and acquiring lower signal (mostly noise). Most resulting FIDs will be out of phase with each other. For these reasons, spectra should not simply all be added together. This could add noise unnecessarily, and the out of phase components will add at least somewhat destructively. A method has been developed for optimal receiver combination that uses the phases and amplitudes of the unsuppressed water peaks[123]. The phase of the water signal from each coil is recorded and adjusted relative to the signal in the first coil. The spectra can then be added constructively. The amplitudes of the water signal determine the relative weighting of each spectrum so that the water suppressed spectra that are acquiring mostly noise will contribute much less than spectra with lots of signal. After

the receivers have been combined, the spectra are ready for frequency and phase correction.

1.2.8.2 Frequency and phase correction

^{1}H-MRS acquisitions often require the combination of many spectra to acquire a spectrum with adequate SNR. During long acquisitions, some frequency drift may occur due to the heating up of the gradients and some phase shifts may occur due to subject motion. That's why it is important to collect the spectra individually and correct the frequency and phase prior to averaging the spectra together. If left uncorrected, the frequency shift between successive spectra will blur the resulting combined spectrum and the phase offset between successive spectra will cause destructive addition. To correct the frequency of each individual spectrum, one simply tracks the frequency of a prominent spectral peak (i.e. Cr, Cho, NAA) and adjusts the frequency to each spectrum relative to that of the first spectrum. To correct the phase, examine the phase of the first few points of the FID and adjust the phase of each spectrum relative to that of the first spectrum. This will ensure the optimal combination of the data (i.e. frequency- and phase-coherent averaging).

1.2.8.3 Averaging

Now that the spectra from each of the receive channels have been combined and the data have been frequency and phase corrected, the individually acquired spectra may now be combined into one higher quality spectrum. With all the preprocessing complete, all that is necessary is to add the spectra together. This will improve the SNR of the spectra at a rate proportional to the root of the number of averages:

$$SNR \propto \sqrt{N_{AVG}} \tag{1.9}$$

where N_{AVG} is the number of averages. This is another reason why stronger B_0 is important for increasing the SNR, as it takes four times as many averages to double the SNR from an

acquisition. For example, it would take 3 minutes 12 seconds to acquire a 64 average spectrum at 7 T. To acquire a spectrum with the same SNR at 3 T, this would take 17 minutes 25 seconds (5.4 times as long), assuming similar voxel conditions (i.e. volume, location, etc) and the main source of the noise is the sample.

1.2.8.4 Lineshape correction

When a FID is acquired it typically does not decay with the perfect lineshape that would be predicted from Eq 1.4. The main contributions to lineshape imperfections come from magnetic field inhomogeneities and eddy-current artifacts. The magnetic field inhomogeneities are often unavoidable but can be minimized by using a good B_0 shimming algorithm. The eddy-current artifacts come from ramping magnetic field gradients pulses shortly prior to signal acquisitions. This induces currents into the cryostat of the scanner, which induces temporally decaying B_0 offsets. These eddy currents tend to be more pronounced in short-TE spectra because the last crusher gradient is played out right before the acquisition of the FID (A longer TE would allow the eddy-currents to dissipate). These can greatly distort the lineshapes of spectral peaks and ultimately make it difficult to predict the lineshape to use for fitting. Through a process called Quality Eddy Current Correction (QUECC), it is possible to remove the eddy current artifacts and remove the majority of the lineshape imperfections due to magnetic field inhomogeneities[124]. QUECC requires a reference lineshape to deconvolve form the spectrum. This lineshape reference is typically the water peak obtained from a water-unsuppressed spectrum. It is, therefore, necessary to acquire a water-unsuppressed spectrum that produces the same eddy-current artifacts as those observed in the water-suppressed acquisition (matched gradient waveforms, i.e. only RF off). Essentially, the water suppressed data is divided (complex division) by the water unsuppressed data and convolved with a Lorentzian function to make all peaks in the spectrum Lorentzian. This is done only until the water signal approaches 0 else there will be a characteristic artifact in the data. The remainder of the signal undergoes phase corrections only (no division by amplitude of reference, only its phase term). QUECC allows one to use the working assumption that the spectral lineshapes are Lorentzian for the purpose of data modelling.

1.2.9 Spectral Fitting

Now that the post-processing is complete, the next step is to quantify the data. Every peak (excluding spectral noise) represents signal from the ^{1}H of a particular metabolite and the area underneath the peak will be proportional to the concentration of that metabolite in the volume of interest. There are usually contributions from ^{1}H nuclei of many metabolites that often overlap and can make the spectrum very complicated. To isolate a metabolite's contribution to the signal, it is first necessary to know their unique spectral signatures.

1.2.9.1 *A priori* information

Fitting a ^{1}H-MRS spectrum requires *a priori* information (prior knowledge) about the relative distribution of resonances from each metabolite's ^{1}H nuclei. Each metabolite has a characteristic pattern of resonances with predictable relative amplitudes and chemical shifts known as a spectral signature. Every resonance from a metabolite varies in amplitude together so it is possible to model the spectral signatures by constraining the predictable information together. There are multiple methods to determine the relative resonances for each metabolite with a specific ^{1}H-MRS pulse sequence and B_0 (because both will influence the fit). First, *in vitro* metabolite solutions (i.e. phantoms) containing only one metabolite and a reference (TMS for reference at 0 ppm) can be scanned and modelled. This will provide a spectrum with the predictable resonance pattern that can be modelled iteratively with the relative amplitudes, chemical shifts, phases, and linewidths of each resonance of the pattern appropriately constrained. This information would be located in two files known as a .ges or a .cst files. The .cst file or "constraint" file, holds all the set relationships between the properties of individual peaks within the metabolite's spectral signature (Fig 1-9A), while the spectrum specific initial parameter estimates for each metabolite (not each resonance) are located in the .ges files (i.e. "guess" file; Fig 1-9B). The information in the .ges file is used to seed the iterative fitting algorithm that will provide an estimate of each metabolite's concentration.

Another method to determine the spectral signatures for each metabolite is to simulate responses of a given spin system with known chemical shifts and coupling constants[104,125] to a particular pulse sequence using density operator calculations or product operator formalism. The advantage to the simulation method is that it can quickly produce exact representations of the spectral signatures for a given TE and TM of the STEAM sequence that can readily be incorporated into .ges and .cst files. Of course, the development of the simulation package for a specific pulse sequence is a specific scientific effort and was not part of this thesis (more details provided in chapter 2)[125].

A full template that can be used for metabolite quantification of *in vivo* spectra can be made by combining .ges and .cst files from each metabolite into one pair of large .ges and .cst files. This works well if a complete list of metabolites contained in the spectrum is known. This is not always the case. For example, the exact molecules producing the broad, so called macromolecular, resonances part of short-TE human brain spectra are typically not known.

1.2.9.2 Macromolecular fitting

One of the biggest challenges in quantification of short-echo ^{1}H-MRS spectra is the issue of modeling the broad, fast-relaxing macromolecular components that overlap metabolite signals throughout the spectrum. This macromolecular baseline is composed of DNA, RNA, proteins and phospholipids. The signal is most prominent at low TE, so one way to reduce their influence in the spectrum is by using very long TE. However, this is not a practical approach for quantifying strongly coupled metabolites such as GLU and GLN that have highest signal at low TE[63]. Another way to account for the macromolecules is to acquire a separate metabolite- (and water-) suppressed spectrum that will leave only signal from the macromolecules remaining. One method to go about this is to use multiple well-timed inversion recovery pulses that effectively saturate the metabolite signal prior to the STEAM acquisition. This macromolecular signal can then be modeled using a Hankel-Lanczos Singular Value Decomposition (HLSVD; Fig.1-10)[126,127] fit,

A

```
[Peaks]
1   {shift}+2.732710 {lw} {glu}*0.031749 >0 {ph}+0.248862 {DT} @{WG}
2   {shift}+2.708890 {lw} {glu}*0.061366 >0 {ph}+0.113159 {DT} @{WG}
3   {shift}+2.705860 {lw} {glu}*0.031057 >0 {ph}+0.095781 {DT} @{WG}
4   {shift}+2.685060 {lw} {glu}*0.030100 >0 {ph}-0.037962 {DT}  @{WG}
...
...
...
```

B

```
[Peaks]
1   2.73    10    0.302294*glu  0    0    0
2   0       0     0             0    0    0
3   0       0     0             0    0    0
4   0       0     0             0    0    0
...
...
...
```

Figure 1-9. Resonance information as it would be listed in (A) .cst and (B) .ges files. The .cst file contains the fitting parameters denoted by the { and } brackets, which contain individual modifications for each resonance. The parameters that would be constrained include the chemical shift (i.e. {shift}), the Lorentzian linewidth (i.e. {lw}), the metabolite specific amplitude parameter (i.e. {glu} for glutamate), the phase (i.e. {ph}), the delay time (i.e. {DT}), and the Gaussian linewidth (i.e. {WG}). The "@" symbol indicates that the final value for the fit should be taken directly from the .ges file. The .ges file includes the initial "guesses" for each parameter. Values are only needed the first time a fitting parameter is used (or if there is an "@" in the .cst file), which is why in this example only peak 1 has any values. The *glu value is a variable that would be specific for modifying glutamate concentrations, located for convenience at the top of the file. Due to the QUECC lineshape correction employed in our lab, all Gaussian widths are set to 0.

which will output a list of resonances that fit the data. These resonances can be constrained together into a macromolecular spectral signature, and then added to the quantification template.

1.2.9.3 fitMAN

Now that a template has been built with the resonances of each metabolite (and the macromolecules) modelled and constrained, it is time to fit the spectrum using the time-domain iterative fitting algorithm, fitMAN[128]. The fitting algorithm takes the initial estimate of the fit (constructed from the information in the .ges and .cst files) and iteratively modifies the model parameters, within the given set of constraints, until the difference between the data (from a .dat file) and the model (i.e. the residuals) is minimized (i.e. the residuals are below a pre-defined acceptable level or after a predefined maximum number of iterations has been reached as indicated in the header of the .cst file). Upon completion, fitMAN will output the final fit parameters for every resonance into a separate .out file to be used in determining the metabolite concentrations.

1.2.9.4 Quantification

The amplitude of each resonance represents the signal contribution at t=0 in the time domain. The total area occupied by the resonances of each metabolite can be determined by adding up the amplitudes of each metabolite's resonances from the .out file. This estimate of the metabolite's area can be used to estimate the metabolite's concentration, [Met], by using the area of the water signal as a reference of known concentration[129]:

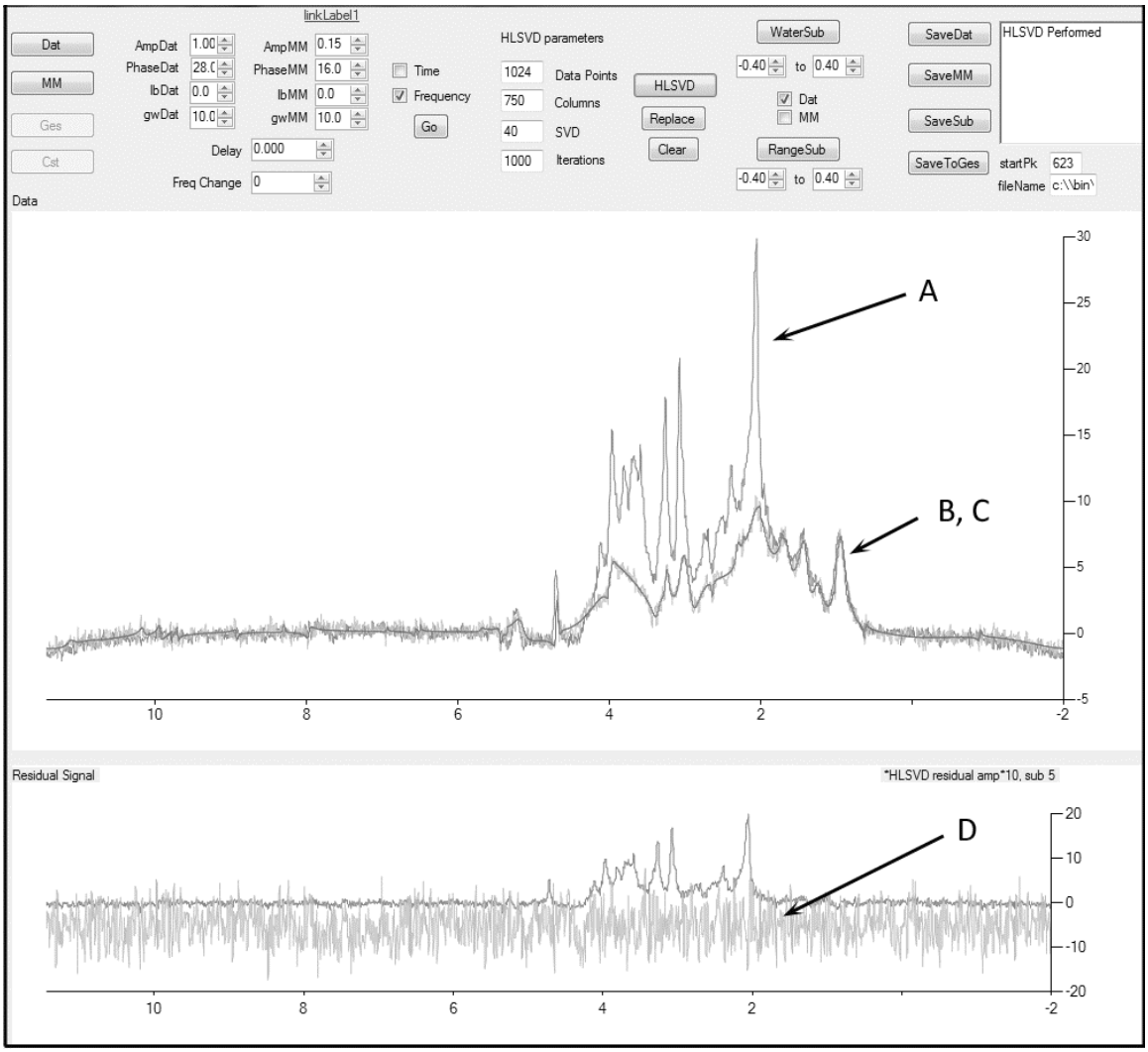

Figure 1-10. datSub, a user interface for the HLSVD fitting of macromolecules. This program allows a user to overlay the (A) water suppressed spectrum with the (B) macromolecular (metabolite and water suppressed) spectrum and (C) perform an HLSVD fit of the macromolecules. (D) The residuals between the HLSVD fit and the macromolecular spectrum can be viewed amplified by a factor of 10.

$$[Met] = \frac{\frac{(\frac{A_M}{N_{AVG\_M}})}{10^{(\frac{G_M}{20})} * Scale_M}}{\frac{(\frac{A_W}{N_{AVG\_W}})}{10^{(\frac{G_W}{20})} * Scale_W}} * 36.9\ \frac{mol}{L} * \%_W * \frac{2}{\#_{protons}} \quad 1.10$$

where A_M and A_W is the spectral area of the metabolite and water, respectively, N_{AVG_M} and N_{AVG_W} is the number of averages of the water suppressed spectrum and water unsuppressed spectrum, respectively, G_M and G_W is the gain used in the water suppressed acquisition and water unsuppressed spectrum, respectively, $Scale_M$ and $Scale_W$ is a metabolite and water scaling factor (used for scaling the real and imaginary points of the data spectrum), respectively, that can be found in the header of the original .dat files, 36.9 mol/L is the concentration of water in the brain, $\#_{protons}$ is the number of protons contributing to the metabolite's spectral area, and $\%_W$ is the percentage of tissue that is water from that voxel. The $\%_W$ is determined based on the amount of gray matter, white matter, and CSF in the tissue[129]:

$$\%_W = \frac{((0.81 * f_{gray}) + (0.71 * f_{white}))}{1 - f_{CSF}} * \frac{\frac{water_{density}}{water_{molecularWeight}} * 1000}{36.9\ \frac{mol}{L}} \quad 1.11$$

where f_{gray}, f_{white}, and f_{CSF} are the fractions of gray matter, white matter, and CSF in the voxel, $water_{density}$ is the density of water at body temperature (0.99299g/cm^3), $water_{molecularWeight}$ is the molecular weight of water at body temperature (18.0152 g/mol), 0.81 is the fraction of water content in grey matter and 0.71 is the fraction of water content in white matter[129]. Using this formula, it is possible to determine the concentrations of metabolite spectra acquired *in vivo*. The typical concentration range of detectable metabolites *in vivo* is 0.5-15 mmol/l for realistic acquisition times and voxel sizes.

1.3 Thesis Objectives

The ultimate purpose of this thesis is to learn more about the health of the glutamatergic system in SZ using advanced hardware and methodology. Outlined below are specific objectives with their associated hypothesis for chapters 2-5 of this thesis, respectively.

1.3.1 Demonstrate the benefits of ultra-high field for GLU and GLN ^{1}H-MRS

Prior to embarking on a challenging study using the new, advanced brain imaging infrastructure that is the 7 T MRI scanner, it is wise to first demonstrate that the resulting benefits are worth the significant effort involved. The first objective is to determine what improvements in quantification can be expected as the B_0 increases. One approach consists in using a spectral simulation framework, such as the one previously mentioned while describing the fitting process, to create metabolite quantification templates. These simulations can generate spectra with known concentrations of a known list of metabolites for a range of B_0 and SNR, then use a Monte Carlo approach to repeatedly fit noisy realizations of the simulated spectrum. With such large simulated datasets, one can evaluate the factors affecting the precision and accuracy of the quantification procedure. It is hypothesized that improvements in B_0 and SNR will generally improve the coefficients of variation of metabolite concentration estimates with the greatest improvements being in J-coupled metabolites (i.e. GLU and GLN), while decreasing the correlations between different metabolite concentration estimates due to the reduced spectral overlap at higher B_0 and reduced influence of noise on the variability of the fit with higher SNR.

As B_0 increases so do the number of metabolite peaks that rise above the level of the noise and should be accounted for in the quantification template. Forming a complete list of the metabolites that should be part of the quantification template is not a simple task. There is currently no data-driven method to determine which metabolite should be included versus omitted. The addition of extraneous metabolite signatures in the quantification template increases the dimensionality of the spectral modelling problem

and negatively affects the precision of all metabolites. If metabolites that should be included are omitted, the spectral fitting algorithm will attempt to minimize residuals by over- or under-estimating other metabolite considerations. This raises the question as to which metabolites absorb the residual signal from these unaccounted metabolites, and how could an incomplete quantification template influence the interpretation of the existing large body of human brain MRS literature. It is hypothesized that metabolites that overlap with each other will be influenced the most by an omitted metabolite, and this will be more pronounced at lower B_0 due to decreased spectral dispersion.

This thesis objective is explored in greater details in the article presented in chapter 2, which was submitted for publication in Magnetic Resonance in Medicine. Revisions have been requested by the reviewers prior to resubmission. These have been addressed in chapter 6 of this thesis.

1.3.2 Examine glutamate, glutamine, and glycine in schizophrenia

The ACC and the thalamus are key nodes implicated in the symptoms of SZ, with NMDA hypofunction as one of the leading theories. Past studies have implicated GLU and GLN in SZ using ^{1}H-MRS at lower B_0[18,22,24]. These studies should be replicated and validated using the expected improvements in metabolite quantification of a 7 T MRI. One limitation of previous studies is that the comparison is only of SZ to healthy controls. The reality is that many of the symptoms of SZ are overlapped with other disorders as well, such as in major depressive disorder (MDD). The inclusion of a psychiatric control group would benefit the study and help improve the specificity of the results. Therefore, metabolite concentrations will be assessed in the SZ group relative to healthy controls and also to a psychiatric control group of MDD. It is possible that NMDA hypofunction could be due abnormalities in GLU and GLN or to the unavailability of GLY (lower glycine concentrations) in the synaptic cleft. It is hypothesized that there will be increases in GLN and decreases in GLU in the SZ group relative to the control groups based on the literature[18,22,24]. In addition, no study to date

has examined GLY in SZ with ^{1}H-MRS. It is hypothesized that there will be abnormal GLY concentration in the SZ group relative to the control groups.

Our exploration of "resting" levels of GLU, GLN, and GLY in SZ compared to healthy and MDD control groups is presented in chapter 3. This article has been prepared for submission to The British Journal of Psychiatry.

1.3.3 Demonstrate glutamate changes with ^{1}H-fMRS in the ACC using a cognitive task

There have been many ^{1}H-MRS studies that have demonstrated GLU and GLN dysfunction in SZ. A limitation of these studies is that the concentrations have all been measured in an uncontrolled "resting" state and at one time point. Of course, glutamate concentrations are adjusted dynamically, at the microscopic level, when transitioning from periods of rest (lower neuronal spiking activity) and periods of activity (higher neuronal firing rates) in glutamatergic neurons. One way to assess the health of the GLU-GLN cycle is to perform ^{1}H-fMRS and assess GLU and GLN concentrations dynamically during prolonged periods of controlled rest (visual fixation) versus periods of prolonged functional activation (i.e. a cognitive task). There are no studies to date using ^{1}H-fMRS at 7 T to show GLU changes during a cognitive task, so the ability of ^{1}H-fMRS to detect such dynamic regulation of glutamate will first need to be demonstrated in healthy controls. Based on other ^{1}H-fMRS studies that have demonstrated GLU changes after visual or motor stimulation[75–77,80,81], it is hypothesized that a color-word Stroop task will stimulate the ACC and increase GLU concentrations upon functional activation.

The results of the study conducted based on these scientific questions have been published in NeuroReport and form the contents of chapter 4.

1.3.4 Examine ^{1}H-fMRS in the ACC using a cognitive task in schizophrenia

Once the ^{1}H-fMRS in the ACC has been established in healthy controls, the next step is to implement this in individuals with SZ and MDD (psychiatric control group). Due to the abnormal GLU and GLN concentrations that have been reported in "resting" ^{1}H-MRS studies in SZ, it is hypothesized that dysfunctions of the GLU-GLN cycle will manifest themselves as abnormal modulation of either GLU or GLN concentrations in response to functional activation.

The results of this study have been accepted for publication in npj Schizophrenia and form the contents of chapter 5.

1.4 References

1. Williamson, P. C. & Allman, J. M. *The Human Illnesses: Neuropsychiatric Disorders and the Nature of the Human Brain*. (Oxford University Press, 2011).

2. Williamson, P. C. *Mind, Brain, and Schizophrenia*. (Oxford University Press, 2006).

3. Angst, J. & Marneros, A. Bipolarity from ancient to modern times: *J. Affect. Disord.* **67,** 3–19 (2001).

4. Jeste, D. V., del Carmen, R., Lohr, J. B. & Wyatt, R. J. Did schizophrenia exist before the eighteenth century? *Compr. Psychiatry* **26,** 493–503 (1985).

5. Saha, S., Chant, D., Welham, J. & McGrath, J. A systematic review of the prevalence of schizophrenia. *PLoS Med.* **2,** 0413–0433 (2005).

6. Ochoa, S., Usall, J., Cobo, J., Labad, X. & Kulkarni, J. Gender Differences in Schizophrenia and First-Episode Psychosis: A Comprehensive Literature Review. *Schizophr. Res. Treatment* **2012,** 1–9 (2012).

7. Gruber, O., Santuccione, A. C. & Aach, H. Magnetic resonance imaging in studying schizophrenia, negative symptoms, and the glutamate system. *Front. Psychiatry* **5,** 1–11 (2014).

8. Sullivan, P. F., Kendler, K. S. & Neale, M. C. Schizophrenia as a Complex Trait. *Arch. Gen. Psychiatry* **60,** 1187–1192 (2003).

9. Howes, O. D. & Kapur, S. A neurobiological hypothesis for the classification of schizophrenia: Type a (hyperdopaminergic) and type b (normodopaminergic). *Br. J. Psychiatry* **205,** 1–3 (2014).

10. Carbon, M. & Correll, C. U. Thinking and acting beyond the positive: the role of the cognitive and negative symptoms in schizophrenia. *CNS Spectr.* **19,** 35–53 (2014).

11. Andreasen, N. C. *Scale for the Assessment of Negative Symptoms (SANS)*. (The University of Iowa, 1984).

12. Poels, E. M. P. *et al.* Imaging glutamate in schizophrenia: review of findings and implications for drug discovery. *Mol. Psychiatry* **19,** 20–9 (2014).

13. Bersani, F. . *et al.* Cingulate Cortex in Schizophrenia : its relation with negative symptoms and psychotic onset . *Eur. Rev. Med. Pharmacol. Sci.* **18,** 3354–3367 (2014).

14. Murphy, B. P., Chung, Y.-C., Park, T.-W. & McGorry, P. D. Pharmacological treatment of primary negative symptoms in schizophrenia: a systematic review. *Schizophr. Res.* **88,** 5–25 (2006).

15. Howes, O., Mccutcheon, R. & Stone, J. Glutamate and dopamine in schizophrenia : An update for the 21 st century. (2015). doi:10.1177/0269881114563634

16. Miyamoto, S., Miyake, N., Jarskog, L. F., Fleischhacker, W. W. & Lieberman, J. a. Pharmacological treatment of schizophrenia: a critical review of the

pharmacology and clinical effects of current and future therapeutic agents. *Mol. Psychiatry* **17,** 1206–1227 (2012).

17. Williamson, P. Are anticorrelated networks in the brain relevant to schizophrenia? *Schizophr. Bull.* **33,** 994–1003 (2007).

18. Marsman, A. *et al.* Glutamate in schizophrenia: A focused review and meta-analysis of 1H-MRS studies. *Schizophr. Bull.* **39,** 120–129 (2013).

19. Ungar, L., Nestor, P. G., Niznikiewicz, M. A., Wible, C. G. & Kubicki, M. Color Stroop and negative priming in schizophrenia: An fMRI study. *Psychiatry Res. - Neuroimaging* **181,** 24–29 (2010).

20. Boksman, K. *et al.* A 4.0-T fMRI study of brain connectivity during word fluency in first-episode schizophrenia. *Schizophr. Res.* **75,** 247–263 (2005).

21. Katsel, P. *et al.* Astrocyte and glutamate markers in the superficial, deep, and white matter layers of the anterior cingulate gyrus in schizophrenia. *Neuropsychopharmacology* **36,** 1171–1177 (2011).

22. Théberge, J. *et al.* Glutamate and glutamine measured with 4.0 T proton MRS in never-treated patients with schizophrenia and healthy volunteers. *Am. J. Psychiatry* **159,** 1944–1946 (2002).

23. Bartha, R., Drost, D. J., Menon, R. S. & Williamson, P. C. Comparison of the Quantification Precision of Human Short Echo Time 1 H Spectroscopy at 1.5 and 4.0 Tesla. *Magn. Reson. Med.* **44,** 185–192 (2000).

24. Théberge, J. *et al.* Glutamate and glutamine in the anterior cingulate and thalamus of medicated patients with chronic schizophrenia and healthy comparison subjects measured with 4.0-T proton MRS. *Am. J. Psychiatry* **160,** 2231–2233 (2003).

25. Théberge, J. *et al.* Longitudinal grey-matter and glutamatergic losses in first-episode schizophrenia. *Br. J. Psychiatry* **191,** 325–334 (2007).

26. Clinton, S. M. & Meador-Woodruff, J. H. Thalamic dysfunction in schizophrenia: Neurochemical, neuropathological, and in vivo imaging abnormalities. *Schizophr. Res.* **69,** 237–253 (2004).

27. Watis, L., Chen, S. H., Chua, H. C., Chong, S. a. & Sim, K. Glutamatergic abnormalities of the thalamus in schizophrenia: A systematic review. *J. Neural Transm.* **115,** 493–511 (2008).

28. Woodward, N. D., Karbasforoushan, H. & Heckers, S. Thalamocortical dysconnectivity in schizophrenia. *Am. J. Psychiatry* **169,** 1092–1099 (2012).

29. Hoflich, a. *et al.* Ketamine-Induced Modulation of the Thalamo-Cortical Network in Healthy Volunteers As a Model for Schizophrenia. *Int. J. Neuropsychopharmacol.* 1–11 (2015). doi:10.1093/ijnp/pyv040

30. Szulc, A. *et al.* Proton magnetic resonance spectroscopy measures related to short-term symptomatic outcome in chronic schizophrenia. *Neurosci. Lett.* **547,** 37–41 (2013).

31. Delamillieure, P., Constans, J. M., Fernandez, J., Brazo, P. & Dollfus, S. Proton magnetic resonance spectroscopy (1H-MRS) of the thalamus in schizophrenia. *Eur. Psychiatry* **15,** 489–491 (2000).

32. Meador-Woodruff, J. H., Clinton, S. M., Beneyto, M. & McCullumsmith, R. E. Molecular Abnormalities of the Glutamate Synapse in the Thalamus in Schizophrenia. *Ann. N. Y. Acad. Sci.* **1003,** 75–93 (2003).

33. Neufeld, R. W. J., Boksman, K., Vollick, D., George, L. & Carter, J. R. Stochastic dynamics of stimulus encoding in schizophrenia: Theory, testing, and application. *J. Math. Psychol.* **54,** 90–108 (2010).

34. Posner, M. I. & Petersen, S. E. The Attention System of the Human Brain. 31 (1989). doi:10.1146/annurev.ne.13.030190.000325

35. Carter, C. S. & van Veen, V. Anterior cingulate cortex and conflict detection: an update of theory and data. *Cogn. Affect. Behav. Neurosci.* **7,** 367–379 (2007).

36. Barch, D. M. *et al.* Anterior cingulate cortex and response conflict: effects of response modality and processing domain. *Cereb. Cortex* **11,** 837–848 (2001).

37. Javitt, D. C. & Zukin, S. R. Recent advances in the phencyclidine model of schizophrenia. *Am. J. Psychiat.* **148,** 1301–1308 (1991).

38. Coyle, J. T. & Tsai, G. The NMDA receptor glycine modulatory site: a therapeutic target for improving cognition and reducing negative symptoms in schizophrenia. *Psychopharmacology (Berl).* **174,** 32–38 (2004).

39. Tamminga, C. A., Holcomb, H. H., Gao, X. M. & Lahti, A. C. Glutamate pharmacology and the treatment of schizophrenia: current status and future directions. *International clinical psychopharmacology* **10 Suppl 3,** 29–37 (1995).

40. Gilbert-Rahola, J. & Villena-Rodriguez, A. Glutamatergic drugs for schizophrenia treatment. *Actas españolas Psiquiatr.* **42,** 234–241 (2014).

41. Lahti, A. C., Weiler, M. a., Michaelidis, T., Parwani, A. & Tamminga, C. a. Effects of ketamine in normal and schizophrenic volunteers. *Neuropsychopharmacology* **25,** 455–467 (2001).

42. Malhotra, A. K. *et al.* Ketamine-induced exacerbation of psychotic symptoms and cognitive impairment in neuroleptic-free schizophrenics. *Neuropsychopharmacology* **17,** 141–150 (1997).

43. Stone, J. M. Glutamatergic antipsychotic drugs: a new dawn in the treatment of schizophrenia? *Ther. Adv. Psychopharmacol.* **1,** 5–18 (2011).

44. Plitman, E. *et al.* Glutamate-mediated excitotoxicity in schizophrenia: A review. *Eur. Neuropsychopharmacol.* **24,** 1591–1605 (2014).

45. Rothman, D. L., Behar, K. L., Hyder, F. & Shulman, R. G. In vivo NMR studies of the glutamate neurotransmitter flux and neuroenergetics: implications for brain function. *Annu. Rev. Physiol.* **65,** 401–427 (2003).

46. Hertz, L., Dringen, R., Schousboe, A. & Robinson, S. R. Astrocytes: Glutamate producers for neurons. *J. Neurosci. Res.* **57,** 417–428 (1999).

47. Hertz, L., Yu, A. C. H., Kala, G. & Schousboe, A. Neuronal-astrocytic and cytosolic-mitochondrial metabolite trafficking during brain activation, hyperammonemia and energy deprivation. *Neurochem. Int.* **37,** 83–102 (2000).

48. Mark, L. P. *et al.* Pictorial review of glutamate excitotoxicity: Fundamental concepts for neuroimaging. *Am. J. Neuroradiol.* **22,** 1813–1824 (2001).

49. Marx, M.-C., Billups, D. & Billups, B. Maintaining the presynaptic glutamate supply for excitatory neurotransmission. *J. Neurosci. Res.* **00,** n/a–n/a (2015).

50. Harvey, R. J. & Yee, B. K. Glycine transporters as novel therapeutic targets in schizophrenia, alcohol dependence and pain. *Nat. Rev. Drug Discov.* **12,** 866–85 (2013).

51. Hu, W., MacDonald, M. L., Elswick, D. E. & Sweet, R. a. The glutamate hypothesis of schizophrenia: evidence from human brain tissue studies. *Ann. N. Y. Acad. Sci.* **1338,** 38–57 (2015).

52. Norenberg, M. D. & Martinez-Hernandez, A. Fine structural localisation of glutamine synthetase in astrocytes of rat brain. *Brain Res.* **161,** 303–310 (1979).

53. Walls, A. B., Waagepetersen, H. S., Bak, L. K., Schousboe, A. & Sonnewald, U. The Glutamine–Glutamate/GABA Cycle: Function, Regional Differences in Glutamate and GABA Production and Effects of Interference with GABA Metabolism. *Neurochem. Res.* **40,** 402–409 (2014).

54. McKenna, M. C., Stevenson, J. H., Huang, X. & Hopkins, I. B. Differential distribution of the enzymes glutamate dehydrogenase and aspartate

aminotransferase in cortical synaptic mitochondria contributes to metabolic compartmentation in cortical synaptic terminals. *Neurochem. Int.* **37,** 229–241 (2000).

55. McKenna, M. C. Glutamate pays its own way in astrocytes. *Front. Endocrinol. (Lausanne).* **4,** 1–6 (2013).

56. Javitt, D. C. Twenty-five years of glutamate in schizophrenia: Are we there yet? *Schizophr. Bull.* **38,** 911–913 (2012).

57. Gluck, M. R., Thomas, R. G., Davis, K. L. & Haroutunian, V. Implications for altered glutamate and GABA metabolism in the dorsolateral prefrontal cortex of aged schizophrenic patients. *Am. J. Psychiatry* **159,** 1165–1173 (2002).

58. Bruneau, E. G., McCullumsmith, R. E., Haroutunian, V., Davis, K. L. & Meador-Woodruff, J. H. Increased expression of glutaminase and glutamine synthetase mRNA in the thalamus in schizophrenia. *Schizophr. Res.* **75,** 27–34 (2005).

59. Kegeles, L. S. *et al.* Elevated Prefrontal Cortex -Aminobutyric Acid and Glutamate-Glutamine Levels in Schizophrenia Measured In Vivo With Proton Magnetic Resonance Spectroscopy. *Arch. Gen. Psychiatry* **69,** 449–459 (2012).

60. De la Fuente-Sandoval, C. *et al.* Glutamate levels in the associative striatum before and after 4 weeks of antipsychotic treatment in first-episode psychosis: a longitudinal proton magnetic resonance spectroscopy study. *JAMA psychiatry* **70,** 1057–66 (2013).

61. Bolkan, S. S., De Carvalho, F. D. & Kellendonk, C. Using human brain imaging studies as a guide toward animal models of schizophrenia. *Neuroscience* (2015). doi:10.1016/j.neuroscience.2015.05.055

62. Marsman, A. *et al.* GABA and glutamate in schizophrenia: A 7 T 1H-MRS study. *NeuroImage Clin.* **6,** 398–407 (2014).

63. Wijtenburg, S. A., Yang, S., Fischer, B. a. & Rowland, L. M. In vivo assessment of neurotransmitters and modulators with magnetic resonance spectroscopy: Application to schizophrenia. *Neurosci. Biobehav. Rev.* **51,** 276–295 (2015).

64. Tayoshi, S. *et al.* Metabolite changes and gender differences in schizophrenia using 3-Tesla proton magnetic resonance spectroscopy (1H-MRS). *Schizophr. Res.* **108,** 69–77 (2009).

65. Bustillo, J. R. *et al.* Glutamate as a marker of cognitive function in schizophrenia: A proton spectroscopic imaging study at 4 tesla. *Biol. Psychiatry* **69,** 19–27 (2011).

66. Lutkenhoff, E. S. *et al.* Proton MRS in twin pairs discordant for schizophrenia. *Mol. Psychiatry* **15,** 308–318 (2010).

67. Shirayama, Y. *et al.* Specific metabolites in the medial prefrontal cortex are associated with the neurocognitive deficits in schizophrenia: A preliminary study. *Neuroimage* **49,** 2783–2790 (2010).

68. Öngür, D. *et al.* Abnormal Glutamatergic Neurotransmission and Neuronal-Glial Interactions in Acute Mania. *Biol. Psychiatry* **64,** 718–726 (2008).

69. Bartha, R. *et al.* Measurement of Glutamate and Glutamine in the Medial Prefrontal Cortex of Never-treated Schizophrenic Patients and Healthy Controls by Proton Magnetic Resonance Spectroscopy. *Arch. Gen. Psychiatry* **54,** 959–965 (1997).

70. Bustillo, J. R. *et al.* 1H-MRS at 4 tesla in minimally treated early schizophrenia. *Mol. Psychiatry* **15,** 629–636 (2010).

71. Stone, J. M. *et al.* Glutamate Dysfunction in People with Prodromal Symptoms of Psychosis: Relationship to Gray Matter Volume. *Biol. Psychiatry* **66,** 533–539 (2009).

72. Rowland, L. M. *et al.* Effects of ketamine on anterior cingulate glutamate metabolism in healthy humans: A 4-T proton MRS study. *Am. J. Psychiatry* **162,** 394–396 (2005).

73. Brenner, E., Kondziella, D., Håberg, A. & Sonnewald, U. Impaired glutamine metabolism in NMDA receptor hypofunction induced by MK801. *J. Neurochem.* **94,** 1594–1603 (2005).

74. Michels, L. *et al.* Frontal gaba levels change during working memory. *PLoS One* **7,** e31933 (2012).

75. Bednařík, P. *et al.* Neurochemical and BOLD responses during neuronal activation measured in the human visual cortex at 7 Tesla. *J. Cereb. Blood Flow Metab.* 1–10 (2015). doi:10.1038/jcbfm.2014.233

76. Mangia, S. *et al.* Sustained neuronal activation raises oxidative metabolism to a new steady-state level: evidence from 1H NMR spectroscopy in the human visual cortex. *J. Cereb. Blood Flow Metab.* **27,** 1055–1063 (2007).

77. Lin, Y., Stephenson, M. C., Xin, L., Napolitano, A. & Morris, P. G. Investigating the metabolic changes due to visual stimulation using functional proton magnetic resonance spectroscopy at 7 T. *J. Cereb. Blood Flow Metab.* **32,** 1484–1495 (2012).

78. Mullins, P. G., Rowland, L. M., Jung, R. E. & Sibbitt, W. L. A novel technique to study the brain's response to pain: Proton magnetic resonance spectroscopy. *Neuroimage* **26,** 642–646 (2005).

79. Gussew, A. *et al.* Time-resolved functional 1H MR spectroscopic detection of glutamate concentration changes in the brain during acute heat pain stimulation. *Neuroimage* **49,** 1895–1902 (2010).

80. Schaller, B., Xin, L., O'Brien, K., Magill, A. W. & Gruetter, R. Are glutamate and lactate increases ubiquitous to physiological activation? A 1H functional MR

spectroscopy study during motor activation in human brain at 7Tesla. *Neuroimage* **93,** 138–145 (2014).

81. Schaller, B., Mekle, R., Xin, L., Kunz, N. & Gruetter, R. Net increase of lactate and glutamate concentration in activated human visual cortex detected with magnetic resonance spectroscopy at 7 tesla. *J. Neurosci. Res.* **91,** 1076–1083 (2013).

82. Kim, T. H., Kang, H. K. & Jeong, G. W. Assessment of Brain Metabolites Change during Visual Sexual Stimulation in Healthy Women Using Functional MR Spectroscopy. *J. Sex. Med.* **10,** 1001–1011 (2013).

83. Richards, T. L. *et al.* Functional MR spectroscopy of the auditory cortex in healthy subjects and patients with sudden hearing loss. *AJNR. Am. J. Neuroradiol.* **18,** 611–620 (1997).

84. Richards, T. L. *et al.* Dyslexic children have abnormal brain lactate response to reading- related language tasks. *Am. J. Neuroradiol.* **20,** 1393–1398 (1999).

85. Lally, N. *et al.* Glutamatergic correlates of gamma-band oscillatory activity during cognition: A concurrent ER-MRS and EEG study. *Neuroimage* **85,** 823–833 (2014).

86. Drobyshevsky, A., Baumann, S. B. & Schneider, W. A rapid fMRI task battery for mapping of visual, motor, cognitive, and emotional function. *Neuroimage* **31,** 732–744 (2006).

87. Neufeld, R. W. J. On the centrality and significance of stimulus-encoding deficit in schizophrenia. *Schizophr. Bull.* **33,** 982–993 (2007).

88. Eidels, A., Townsend, J. T. & Algom, D. Comparing perception of Stroop stimuli in focused versus divided attention paradigms: Evidence for dramatic processing differences. *Cognition* **114,** 129–150 (2010).

89. Schweickert, R. Journal of Experimental Psychology : Learning , Memory , and Cognition in Sentence Verification and the Stroop Effect. **9,** (1983).

90. Heathcote, a, Popiel, S. J. & Mewhort, D. J. K. Analysis of Response-Time Distributions - an Example Using the Stroop Task. *Psychological Bulletin* **109,** 340–347 (1991).

91. Lindsay, D. S. & Jacoby, L. L. Stroop process dissociations: the relationship between facilitation and interference. *J. Exp. Psychol. Hum. Percept. Perform.* **20,** 219–234 (1994).

92. Logan, G. D., Zbrodoff, N. J. & Williamson, J. Strategies in the color-word Stroop task. *Bulletin of the Psychonomic Society* **22,** 135–138 (1984).

93. Reid, M. A. *et al.* Assessments of function and biochemistry of the anterior cingulate cortex in schizophrenia. *Biol. Psychiatry* **68,** 625–633 (2010).

94. Minzenberg, M. J., Laird, A. R., Thelen, S., Carter, C. S. & Glahn, D. C. Meta-analysis of 41 functional neuroimaging studies of executive function in schizophrenia . PubMed Commons. *Arch. Gen. Psychiatry* **66,** 1–2 (2014).

95. Harrison, B. J. *et al.* Functional connectivity during Stroop task performance. *Neuroimage* **24,** 181–191 (2005).

96. Matsuzawa, D. *et al.* Negative correlation between brain glutathione level and negative symptoms in schizophrenia: A 3T 1H-MRS study. *PLoS One* **3,** (2008).

97. Banich, M. T. *et al.* fMri studies of Stroop tasks reveal unique roles of anterior and posterior brain systems in attentional selection. *J. Cogn. Neurosci.* **12,** 988–1000 (2000).

98. Umbricht, D. *et al.* Effect of Bitopertin, a Glycine Reuptake Inhibitor, on Negative Symptoms of Schizophrenia: A Randomized, Double-Blind, Proof-of-Concept Study. *JAMA psychiatry* **71,** 637–46 (2014).

99. Hashimoto, K., Malchow, B., Falkai, P. & Schmitt, A. Glutamate modulators as potential therapeutic drugs in schizophrenia and affective disorders. *Eur. Arch. Psychiatry Clin. Neurosci.* **263,** 367–377 (2013).

100. Kaufman, M. J. *et al.* Oral glycine administration increases brain glycine/creatine ratios in men: A proton magnetic resonance spectroscopy study. *Psychiatry Res. - Neuroimaging* **173,** 143–149 (2009).

101. J.H., S., W.T., J., J., S. & a., S. The selective glycine uptake inhibitor org 25935 as an adjunctive treatment to atypical antipsychotics in predominant persistent negative symptoms of schizophrenia: Results from the GIANT trial. *J. Clin. Psychopharmacol.* **34,** 190–198 (2014).

102. Hons, J., Vasatova, M., Cermakova, E., Doubek, P. & Libiger, J. Different serine and glycine metabolism in patients with schizophrenia receiving clozapine. *J. Psychiatr. Res.* **46,** 811–818 (2012).

103. Yamamori, H. *et al.* Changes in plasma d-serine, l-serine, and glycine levels in treatment-resistant schizophrenia before and after clozapine treatment. *Neurosci. Lett.* **582,** 93–98 (2014).

104. Govindaraju, V., Young, K. & Maudsley, a a. Proton NMR chemical shifts and coupling constants for brain metabolites. *NMR Biomed.* **13,** 129–153 (2000).

105. Prescot, A. P. *et al.* In vivo detection of brain glycine with echo-time-averaged 1H magnetic resonance spectroscopy at 4.0 T. *Magn. Reson. Med.* **55,** 681–686 (2006).

106. Gambarota, G. *et al.* In vivo measurement of glycine with short echo-time 1H MRS in human brain at 7 T. *Magn. Reson. Mater. Physics, Biol. Med.* **22,** 1–4 (2009).

107. Levitt, M. H. *spin dynamics: Basics of Nuclear Magnetic Resonance*. (John Wiley & Sons Ltd., 2008).

108. Harris, R. K. *Nuclear Magnetic Resonance Spectroscopy*. (Addison Westley Longman Limited, 1986).

109. Keeler, J. *Understanding NMR Spectroscopy*. (John Wiley & Sons Ltd., 2005).

110. Haacke, M. E., Brown, R. W., Thompson, Michael, R. & Venkatesan, R. *Magnetic Resonance Imaging: Physical Principles and Sequence Design*. (John Wiley & Sons Inc., 1999).

111. Drost, D. J., Riddle, W. R. & Clarke, G. D. Proton magnetic resonance spectroscopy in the brain: report of AAPM MR Task Group #9. *Med. Phys.* **29,** 2177–2197 (2002).

112. Ross, B. & Bluml, S. Magnetic resonance spectroscopy of the human brain. *Anat. Rec.* **265,** 54–84 (2001).

113. Keevil, S. F. Spatial localization in nuclear magnetic resonance spectroscopy. *Phys. Med. Biol.* **51,** R579–R636 (2006).

114. Deelchand, D. K. *et al.* In vivo 1H NMR spectroscopy of the human brain at 9.4 T: initial results. *J. Magn. Reson.* **206,** 74–80 (2010).

115. Tkác, I. *et al.* In vivo 1H NMR spectroscopy of the human brain at 7 T. *Magn. Reson. Med.* **46,** 451–6 (2001).

116. Curtis, A. T., Gilbert, K. M., Klassen, L. M., Gati, J. S. & Menon, R. S. Slice-by-slice B1+ shimming at 7 T. *Magn. Reson. Med.* **68,** 1109–16 (2012).

117. Vaughan, J. T. *et al.* 7T vs. 4T: RF power, homogeneity, and signal-to-noise comparison in head images. *Magn. Reson. Med.* **46,** 24–30 (2001).

118. Frahm, J., Merboldt, K.-D. & Hänicke, W. Localized proton spectroscopy using stimulated echoes. *J. Magn. Reson.* **72,** 502–508 (1987).

119. Bottomley, P. a. Spatial localization in NMR spectroscopy in vivo. *Ann. N. Y. Acad. Sci.* **508,** 333–348 (1987).

120. Kim, H., Thompson, R. B., Hanstock, C. C. & Allen, P. S. Variability of metabolite yield using STEAM or PRESS sequences in vivo at 3.0 T, illustrated with myo-inositol. *Magn. Reson. Med.* **53,** 760–769 (2005).

121. Christiansen, P. *et al.* MR-visible water content in human brain: A proton MRS study. *Magn. Reson. Imaging* **12,** 1237–1244 (1994).

122. Tkáć, I. & Gruetter, R. Methodology of 1 H NMR Spectroscopy of the Human Brain at Very High Magnetic Fields. *Appl. Magn. Reson.* **29,** 139–157 (2005).

123. Brown, M. A. Time-domain combination of MR spectroscopy data acquired using phased-array coils. *Magn. Reson. Med.* **52,** 1207–1213 (2004).

124. Bartha, R., Drost, D. J., Menon, R. S. & Williamson, P. C. Spectroscopic lineshape correction by QUECC: Combined QUALITY deconvolution and eddy current correction. *Magn. Reson. Med.* **44,** 641–645 (2000).

125. Soher, B. J., Young, K., Bernstein, A., Aygula, Z. & Maudsley, A. a. GAVA: Spectral simulation for in vivo MRS applications. *J. Magn. Reson.* **185,** 291–299 (2007).

126. De Beer, R. & Van Ormondt, D. Analysis of NMR Data Using Time Domain Fitting Procedures. *NMR Basic Princ. Prog.* **26,** 201–248 (1992).

127. Van den Boogaart, a, Ala-Korpela, M., Jokisaari, J. & Griffiths, J. R. Time and frequency domain analysis of NMR data compared: an application to 1D 1H spectra of lipoproteins. *Magn. Reson. Med.* **31,** 347–358 (1994).

128. Bartha, R., Drost, D. J. & Williamson, P. C. Factors affecting the quantification of short echo in-vivo 1 H MR spectra : prior knowledge, peak elimination, and filtering. *NMR Biomed.* **12,** 205–216 (1999).

129. Stanley, J. A., Drost, D. J., Williamson, P. C. & Thompson, R. T. The use of a priori knowledge to quantify short echo in vivo 1H MR spectra. *Magn. Reson. Med.* **34,** 17–24 (1995).

Chapter 2

2 Sources of Variability in the quantification of short-echo time human brain ^{1}H-MRS spectra

The work presented in this chapter was done to learn more about how specific sources of variability can influence metabolite quantification, with a focus on J-coupled metabolites and magnetic field strength. A version of this work is currently being edited for a resubmission to publish in Magnetic Resonance in Medicine. The reviewers' comments to the initial submission are addressed in chapter 6.

2.1 Introduction

Proton MR Spectroscopy (^{1}H-MRS) is a useful technique for non-invasively determining *in-vivo* metabolite concentrations of the human brain. Brain disorders, such as neuropsychiatric illnesses, have been studied extensively with ^{1}H-MRS[1]. Detection of Glutamate (GLU) and glutamine (GLN) with ^{1}H-MRS is of particular interest in neuropsychiatric disorders thought to feature abnormalities of neurotransmitter metabolism[2]. GLU and GLN have only slightly different molecular structures and, as such, the protons have similar electromagnetic environments. In a ^{1}H-MRS spectrum, this translates to overlapping spectral signatures and makes independent estimates of their concentration more challenging. Quantitative estimates of metabolite concentrations are also influenced by ^{1}H-MRS data quality, modeling method and model completeness.

Low signal-to-noise ratios (SNR) are an inherent feature of ^{1}H-MRS spectra, often making it difficult to differentiate metabolite signals from background noise. Previous publications have used simulations to study how SNR influences ^{1}H-MRS quantitation of metabolites[3–5]. It was shown that the SNR had an effect on the standard deviation of metabolite concentrations estimates. Therefore, SNR is an important variable to control for in any simulation study.

It is often difficult to observe metabolite spectral peaks independently due to strong spectral overlap. It is believed that as peak overlap is reduced there is less covariation in metabolite concentration estimates. Mitigation of overlap can be achieved through various strategies. One strategy, increasing the external magnetic field strength (B_0), leads to increased spectral dispersion, reduced influence of J-dephasing for metabolites with strongly coupled spin (higher-order J-coupling) and a linear SNR increase (assuming body noise dominance). Particularly, higher B_0 reduces overlap in GLU and GLN signals (C4 protons) and reduces signal loss through J-dephasing (Fig. 2-1). However, even at B_0 as high as 7.0T, there is still much overlap as some of the gain in peak separation from spectral dispersion is offset by shortening of T_2^*(increased peak linewidths (LW)). It is expected that spectral dispersion linewidths and J-coupling will affect the quantification precision (modeling) of data from coupled metabolites.

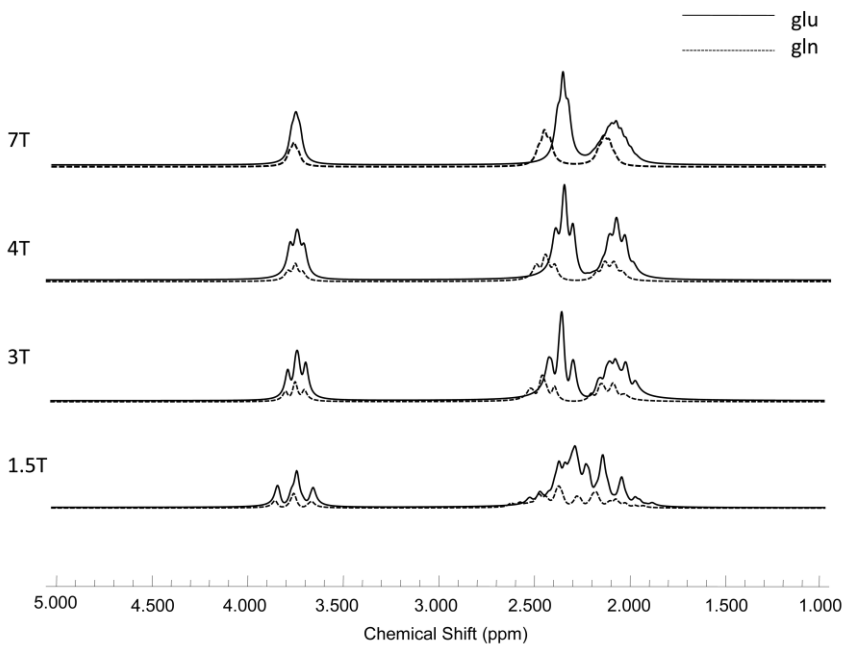

Figure 2-1. Simulated chemical signatures of GLU and GLN.
GLU and GLN are two strongly coupled and overlapping metabolites in ^{1}H-MRS spectra. They are simulated across four B_0, demonstrating apparent decreased overlap as B_0 increases.

Metabolite peak separation will influence the quantification algorithm's ability to converge to correct metabolite concentrations. Many metabolite quantification algorithms

utilize *a priori* information for the metabolites' spectral signatures[6–8], which are determined individually by acquiring the signal from a metabolite phantom or through the use of simulation software. Fitting parameters for a metabolite's peaks need to be constrained to have specific, pre-determined amplitude ratios, 0^{th} order phase offsets, chemical shift offsets and LW offsets. Iterative fitting algorithms will require initial values (seed values) for these parameters in order to compute the residual between the data and the model. The algorithm will perform repeated trials of parameter changes until convergence toward minimum residuals is achieved. When searching a vast multidimensional minimization space for a global minimum, the final solution returned by the fitting algorithm can become sensitive to the accuracy of the initialization parameters and converge toward a local minimum. If it were possible to initialize the algorithm with the known correct answer, the only source of metabolite concentration variability would be random noise. Of course, this is not possible with *in vivo* data as the correct answer is not known with certainty. Therefore, for in vivo ^{1}H-MRS data, variability due to noise cannot be separated from variability due to intra- and inter-individual variability.

The ^{1}H-MRS spectrum is composed of contributions from the protons of many metabolites. Many of these are often not included in basis sets for quantification because they are not represented by prominent peaks in human brain 1H-MRS spectra. This can be due to low concentrations or because their peaks have been split into too broad of a multiplet and as a result are on the order of the spectral noise. The inclusion of such contributions is thought to unnecessarily complicate fits and increase overall variability of concentration estimates. Either way, a metabolite that is not accounted for by the basis set will leave additional spectral area that the fitting algorithm will still try to minimize given the basis set provided. This can lead to errors in the estimates of metabolite concentrations and it is not well known how these areas will propagate (only nearby metabolites or remote metabolites). Therefore, if a basis set is not complete, measurements of metabolite concentrations may actually represent contributions from a number of metabolites and may decrease the quantification accuracy.

The goal of this paper is to study factors influencing the quantification precision of brain metabolites in controlled conditions similar to those encountered *in vivo*. Specifically, simulations were conducted in this study to isolate and examine the effects of spectral dispersion, weakened J-coupling versus changes in B_0, the effect of noise, the effect of inaccurate seeding values and the effect of template incompleteness on the variability of metabolite concentration estimates.

2.1.1 Hypotheses

Due to the increased metabolite separation as B_0 increases, the correlations between metabolite concentration estimates in metabolites that experience strong coupling at low B_0 should generally decrease as B_0 increases. This should also increase the precision of metabolite concentration quantification.

It is hypothesized that higher SNR will result in higher inter-metabolite correlation coefficient ($r_{(METa,METb)}$) between the concentration estimates of two metabolite (a and b) due to the decreasing interference of noise with the iterative modelling of the spectrum.

While fitting algorithms blindly perform the mathematical act of minimizing residuals, spectral area from a metabolite not included in the quantification template can be incorrectly assigned to another metabolite part of the template. It is hypothesized that any metabolite omitted from a spectral basis set will result in corresponding quantification errors in overlapping metabolites and that omitted metabolites will have greater influence at lower B_0 as there is greater spectral overlap between metabolites.We hypothesize that the more inaccurate seed values of the fitting algorithm will result in poorer precision of metabolite concentration estimates and greater amplitudes of inter-metabolite correlations coefficients.

Finally, it is expected that the accuracy (measured mean concentrations minus expected mean concentrations) will be generally unaffected by variations in B_0, SNR, and initial seed values of the fitting algorithm, whereas omitted metabolites will translate to reduced accuracy of metabolites overlapping the omitted metabolite.

2.2 Methods

Two sets of simulations were designed for this study. The first set thoroughly analyzed the influences of B_0, SNR, and the initial seeding of the quantification template. The second set examined completeness of the basis set for quantification. They were all made to be representative of *in vivo* human brain spectra at four common B_0 (1.5 T, 3 T, 4 T, 7 T) that would be acquired with an ultra-short echo STEAM sequence (TE=6ms, TM=32ms)[9] and two SNR representative of what could be acquired with the averages (nt) set to 64 and 256. TE values within 2ms have been used previously at all these B_0[9–12]. The metabolite spectra included spectral signatures from 22 metabolites (glutamate (GLU), glutamine (GLN), N-acetylaspartate (NAA), N-acetylaspartylglutamate (NAAG), creatine (Cr), phosphocreatine (PCr), myo-inositol (Myo), choline (Cho), Phosphorylcholine (PCho), glycerophosphorylcholine (GPCho), gamma aminobutyric acid (GABA), serine (Ser), glycine (GLY), scyllo-inositol (Scy), phosphorylethanolamine (PE), α-glucose (α-glc), β-glucose (β-glc), aspartate (Asp), alanine (Ala), glutathione (GSH), lactate (Lac), taurine (Tau)). To provide an amplitude reference for calibration of the SNR of simulated spectra that would be comparable to that commonly used in SNR measurements of *in vivo* spectra, a singlet equivalent in concentration to the CH_3 singlet of NAA (10.3mmol/kg_{ww})[13] was added to the simulation, set upfield at 0.0 ppm so as to not interfere with quantification. SNR was determined using the peak area definition of SNR, which comes from the relative amplitude of the signal in the time-domain at t=0 compared to the standard deviation of the noise. The peak area definition is advantageous because it is not influenced by the T_2^* changes with B_0. Reference values from the literature[14] along with the assumption of linear SNR change with B_0 and the common SNR-to-nt (averages) relationship $SNR_1/SNR_2=(nt_1/nt_2)^{0.5}$ were used to determine representative SNR for nt=256 and nt=64. The resulting SNR for each B_0 were 117 and 58.5 (7 T), 67 and 33.5 (4 T), 50 and 25 (3 T), 25 and 12.5 (1.5 T), for nt of 256 and 64, respectively. Figure 2-2 shows example spectra for each B_0 with nt=256. Additional simulations were created for each B_0 at an SNR of 1024 to minimize the variability associated with the random distribution of noise. Each spectral signature was simulated using GAVAgui, an in-house program designed by a medical physicist (J.T.). The program is an interface to code designed by Brian Soher that uses the GAMMA

simulations package to predict the response of spin systems to the STEAM pulse sequence[15]. The interface allows the selection of a given echo time (TE), mixing time (TM), B_0 and spin system and transforms the output of the GAMMA simulation in a list of the predicted resonances and their relative parameters compatible with the file format of the Lawson Fitman Spectral Analysis Suite[7,16]. J-coupling constants and chemical shifts used were derived from the literature[13,17]. A macromolecule (MM) signature was added as well, composed of 15 resonances with combinations of Gaussian and Lorentzian lineshapes, empirically determined to match a typical MM spectra (Fig. 2-3).

To model a spectrum containing MR signals from more than one metabolite, the superposition of metabolites' respective resonances must be constrained in order to preserve their natural relative chemical shift (δ), LW, amplitude (A_n), 0^{th} order phase (ϕ_0) and 1^{st} order phase (*d*). Model constraints reduce the degrees of freedom of the minimization problem submitted to the iterative fitting algorithm. Specifically, δ, LW, ϕ_0, and *d* of each resonance were linked within and between metabolites, whereas the amplitudes of each resonance were linked within metabolites only ($A_{MET(1\text{-}22)}$) and within MM resonances (A_{MM}). An additional chemical shift constraint was placed on the MM signals, leading to a total of 28 fitting parameters (δ, δ_{MM}, LW, ϕ_0, *d*, $A_{met\ (1\text{-}22)}$, A_{MM}). ϕ_0 and *d* order phases were initialized to 0. The LW has been shown to influence the standard deviation of metabolite concentration estimates[3,5] so, it will be set to 1.35 Hz/T for each B_0 based on work by Deelchand et al[18].

To evaluate precision, 200 noisy realizations were produced and fit (in the time domain) using fitMAN analysis software[7] for each B_0 and fitting template. The quantification algorithm was seeded with the correct parameter values (exact seeding) and again with two inexact metabolite templates that randomly varied the initial estimates of all fitting parameters (inexact seeding). These inexact seeds more realistically represent the variability associated with the manual iterative algorithm seeding step used to provide the starting point of in vivo data modelling. Seed values for parameters ϕ_0, LW, δ, δ_{MM}, $A_{met\ (1\text{-}22)}$, A_{MM} varied with a Gaussian distribution around 0.05 rad, 5%, 0.0025 ppm, 0.0025 ppm, 10% and 10%, respectively, for the first inexact seeding (IE1) and double these values for the second inexact seeding (IE2) approach. Pseudo-random noise with

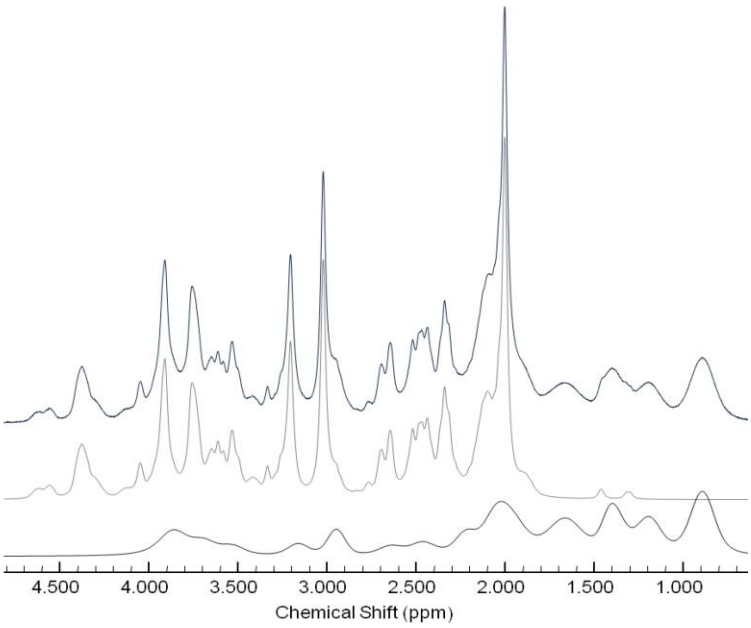

Figure 2-2. The full simulated set (top) of metabolites (middle) and macromolecules (bottom).

Gaussian distribution was added to each simulated spectra using Datsim, a program developed in-house (J.T.) and part of the Lawson Fitman Spectral Analysis Suite[7,16]

Once all 200 noisy realizations have been fit for each B_0, SNR, and template seeding combination, the mean concentration (μ) of each metabolite is computed along with its standard deviation (σ) to get the Coefficient of Variation (CV):

$$CV = \frac{\sigma}{\mu} \times 100\% \qquad 2.1$$

The CV is taken to represent the quantification precision of a given metabolite's concentration. CV was chosen instead of Cramer-Rao Lower Bounds (CRLB)[19] because CV is a measure of the observed amount of variability including all sources, whereas CRLBs are related to the minimum amount of variability observable given a specific spectral quantification model. The interaction of the metabolite models during

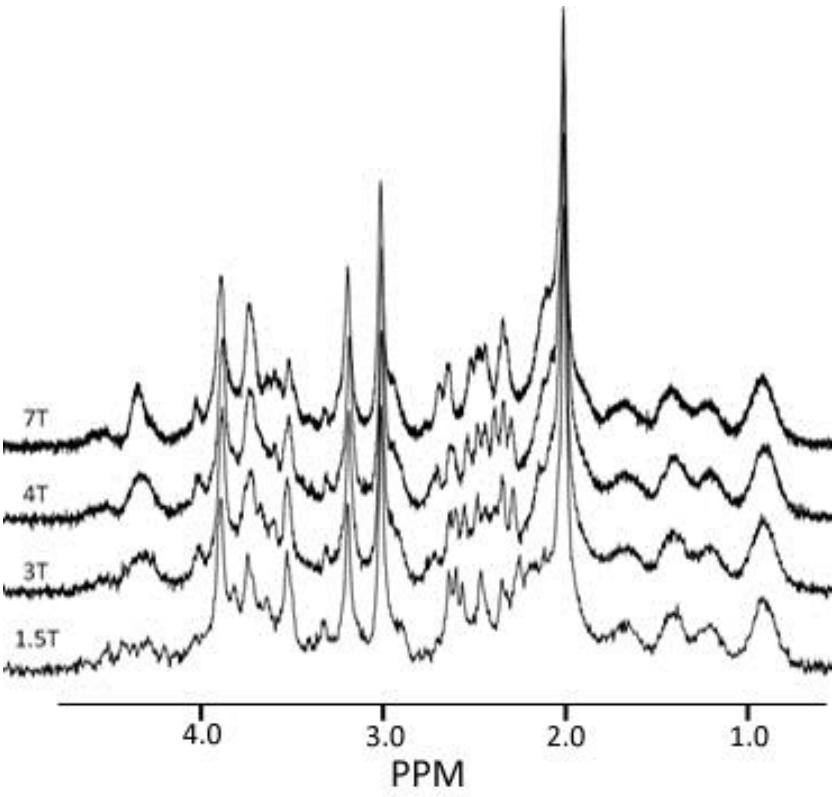

Figure 2-3. Example spectra for each B_0 with 256 averages

quantification can be assessed using the following formula describing the inter-metabolite correlation coefficient of metabolite 'a' (*METa*) and metabolite 'b' (*METb*):

$$r_{(METa,METb)} = \frac{\mathrm{cov}_{(METa,METb,)}}{\sigma_{METa}\sigma_{METb}} \qquad 2.2$$

where σ_{METa} and σ_{METb} are the standard deviations and $cov_{(METa,METb)}$ is the covariation, represented by:

$$\mathrm{cov}_{(METa,METb)} = \frac{\sigma^2_{(METa+METb)} - \sigma^2_{METa} - \sigma^2_{METb}}{2} \qquad 2.3$$

where $\sigma^2_{(METa+METb)}$ represents the variance of the sum of the two metabolites' amplitudes.

The accuracy will be assessed by comparing the mean concentration estimates for each metabolite over all 200 noisy realizations relative to the actual known concentration.

Together, the CV, accuracy, and $r_{(METa,METb)}$ allow for a quantitative assessment of the variability of concentration estimates of metabolite pairs and their interactions. Pearson's correlation were calculated and Sidak's adjustment for multiple correlations corrected the alpha value accordingly ($p<0.00004$ from $p<0.01$).

The same experimental design was used to evaluate the influence of a metabolite's omission from the basis set with IE1 seeding for 3 T and 7 T, with nt=64. Individual metabolites were removed from the full quantification template, and 200 noisy realizations of the complete spectra were then fit with the metabolite omitted. Omission of the MM baseline was similarly explored. The correct concentration of each metabolite is known, making it possible to determine which metabolites assume the remaining spectral area of an omitted metabolite. The total spectral quantification error is defined to be the resultant cumulative error in the remaining metabolites' concentration estimates (measured-expected, μmol/g) when a metabolite is removed from the fitting template. In total, 16800 simulated spectra were fit.

2.3 Results

Quantification precision (CV), accuracy, and $r_{(METa,METb)}$ were analyzed for every set of simulations, excluding the metabolite omission simulations, which only looked at accuracy of metabolite concentration estimates. Correlation tables were created for each B_0, SNR, and template seeding combination, with 253 possible correlations per table. Significant $r_{(METa,METb)}$ are summarized in Table 2-1. The SNR had little impact on the total significant $r_{(METa,METb)}$ (positive or negative) when the template was seeded with the correct final answer. When seeded using IE1 or IE2, the total number of significant $r_{(METa,METb)}$ increased with SNR. IE2 generally had more significant $r_{(METa,METb)}$ than IE1.

The magnitude of $r_{(METa,METb)}$ decreases with B_0 when GLU and other coupled metabolites (GLN, GABA, NAAG) are part of the metabolite pairs (Fig.2-4b). Metabolite

pairs that make up the three largest singlet peaks in the spectrum at 2.01 ppm (NAA-NAAG), 3.03 ppm (Cr-PCr), and 3.21 ppm (GPCho-PCho) all still had strong $r_{(METa,METb)}$ that did not seem to fluctuate with B_0 (Fig 2-4c). Some metabolite pairs with GSH seemed to initially decrease the magnitude of $r_{(METa,METb)}$ to a level below the significance level, but eventually reached significance with opposite polarity from 1.5 T to 7 T (Fig. 2-4a).

Table 2-1. Significant correlations between metabolite concentration estimates

		EX[a]			IE1[b]			IE2[c]		
SNR	**B_0**	**+[d]**	**-[e]**	**Total**	**+**	**-**	**Total**	**+**	**-**	**Total**
1024	**7 T7 T**	2	4	**6**	57	59	**116**	58	59	**117**
	4 T	6	3	**9**	56	61	**117**	56	60	**116**
	3 T	6	4	**10**	61	66	**127**	65	75	**140**
	1.5 T	7	3	**10**	62	70	**132**	72	67	**139**
nt[f]=256	**7 T7 T**	3	6	**9**	37	44	**81**	44	45	**89**
	4 T	7	4	**11**	35	45	**80**	49	53	**102**
	3 T	5	6	**11**	33	48	**81**	46	59	**105**
	1.5 T	8	3	**11**	29	37	**66**	41	45	**86**
nt=64	**7 T7 T**	2	7	**9**	26	37	**63**	31	42	**73**
	4 T	8	6	**14**	23	35	**58**	32	45	**77**
	3 T	8	4	**12**	22	22	**44**	29	45	**74**
	1.5 T	7	4	**11**	18	27	**45**	21	33	**54**

[a] Exact seeding

[b, c] Inexact seeding 1 and inexact seeding 2, as described in the "Methods" section

[d, e] Number of significant positive or negative correlations ($p<0.01$, Bonferroni corrected to $p<0.00004$)

[f] Number of averages

Table 2-2. Metabolite precision (CV; %) across B_0 with the SNR=1024 and IE1

	1.5 T	3 T	4 T	7 T
GLN	0.50	0.44	0.35	0.30
GLU	0.56	0.34	0.29	0.23
NAAG	1.82	2.38	2.54	2.35
GABA	4.18	2.14	2.29	1.98
GSH	0.38	0.50	0.46	0.29
Tau	4.14	4.08	3.18	2.57
Ser	17.23	27.42	20.38	19.35
Cho	9.75	10.63	9.82	9.75
PCho	8.55	8.24	9.69	8.45
GPCho	4.40	4.28	4.78	4.10
Cr	3.56	4.04	4.60	4.35
PCr	5.89	5.59	7.14	6.58
Asp	2.09	3.91	5.65	6.79
α-Glc	2.72	5.39	4.71	2.85
β-Glc	2.31	3.48	3.98	4.14
NAA	0.72	0.84	0.94	0.97
Ala	3.53	3.76	4.01	2.81
Myo	0.88	0.85	0.66	0.39
PE	3.37	4.79	1.85	2.35
Lac	3.10	4.92	4.75	4.27
GLY	4.71	4.32	3.52	1.39
Scy	2.57	1.37	1.33	1.06

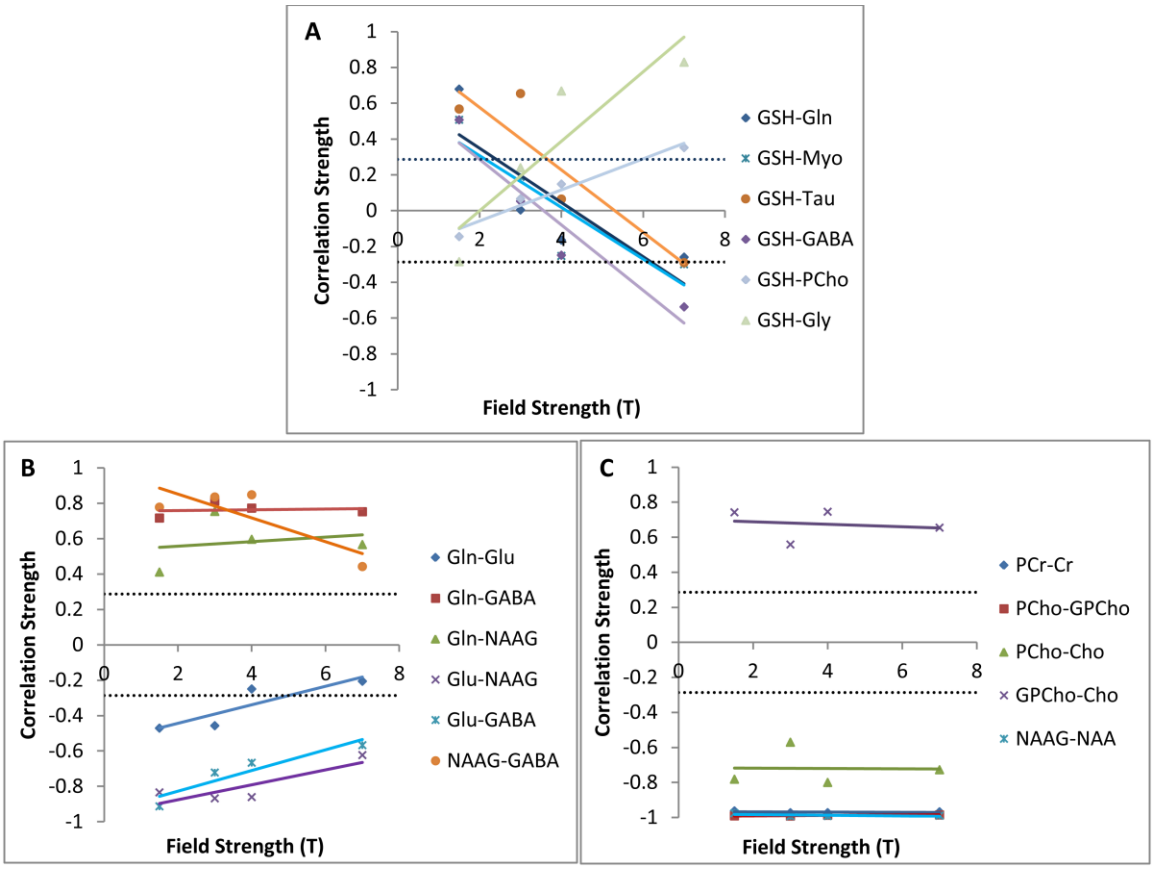

Figure 2-4. Correlations between metabolite concentration estimates.

Some of the main correlations found between metabolite concentration estimates as a function of B_0 with the IE1 template are displayed with linear lines of best fit. Interacting metabolites are shown together in the legend. The dashed line in each figure represents the significance threshold. A) Coupled metabolites are paired with other coupled metabolites. B) Overlapping metabolites that make up the tallest spectral peaks are paired. C) Metabolites paired with GSH that seemed to reverse the polarity of the correlation strength

Table 2-3. The increase in CV due to doubling initial fit seeding offsets

	SNR	IE2/IE1[a]
1.5 T	12.5	1.36
	25	1.40
	1024	1.60
3 T	25	1.42
	50	1.41
	1024	1.80
4 T	33.5	1.47
	67	1.31
	1024	1.90
7 T	58.5	1.45
	117	1.37
	1024	1.88

[a] Inexact seeding 1 and 2, as defined in the "Methods" section

.

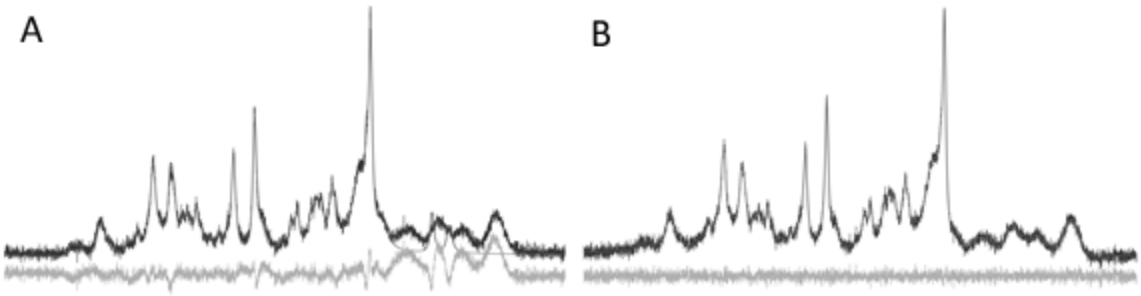

Figure 2-5. Metabolite spectra (top) with their fits overlaid along with the residual from the fits (bottom) A) when MM has been omitted and B) with a complete template

Table 2-4. Metabolite precision (%) across B_0 with nt=256 and IE1

	1.5 T	3 T	4 T	7 T
GLN	5.18	3.07	1.82	0.97
GLU	3.37	1.67	1.12	0.68
NAAG	13.30	13.13	10.47	5.43
GABA	20.29	10.27	8.23	4.26
GSH	4.64	2.88	2.22	1.17
Tau	17.79	15.62	13.67	7.22
Ser	52.29	42.59	29.70	31.38
Cho	13.25	13.17	14.46	14.41
PCho	9.45	9.44	8.85	9.18
GPCho	6.26	5.74	5.63	4.67
Cr	6.76	6.37	6.26	5.70
PCr	8.57	6.97	8.81	8.05
Asp	20.17	18.60	18.05	12.69
α-Glc	20.69	13.56	11.30	8.52
β-Glc	19.69	17.07	16.96	11.25
NAA	4.81	4.43	3.83	2.26
Ala	18.44	13.48	10.07	7.19
Myo	3.57	2.40	1.87	1.04
PE	14.06	10.78	7.75	6.52
Lac	24.47	18.57	16.77	9.37
GLY	10.24	10.24	9.41	5.21
Scy	8.56	5.65	5.87	4.01

Table 2-5. Metabolite omissions from the fitting template (nt=64, IE1)

	7 T			3 T		
Met removed[a]	**Total Spectral Quantification error[b] (**µmol/g**)**	**Largest Error[c] (Met,** µmol/g**)**		**Total Spectral Quantification error (**µmol/g**)**	**Largest Error (Met,** µmol/g**)**	
None[d]	0.13	Cr	0.03	0.30	NAA	-0.05
GLN	4.62	GLU	1.81	6.30	GLU	2.61
GLU	10.02	GLN	3.34	13.37	GLN	5.05
NAAG	3.09	GLU	0.69	3.16	GLU	0.79
Cr	8.39	PCr	4.04	9.92	PCr	3.80
Myo	4.79	α-Glc	0.60	7.04	GLY	2.52
Tau	1.84	β-Glc	0.57	1.75	β-Glc	0.45
Ser	0.77	PE	0.28	1.05	PCr	0.26
Cho	0.71	PE	0.21	1.03	PCr	0.35
PCho	1.93	GPCho	0.49	5.56	NAA	-1.33
GABA	2.63	GLU	0.42	3.27	GLU	1.01
GSH	4.79	GLN	1.20	10.18	α-Glc	2.11
Lac	0.28	Ser	-0.05	0.46	NAA	0.06
Asp	1.13	Ser	0.25	0.92	Tau	0.33
α-Glc	1.39	Ser	0.36	1.54	Ser	0.23
β-Glc	0.90	Tau	0.32	1.40	Tau	0.45
NAA	19.94	NAAG	7.13	19.37	NAAG	8.23
Ala	0.48	α-Glc	0.09	0.45	α-Glc	0.08
PCr	5.82	Cr	2.31	7.24	Cr	1.79
PE	2.16	Ser	0.89	2.57	Ser	0.76
GPCho	4.89	PE	1.72	4.82	PE	2.00
MM	24.92	NAAG	2.80	23.16	Lac	3.18
GLY	1.17	Myo	0.49	1.30	Myo	0.67
Scy	0.93	Cho	-0.14	1.67	Tau	0.68

[a] 200 noisy realizations of the same data were fit with one (or zero) metabolites removed from the fitting template

[b] The resultant cumulative error in the remaining metabolites' concentration estimates (measured-expected, µmol/g) when a metabolite is removed from the fitting template

[c] The metabolite that had the largest spectral quantification error

[d] No metabolites were removed from the fitting template

The SNR, B_0, and the seeding of the template all had important influences on the CV of concentration estimates. When SNR doubled (from nt=64 to nt=256) the CV improved by a factor of 1.96 on average over all metabolites and over all B_0 using exact seeding of the fitting algorithm. Using the IE1 and IE2 seeds, doubling SNR improved the CV by 1.52 and 1.47, respectively. Table 2-2 shows that there is lower CV at low B_0 and high SNR (1024) when exact seeding is used, but this is not consistent with the inexact seeding models. There were improvements in some metabolites, namely GLU, GLN, GABA, Myo, Tau, Scy, and GLY, while the remaining metabolites showed little variation, with the exception of Asp and β-Glc, which seemed to get worse as B_0 increased. There is also a reduction in precision observed over all metabolite concentration estimates when going from IE1 to IE2 (Table 2-3). This reduction factor increases at very high SNR

To isolate the influences on the CV specifically due to the changes in spectral signatures of metabolites when the B_0 changes, the SNR had to be equated. This was achieved by running simulations with the SNR set to 1024 for all B_0. The CV increased for every metabolite as the B_0 increased from 1.5 T to 7 T when using the exact seeding. However, using the inexact seeding approach, GLU, GABA, GLN, Myo, Scy, GLY, and Tau all exhibited decreased CV's going from 1.5 T to 7 T for both the IE1 (Table 2-2) and IE2 (not shown) seeding techniques. All the remaining metabolites either had no change or increased CV's when B_0 increased. Table 2-4 demonstrates improved CV's at higher B_0 when nt=256 at realistic SNR for each B_0.

An additional evaluation of the influence of spectral lineshape changes due to B_0 on CV comes from the 1.5 T spectra with nt=256 and the 3 T spectra with nt=64 that both have an SNR of 25. The quantity of significant $r_{(METa,METb)}$ were similar for exact seeding, but were reduced in both the IE1 and IE2 seeding templates (Table 2-1) at 3 T compared to 1.5 T. The CV's for GLU and GABA improved by factors of 1.34 and 1.35, respectively, for 3 T using IE1, but, on average, all metabolite CV's were 8% lower at 1.5 T.

The accuracy of the metabolites did not seem to be affected by the SNR, B_0, nor the type of seeding used. It was only the metabolite omissions that affected accuracy.

The total spectral quantification error increased when any metabolite was excluded from the basis set (Table 2-5). For comparison, the typical error that would be expected from the full spectrum (i.e. no metabolite omissions) is also included in Table 2-5. As would be expected, excluding the MM from the template created the largest errors in the fit as its spectral area is broad and extends across all metabolites.

The fitting algorithm was able to efficiently account for the MM spectral area using the remaining metabolites when the MM were not included in the basis set (Fig. 2-5). Where there is little overlap between MM and other metabolites, the residual spectral area resembles the corresponding portion of the MM spectrum with the exception of the enlarged Lac doublet. However, where metabolites and MM overlap there is little residual remaining. Omitting MM decreased total fitted spectral area by 10.10% and 8.82% at 3 T and 7 T, respectively. The only metabolite (with MM not considered to be a metabolite) to alter the total spectral area of fitted metabolites by more than 1% when omitted was NAA. The omission of NAA lead to total increases of 2.70% at 3 T and 2.56% at 7 T. Serine concentration estimates were the most susceptible to fitting errors from incomplete fitting templates and were not within 10% of the correct concentration when any metabolite was omitted.

2.4 Discussion

In this study, simulations were used to isolate some of the sources of variation encountered in ^{1}H-MRS such as: B_0, SNR, algorithm seeding accuracy and quantification template completeness. Quantitative understanding of these sources of variability is important for study protocol optimization. Simulations were chosen to minimize or remove competing sources of variability. A large number of simulated spectra could easily be generated to improve statistical confidence.

Inexact seeding was chosen to examine variability associated with the initialization of the quantification algorithm parameters. Iterative fitting algorithms are more likely to

encounter a local minimum and return an incorrect parameter estimate when poorly seeded. Therefore, when one parameter is fit poorly the other parameters must compensate. This led to correlation between metabolite concentration estimates as there were more correlations and decreased precision observed when the initial parameters were fit with greater seeding variability. Quantitative relationships between IE1 and IE2 are more apparent when the influence of noise is minimized. With high SNR (1024) the CV's of IE2 are almost twice that of IE1. Therefore, greater seeding variability resulted in a near linear increase in CV in the absence of noise. This demonstrates that a substantial improvement can be seen in the CV of metabolite estimates by taking the time to provide accurate initial estimates of the parameters to the fitting algorithm. Future studies that aim to use simulations to study quantitative relationships should consider using inexact fitting templates to better represent *in vivo* fitting.

The variability introduced with the initial seeding of the basis set can also be seen when comparing to the exact seeding data with SNR of 1024. With the noise minimized and the variability associated with the initial seeding removed, the main sources of variability become the spectral separation and the linewidths. Both spectral separation and metabolite linewidths increase with B_0, so it would be expected that the spectral separation would improve quantification precision while the linewidth would worsen it. Because the precision was worse at higher B_0, the increase in metabolite linewidths influenced the fit more than the increase in spectral dispersion. This was not observed when using inexact seeding, but can be explained by looking at the signal in the time domain. The SNR definition chosen for this study corresponded to the amplitude of the signal in the time domain at t=0, relative to the standard deviation of the noise. T_2^* reduces as B_0 increases leading to faster signal decay. Although the SNR, by definition, remains the same between the different B_0 examined, there is more signal at low B_0 than that which remains above the level of the noise during the sampling of the FID at higher B_0. The inexact seeding model better represents how the spectral dispersion and J-coupling will affect the quantification precision, so the reduced CV at high B_0 in J-coupled metabolites indicates that the relative reduction in J-coupling (in ppm only) improves the quantification precision, despite T_2^* reduction.

When SNR=1024, two strongly coupled metabolites, GLU and GABA, showed improvements in CV and reduced quantity of $r_{(METa,METb)}$ at 3 T compared to 1.5 T with inexact seeding. This illustrates the benefits of weaker higher order J-coupling at higher field strengths. In contrast, the majority of metabolites showed a slight reduction in CV at 1.5 T. The observed slight improvement in CV at 1.5 T compared to 3 T in most metabolites is likely due to the signal decaying much slower at 1.5 T, resulting in more points above the noise threshold to help the fitting algorithm converge to a final estimate. Therefore, in the absence of the natural improvement in SNR at 3 T, the increased peak separation did not translate to improved CV for the majority of metabolites.

Doubling SNR improved metabolite quantification, which agrees well with what has been observed in previous studies[3,4], and was consistent at each B_0. The nearly two-fold (1.96) increase in quantification precision when SNR is doubled using exact seeding demonstrates an almost linear relationship between SNR and quantification precision. The exact seeding presents an upper limit of improvements in CV from SNR alone so it makes sense that quantification precision is reduced from this ideal relationship when seeding variability is introduced. As the SNR increased, so did the number of significant $r_{(METa,METb)}$. It is likely that at low SNR the metabolite estimates are more heavily influenced by the local noise around the spectral peaks than the overlapping metabolites, and as the SNR improves more correlations become apparent.

Almost all metabolites showed large reductions in CV when increasing B_0 using SNR values that could be acquired *in vivo* (Table 2-2) with GLU, GLN, GABA, Myo, and GSH having the greatest reductions. There seems to be additive improvements in CV coming from both the increase in SNR and the weakened J-coupling at 7 T. This agrees with Bartha et al[20] who demonstrated an average increase in metabolite quantification precision *in vivo* at 4 T compared to 1.5 T. However, Cho, PCho, GPCho, Cr, and PCr did not have CV's that varied greatly. This is somewhat surprising, as it would be expected that their precision would improve as the influence of noise is reduced. These metabolites must be easier to fit even in low SNR conditions due to their strong singlets.

Despite a reduction in the number of significant correlations observed at 1.5 T compared to 7 T, there still remain many correlations significant at 7 T. This is perhaps not surprising, as the ^{1}H-MRS spectrum is a superposition of spectral signatures from many metabolites in close proximity. However, the magnitude of significant correlations of J-coupled metabolites paired with GLU was generally decreased, which indicates that there are indeed improvements in metabolite quantification due to the separation of some metabolites at higher B_0. It is apparent, through the strong dependency of the GLU-GLN correlation on B_o, that GLU and GLN are increasingly more independently quantified at higher B_0 despite increases in LW. Metabolite pairs with spectral signatures dominated by strong singlets and overlapping heavily (Fig. 2-4b) will have strong $r_{(METa,METb)}$ even at high B_0. The improvements in spectral dispersion appear to be insufficient to separate their quantitative dependence on each other. Therefore, any incorrect estimate in one metabolite is likely to introduce error into the other.

GSH demonstrated unexpected behavior as it moved from one polarity of $r_{(METa,METb)}$ to the other as B_0 increased (Fig. 2-4c). It may be because changes in spectral dispersion and J-coupling can also lead to increased spectral overlap as peaks are shifting from multiple metabolites. It would be interesting to see if these GSH pairings would continue to approach maximum correlation ($r_{(METa,METb)}$=1 or -1) when B_0 increased further or if they would reverse the trend and reduce correlation strength.

One study examined $r_{(METa,METb)}$at 2.9T using a 2D J-resolved ^{1}H-MRS sequence in the anterior cingulate and the posterior cingulate[21]. Some of the correlations from the anterior cingulate that the authors chose to highlight include GLU-GLN, GLU-GABA, GABA-CR, GLY-Myo, GPCho-PCho, NAA-NAAG. The same metabolite pairs were significant in this study (using 3 T, nt=256, IE1 seeding, for comparison). However, there are some notable differences between the two studies. Prescot et al[21] determined the $r_{(METa,METb)}$ from the inverted Fisher matrix, so they represent lower bounds of the covariance rather than the measured or observed variance. They employed a 2D J-resolved PRESS sequence, whereas the simulations in this study were made to represent the STEAM sequence. As the authors mentioned, they did not include a MM basis set for quantification. This had a substantial influence on concentration estimates in this study,

although there was likely a greater presence of the fast relaxing MM due to the short TE. Finally, Prescot et al[21] conducted an *in vivo* study whereas this study used simulations. By using simulations, the experiment was able to be repeated many times with potential sources of variation, which would be present in an *in vivo* study, minimized or removed. Considering this, it is difficult to truly compare the results, but it is encouraging that similar significantly correlated metabolite pairs were discovered.

The SNR, B_0, and type of seeding used had no influence on the accuracy of concentration estimates. This means that these variables did not lead to errors consistently above or below any metabolite's known concentration, it was only the variance around the estimate that changed. Macri et al.[22] observed that when SNR was decreased by a factor of 2 there were variations in some metabolites' amplitudes. The difference in results is likely due to the difference in methods. Macri et al.[22] used the simulated deterioration of *in vivo* spectra, whereas this study used fully simulated results with exact concentrations known.

The omission of any metabolite leads to increased error from decreased accuracy in estimates of metabolite concentrations (although Lac and Ala had very small influences). This agrees with what has been found in a previous study, in that exclusion of lower concentration metabolites during the fit can reduce accuracy of GLU and GLN quantitation[23]. Metabolites that do not share spectral area with a particular metabolite can still influence its concentration estimate indirectly through correlations with other metabolites. The whole metabolite spectral signature, which often consists of many resonances, must be increased uniformly due to the amplitude constraints put on each metabolite. This can lead to compensatory variations throughout the spectrum. The fitting algorithm can come to very different final results with only one metabolite's spectral signature omitted.

There were comparable consequences for omitting a metabolite at 7 T and 3 T. Although it is common for high field ^{1}H-MRS studies to include large quantification templates due to the increased spectral dispersion and SNR, lower field strengths may require full metabolite templates as well. It is important to include as many metabolites as reasonably

possible (based on limitations of data quality) for reliable Ser estimates, for example. Strict constraints would be necessary for metabolites with peak amplitudes on the order of noise to reduce implications of inaccurate fits. Caution is to be taken and careful interpretations of results are required when looking at any study with a limited basis set. For example, in many studies GLU is fit as "GLX", which can mean anything from GLU + GLN, to everything within that area (GLU, GLN, GABA, NAAG, GSH, MM). The GLU spectral signature accounted for GLN, NAAG, and GABA spectral areas more than other metabolites. If these metabolites are not included in the basis set, "GLX" would include a large contribution from each.

As it was hypothesized, the strongly coupled metabolites benefited the most from increases in B_0. Other metabolites with strong singlets, such as Cr and Cho, did not show much improvement in quantification, meaning studies with these metabolites of interest may not require a high field scanner. Definite improvements can be seen in quantification by including as many metabolites as possible in the template, and by providing accurate first estimates of the fitting parameters. Attempts should always be made to maximize SNR as well.

The main limitation of this study is also its main strength, in that it does not use *in vivo* data. It would not be feasible to do such a study with *in vivo* data as there would be too many variables. For example, both eddy current distortions and chemical shift displacement would be difficult issues to address across B_0, but both can be removed by using simulations. This study used a parameterized MM baseline that was known to be correct in the simulations. *In vivo*, MM are more difficult to parameterize. This could increase the observed CVs in this study. An ultra-short TE STEAM sequence was chosen due to its availability and popularity at all B_0. However, others have demonstrated that STEAM is not the ideal sequence at some B_0[24–26]. Future studies should address how other pulse sequences and perhaps different echo times would respond to the sources of variation identified in this work.

This study has explored specific sources of quantification variability commonly found in human brain ^{1}H-MRS spectra. Quantitative knowledge of the influence of these sources

of variability is important in acquisition protocol design and in data analysis method design. The results of this study suggest that for most reliable concentration estimates of GLU and GLN, one requires the highest field strength, highest SNR, most complete template, and high accuracy seeding of the iterative fitting algorithm. Even in those conditions, the largest sources of variability for GLU and GLN are overlap/correlation with each other, NAAG, and GABA.

2.5 References

1. Dager, S. & Oskin, N. Research applications of magnetic resonance spectroscopy (MRS) to investigate psychiatric disorders. *Top Magn Reson Imaging.* **19,** 81–96 (2008).

2. Ramadan, S., Lin, A. & Stanwell, P. Glutamate and glutamine: A review of in vivo MRS in the human brain. *NMR Biomed.* **26,** 1630–1646 (2013).

3. Kanowski, M., Kaufmann, J., Braun, J., Bernarding, J. & Tempelmann, C. Quantitation of Simulated Short Echo Time 1H Human Brain Spectra by LCModel and AMARES. *Magn. Reson. Med.* **51,** 904–912 (2004).

4. Stanley, J. A., Drost, D. J., Williamson, P. C. & Thompson, R. T. The use of a priori knowledge to quantify short echo in vivo 1H MR spectra. *Magn. Reson. Med.* **34,** 17–24 (1995).

5. Bartha, R. Effect of signal-to-noise ratio and spectral linewidth on metabolite quantification at 4 T. *NMR Biomed.* **20,** 512–521 (2007).

6. Provencher, S. Estimation of metabolite concentrations from localized in vivo proton NMR spectra. *Magn. Reson. Med.* **30,** 672–679 (1993).

7. Bartha, R., Drost, D. J. & Williamson, P. C. Factors affecting the quantification of short echo in-vivo 1 H MR spectra : prior knowledge, peak elimination, and filtering. *NMR Biomed.* **12,** 205–216 (1999).

8. Mierisová, Š. *et al.* New approach for quantitation of short echo time in vivo 1H MR spectra of brain using AMARES. *NMR Biomed.* **11,** 32–39 (1998).

9. Tkáć, I. & Gruetter, R. Methodology of 1 H NMR Spectroscopy of the Human Brain at Very High Magnetic Fields. *Appl. Magn. Reson.* **29,** 139–157 (2005).

10. Knight-Scott, J., Shanbhag, D. D. & Dunham, S. A. A phase rotation scheme for achieving very short echo times with localized stimulated echo spectroscopy. *Magn. Reson. Imaging* **23,** 871–876 (2005).

11. Mlynárik, V., Gruber, S., Starcuk, Z. & Moser, E. Very short echo time proton MR spectroscopy of human brain with a standard transmit/receive surface coil. *Magn. Reson. Med.* **44,** 964–7 (2000).

12. Tkác, I. *et al.* In vivo 1H NMR spectroscopy of the human brain at 7 T. *Magn. Reson. Med.* **46,** 451–6 (2001).

13. Govindaraju, V., Young, K. & Maudsley, a a. Proton NMR chemical shifts and coupling constants for brain metabolites. *NMR Biomed.* **13,** 129–153 (2000).

14. Mangia, S. *et al.* Sustained neuronal activation raises oxidative metabolism to a new steady-state level: evidence from 1H NMR spectroscopy in the human visual cortex. *J. Cereb. Blood Flow Metab.* **27,** 1055–1063 (2007).

15. Soher, B. J., Young, K., Bernstein, A., Aygula, Z. & Maudsley, A. a. GAVA: Spectral simulation for in vivo MRS applications. *J. Magn. Reson.* **185,** 291–299 (2007).

16. Théberge, J. Lawson Imaging Website [Dr. Jean Théberge's principal investigator page on the Internet. (2010). at <http://www.lawsonimaging.ca/~jtheberge/software.php>

17. Krawczyk, H. & Gradowska, W. Characterisation of the 1H and 13C NMR spectra of N-acetylaspartylglutamate and its detection in urine from patients with Canavan disease. *J. Pharm. Biomed. Anal.* **31,** 455–463 (2003).

18. Deelchand, D. K. *et al.* In vivo 1H NMR spectroscopy of the human brain at 9.4 T: initial results. *J. Magn. Reson.* **206,** 74–80 (2010).

19. Cavassila, S., Deval, S., Huegen, C., Van Ormondt, D. & Graveron-Demilly, D. Cramer-Rao bounds: An evaluation tool for quantitation. *NMR Biomed.* **14,** 278–283 (2001).

20. Bartha, R., Drost, D. J., Menon, R. S. & Williamson, P. C. Comparison of the Quantification Precision of Human Short Echo Time 1 H Spectroscopy at 1.5 and 4.0 Tesla. *Magn. Reson. Med.* **44,** 185–192 (2000).

21. Prescot, A. P. & Renshaw, P. F. Two-dimensional J-resolved proton MR spectroscopy and Prior Knowledge Fitting (ProFit) in the frontal and parietal lobes of healthy volunteers: Assessment of metabolite discrimination and general reproducibility. *J. Magn. Reson. Imaging* **37,** 642–651 (2013).

22. Macrì, M. A. *et al.* In vivo quantitative 1H MRS of cerebellum and evaluation of quantitation reproducibility by simulation of different levels of noise and spectral resolution. *Magn. Reson. Imaging* **22,** 1385–1393 (2004).

23. Hofmann, L. *et al.* Quantitative 1H-magnetic resonance spectroscopy of human brain: Influence of composition and parameterization of the basis set in linear combination model-fitting. *Magn. Reson. Med.* **48,** 440–453 (2002).

24. Mullins, P. G., Chen, H., Xu, J., Caprihan, A. & Gasparovic, C. Comparative reliability of proton spectroscopy techniques designed to improve detection of J-coupled metabolites. *Magn. Reson. Med.* **60,** 964–969 (2008).

25. Hancu, I. Optimized glutamate detection at 3 T. *J. Magn. Reson. Imaging* **30,** 1155–1162 (2009).

26. Mekle, R. *et al.* MR spectroscopy of the human brain with enhanced signal intensity at ultrashort echo times on a clinical platform at 3 T and 7 T. *Magn. Reson. Med.* **61,** 1279–1285 (2009).

Chapter 3

3 Neurometabolic abnormalities observed with magnetic resonance spectroscopy at 7 T in the anterior cingulate cortex and thalamus of patients with schizophrenia and Major Depressive Disorder

The work presented in this chapter examined brain areas that are commonly implicated in SZ using an ultra-high field MRI and ^{1}H-MRS. A version of this chapter is currently being edited for submission to the British Journal of Psychiatry.

3.1 Introduction

Current treatments of schizophrenia mostly target dopaminergic neurotransmission via dopamine receptors and are effective at alleviating positive symptoms, but are often unable to reduce negative and cognitive symptoms. Drugs that do have some degree of effectiveness in treating cognitive and negative symptoms typically come with undesirable side effects, and their mechanism is only partly understood[1,2]. To better understand the source of SZ symptoms, an alternative mechanism to dopamine abnormalities must be explored.

Glutamatergic theories of SZ propose that positive, negative, and cognitive symptoms in SZ share a common origin in dysfunction of glutamate (GLU) neurotransmission[3–5]. This proposal largely originated from animal studies that observed that agonist towards the N-methyl-D-aspartate (NMDA) receptors, specifically, ketamine and phencyclidine (PCP), replicate symptoms of SZ in their otherwise healthy hosts[6]. Later studies of humans confirmed that the drugs similarly induce symptoms in healthy controls, and actually worsen symptoms in people with SZ[6].

The exact mechanism by which GLU dysfunction could occur is not yet understood, but the NMDA receptor may be involved. In the neuron, GLU is stored in vesicles until it is required for neurotransmission and released into the synaptic cleft. GLU will then bind with one of a number of receptors on the post-synaptic membrane, including the NMDA receptor. When GLU has been released from the post-synaptic membrane receptor it is actively transported into the adjacent glial cell where it can be converted to glutamine (GLN) via glutamine synthetase and safely transported back into the presynaptic neuron and effectively recycled for re-use in neurotransmission[7]. Both GLU and GLN have been somehow implicated in SZ through studies using proton magnetic resonance spectroscopy (^{1}H-MRS) that have demonstrated abnormal concentrations throughout the brain, with a tendency for GLN to be increased and GLU to be decreased early in the illness with faster decline with age relative to controls[8].

Another possible source of dysfunction in glutamatergic neurotransmission is glycine (GLY), an agonist for the NMDA receptor. For GLU to successfully bind with the NMDA receptor, GLY is also required to bind with the receptor at a separate site. The GLY pathway has been the target of new drug interventions with limited success so far[2,5,9]. To date, there have been no ^{1}H-MRS studies of GLY in SZ, but it would be ideal to be able to study this *in vivo* and in a localized area of the brain.

Of particular interest in SZ is the involvement of GLU, GLN, and GLY in critical brain pathways that seem to be implicated in SZ known as the limbic basal ganglia thalamo-cortical (BGTHC) circuits[10] by which motivation is translated to behaviour. Each circuit cycles through the basal ganglia and through to the thalamus before reaching back out to the cortex. The thalamus, therefore, plays a critical role in motivation and behaviour. The anterior cingulate cortex (ACC) is another node of a BGTHC that has been implicated in SZ through ^{1}H-MRS[8,11] and functional magnetic resonance imaging studies[12]. The dorsal component of the ACC is involved in error detection and organization of conflicting stimuli, to which activities that stimulate the ACC have demonstrated hypofunction in SZ [12]. Both the thalamus and the ACC are good brain areas to study a potential dysfunction in glutamatergic neurotransmission in SZ.

Most ^{1}H-MRS studies of the ACC and thalamus in SZ have been quantified at lower magnetic resonance imaging (MRI) field strengths, where GLU and GLN spectral signatures overlap and difficult to reliably quantify individually. Recent advances in technology have created stronger magnetic field strength MRI facilities. Stronger magnetic field strengths translate to an increase in sample magnetization and a linear increase in the signal-to-noise ratio (SNR), assuming body noise dominance. This is very important in ^{1}H-MRS acquisitions, as ^{1}H-MRS is a low-SNR technique that can require long scan times to acquire one quality spectrum from a localized voxel in the brain, and longer scans increase the likelihood of subject movement during a scan. An additional essential feature of stronger MRI field strengths is increased metabolite separation in the ^{1}H-MRS spectra, as the ratio of the magnitude of metabolites' J-coupling constants to their chemical shift dispersion (both measure in Hertz) decreases. This means that metabolites that overlap significantly at low MRI field strengths, such as GLU and GLN, become more resolvable at higher field strengths. It also becomes more likely that reliable detection of lower concentration metabolites that are traditionally difficult to quantify, such as GLY, may be quantifiable with the higher SNR and improved metabolite spectral signature separation.

Specificity of results is difficult to address in studies comparing a psychiatric group to healthy controls. Major Depressive Disorder (MDD) has previously been assessed with ^{1}H-MRS although findings have been inconsistent[13]. As symptoms of SZ can overlap with those of MDD and GLU has also been implicated in mood disorders, the purpose of this study was to examine metabolite signals in voxels located in the ACC and thalamus of patients with SZ compared to healthy controls and a psychiatric control group of people with MDD using ^{1}H-MRS with a 7 Tesla head-only MRI.

Due to the previous findings of increased GLN[8,11], and decreased GLU[8] early in frontal brain areas in SZ, these changes were expected in the ACC and TH of volunteers with SZ relative to the healthy controls and the MDD group. GLY abnormalities were also expected, but it is unknown which direction to expect the abnormalities. It has recently been demonstrated that there is reduced *myo*-inositol (MYO) in MDD[13–15], which was

also expected in the present study. No specific hypotheses were made regarding remaining metabolites.

3.2 Methods

3.2.1 Participants

There were 16 participants in the SZ group, 17 in the MDD group, and 18 in the healthy control group. All gave informed written consent according to the guidelines of the Review Board for Health Sciences Research Involving Human Subjects at the University of Western Ontario. Volunteers with neurological or major medical illnesses, clinically significant head injury, other psychiatric disorders, MRI contra-indications, or substance abuse within the previous year were excluded from the study. Any healthy volunteer with a known family history of psychiatric disorder in a first or second degree relative was also excluded.

A consensus diagnosis was established on all participants by a psychiatrist and trained assistant with the Structured Clinical Interview for DSM-IV[16]. SZ subjects were rated with the Scale for Assessment of Negative Symptoms and the Scale for the Assessment of Positive Symptoms[17,18] and MDD patients were assessed with the Montgomery Asberg Depression Scale[19] and the Young Mania Rating Scale[20]. Fourteen SZ patients were being treated with atypical neuroleptics (Chlorpromazine Equivalent 409 ± 293mg) and 2 patients were not medicated. Eleven of the 17 MDD patients were being treated with antidepressant medications at the time of the scan. Demographic information including age, gender, handedness, education, parental education, clinical rating scores, and length of illness were collected as in our previous study[21] and are shown in Table 3-1.

Table 3-1. Participant demographics

Group	Controls	MDD	SZ	*p*
n	18	17	16	
Age	23.9 ± 4.6	22.5 ± 4.6	22.7 ± 2.9	0.570
M/F	11/7	6/11	13/3	**0.018**
R/L	16/2	15/2	15/1	0.824
Educ	3.1 ± 0.8	2.6 ± 0.6	2.2 ± 0.8	**0.010**
PEduc	3.1 ± 0.9	2.9 ± 0.8	3.3 ± 0.8	0.424
HAM-A		12.8 ± 10.5		
HAM-D		12.8 ± 8.9		
Mania		5.1 ± 6.7		
Montg		18.0 ± 10.4		
CPZ (mg)			358 ± 307	
SANS			9.7 ± 7.7	
SAPS			7.6 ± 10.4	
Illness Duration (months)		28.6 ± 14.4	29.5 ± 15.7	

M/F – male/female
R/L – right/left
Educ – education rating of the participant (1- gr. 10 or lower, 2- completed high school, 3- 1-3 years of college/university, 4- >3 years of college/university)
Peduc – education rating of the participant's parent (1- gr.10 or lower, 2- completed high school, 3- 1-3 years of college/university, 4- >3 years of college/university)
H Anx – Hamilton Anxiety Scale
H Dep – Hamilton Depression Scale
Mania – mania rating from the Young Mania Rating Scale
Montg – result of the Montgomery Asperg Depression Scale
CPZ – chlorapromazine equivalent
SANS – Scale for Assessment of Negative Symptoms
SAPS – Scale for Assessment of Positive Symptoms
p – ANOVA test for significance (alpha=0.05, two-tailed), bolded values indicate significance

3.2.2 ^{1}H-MRS Data Collection and Analysis

All measurements were acquired on a 7.0 T Agilent/Magnex head-only MRI (Agilent, Inc, Walnut Creek, California, USA) with a Siemens AC84 head gradient coil (Siemens, Erlangen, Germany), located at the Center for Functional and Metabolic Mapping at Western University. A transmit-only, receive-only (TORO) head coil with 15 transmitters and 23 receivers[22] was used for all scans. A map of the transmit field for each transmitter

was acquired at the beginning of the session to facilitate optimized homogeneity correction of the transmit field for each scan using an automated B_1-shimming approach[23]. The magnetic field uniformity (B0-shim) was adjusted automatically over the field of view with first-order and second-order shims using RASTAMAP[24] before all acquisitions.

The ^{1}H-MRS voxels were 2.0 x 2.0 x 2.0 cm (8cm^3) in size and located in the left thalamus and left dorsal anterior cingulate. Voxels were placed and angled using anatomical landmarks (Fig 3-1) on two, fast low-angle shot 2D anatomical imaging sequences in the sagittal (45 slices, repetition time (TR) = 950 ms, echo time (TE)=5.23 ms, flip-angle (α)= 30°, gap between slices=1 mm, thickness= 2 mm, field of view (FOV) 220 × 220 mm, and matrix size of 220 × 200) and axial (20 slices, TR = 500 ms, TE =5.23 ms, α =30°, gap between slices=1 mm, thickness= 2 mm, FOV =220 × 220 mm, and matrix size 220 × 220) directions, both with lipid saturation.

Spectra were acquired using an ultra-short TE stimulated echo acquisition mode (STEAM) sequence with outer volume suppression[25] (TR=3s, TE=10 ms, mixing time ™ =32ms, 4000 complex pairs, 4 steady state scans, 1s acquisition time, 8 step phase cycle). There were 64 averages of water suppressed spectra acquired individually for each voxel location, with 16 water-unsuppressed spectra acquired to correct metabolite lineshapes and as internal concentration reference. An 8-pulse VAPOR preparation sequence with an additional water suppression pulse during the TM period[25] was used for water suppression. A separate metabolite suppressed spectrum was acquired to assess the macromolecule content with inversion times as published in Penner et al[26]. Each acquisition produced 23 spectra, one for each receiver, which required channel combination before use[27]. Spectra were frequency and phase corrected before being averaged together in a phase- and frequency-coherent manner. QUality Eddy Current Correction (QUECC)[28] reduced linewidth distortions before spectral fitting with fitMAN, a time-domain fitting algorithm[29]. Metabolite concentrations were corrected for gray and white matter content. All spectra were inspected visually for quality by a trained spectroscopist.

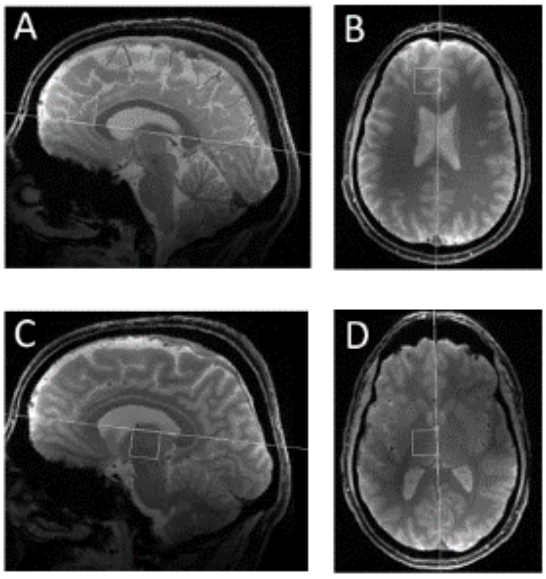

Figure 3-1. Sagittal and transverse cross-sections depicting the voxel locations. Voxel were located in the left anterior cingulate cortex (A,B) and the left thalamus (C,D) in neurological orientation. The AP line and midline shown as anatomical landmarks for the sagittal and transverse cross sections, respectively.

Only metabolites with Cramer-Rao lower bounds (CRLB) less than 20% were included in the analysis, with the exception of GLY, which had a CRLB limit of 30%. Metabolite concentration estimates were also tested for outliers at the group-level.

One-tailed t-tests ($p<0.05/3$) will be employed to explore the directional hypotheses of increased GLU and GLN in SZ relative to the healthy controls and the MDD group. A one-tailed test will also be used for the decreased MYO in the MDD group relative to controls and the SZ group. The statistical tests for GLY will be two-tailed t-tests ($p<0.05/3$). A multivariate analysis of variance (MANOVA) will test for significant differences in the remaining metabolites (glutathione (GSH), taurine (TAU), aspartate (ASP), *scyllo*-inositol (SCY), ascorbate (ASC), total choline (TCH; choline + phoshporylcholine + glycerophosphorylcholine), total creatine (TCR; creatine + phosphocreatine), and total N-acetylaspartate (TNAA; N-acetylaspartate + N-acetylaspartylglutamate)). All statistical tests were completed using SPSS v.20 (IBM Corp, Armonk, New York, USA).

3.3 Results:

^{1}H-MRS spectra were acquired with voxels in the ACC and thalamus of all participants with the exception of one healthy control who did not wish to finish the scan of the thalamus due to dizzyness. Average water linewidths were 13.2 ± 1.3Hz and 16.9 ± 2.1 Hz for the healthy controls, 12.1 ± 0.9Hz and 16.0 ± 1.8Hz for the MDD group, and 12.8 ± 1.6Hz and 16.9 ± 2.2Hz for the SZ group in the ACC and thalamus, respectively, indicating well shimmed data. There were no significant differences in the water linewidths between groups. One spectrum from the ACC of volunteers from each of the MDD and SZ groups needed to be excluded due to poor quality spectra, likely due to excessive movement. Example spectra from each brain region along with the respective fits of GLU, GLN, and GLY can be seen in Fig.3-2. In the thalamus, one subject from the SZ group and one healthy control each presented with GLY concentrations CRLB of 35% and had to be excluded. The remaining GLY measurements were within the CRLB criterion.

Increased GLN concentrations were observed in the thalamus of the SZ group relative to the healthy controls (p=0.009) but not to the MDD group (p=0.072). There were no significant between-group differences in GLU concentrations in neither the ACC (Table 3-2) nor the thalamus (Table 3-3). GLY concentrations were significantly reduced in the thalamus of the SZ group relative to both the healthy controls (p=0.017) and the MDD group (p=0.012), but no differences in GLY were observed in the ACC (p=0.385, p=0.184, respectively). MYO was reduced in the MDD group relative to the healthy controls (ACC: p=0.009; thalamus: p=0.014) and the SZ group (ACC: p=0.001; thalamus: p=0.002). The MANOVA for the remaining metabolites was not significant for the thalamus (p=0.126, Wilk's Lambda) nor for the ACC (p=0.297, Wilk's Lambda).

Although the MANOVA was not significant, a closer look at the pairwise comparisons reveals a significant decrease in SCY in the ACC of the MDD group relative to the SZ group (p=0.004) and a trend when compared to the healthy controls (p=0.026).

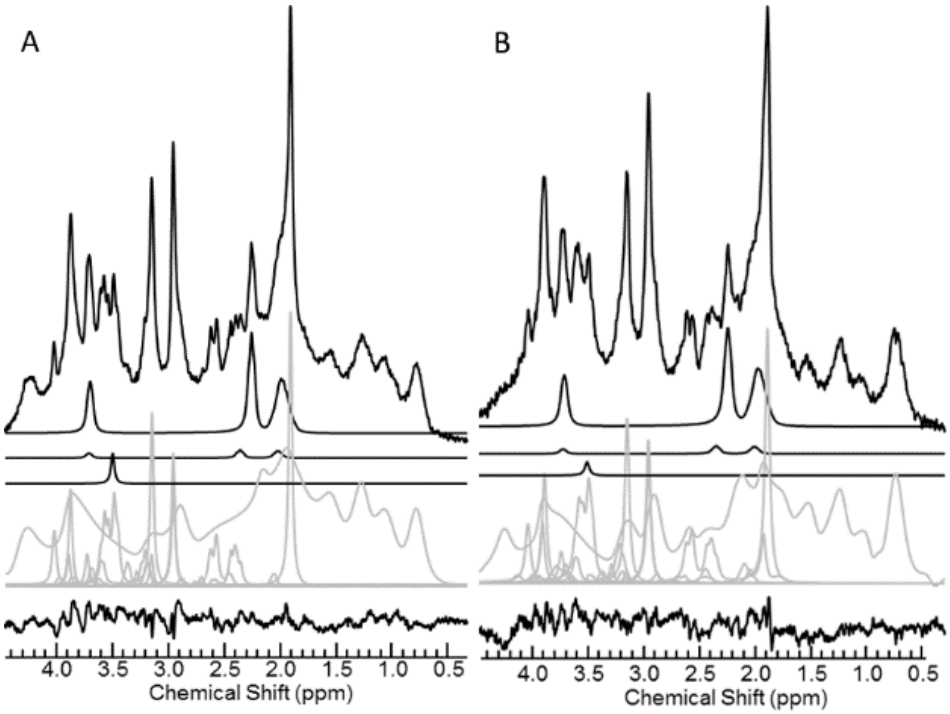

Figure 3-2. Example 64 average spectra from (A) the ACC and (B) the thalamus. Spectral fits are shown for GLU, GLN, GLY, and all remaining metabolites, with the residual of the fit minus the data.

Concentrations of each metabolite, with the pairwise comparisons for each group can be seen for the ACC and the thalamus in Table 3-2 and Table 3-3, respectively.

3.4 Discussion

3.4.1 GLU and GLN

The significant increase in GLN concentrations in the thalamus in the SZ subject group was consistent with the originally stated hypothesis of increased GLN concentrations of subjects with SZ relative to healthy controls ($p=0.009$) and agrees with previous studies[8,11]. The increased GLN could mean a reduced efficiency of converting back to GLU via glutamine synthetase or it could be directly related to NMDA receptor

Table 3-2. Metabolite concentrations (mmol/kg$_{ww}$ ± standard deviations) with statistical comparisons for each subject group for a voxel in the ACC

ACC						
	HC	MDD	SZ	p(HC-MDD)	p(HC-SZ)	p(MDD-SZ)
GLU	10.01 ± 1.25	10.37 ± 0.66	10.73 ± 1.21	0.354	0.064	0.363
GLN	2.04 ± 0.53	1.90 ± 0.72	1.96 ± 0.96	0.592	0.385	0.408
GLY	0.88 ± 0.28	0.99 ± 0.22	0.86 ± 0.24	0.234	0.837	0.184
GSH	1.28 ± 0.41	1.16 ± 0.24	1.41 ± 0.35	0.334	0.303	0.060
TAU	1.64 ± 0.33	1.58 ± 0.39	1.73 ± 0.41	0.671	0.484	0.284
ASP	2.81 ± 1.46	2.10 ± 1.19	2.86 ± 1.34	0.134	0.925	0.128
MYO	8.02 ± 0.79	7.19 ± 0.72	8.36 ± 1.34	**0.009**	0.327	**0.002**
SCY	0.51 ± 0.15	0.39 ± 0.11	0.55 ± 0.18	0.026	0.406	**0.004**
ASC	1.11 ± 0.35	1.10 ± 0.71	1.37 ± 0.68	0.984	0.237	0.249
TCH	2.38 ± 0.33	2.36 ± 0.22	2.40 ± 0.25	0.805	0.792	0.625
TCR	8.89 ± 0.99	8.92 ± 0.74	9.52 ± 0.95	0.929	0.052	0.075
TNAA	11.02 ± 1.36	11.45 ± 0.63	11.60 ± 0.82	0.236	0.107	0.673

HC – healthy controls; MDD- major depressive disorder; SZ – schizophrenia
GLU – glutamate; GLN – glutamine; GLY – glycine; GSH – glutathione; TAU – taurine; ASP – aspartate; MYO – *myo*-inositol; SCY – *scyllo*-inositol; ASC – ascorbate; TCH – total choline; TCR – total creatine; TNAA – total NAA.
p(HC-MDD) – HC vs MDD, alpha=0.05/3 (Bonferroni corrected), two-tailed. Bolded values indicate significance
p(HC-SZ) – HC vs SZ, alpha=0.05/3 (Bonferroni corrected), two-tailed. Bolded values indicate significance
p(MDD-SZ) – MDD vs SZ, alpha=0.05/3 (Bonferroni corrected), two-tailed. Bolded values indicate significance

Table 3-3. Metabolite concentrations (mmol/kg$_{ww}$ ± standard deviations) with statistical comparisons for each subject group for a voxel in the TH

Thalamus												
	HC			MDD			SZ			p(HC-MDD)	p(HC-SZ)	p(MDD-SZ)
GLU	7.38	±	0.61	7.79	±	0.85	7.39	±	1.03	0.161	0.493	0.173
GLN	1.27	±	0.59	1.51	±	0.69	1.85	±	0.63	0.309	**0.009**	0.072
GLY	0.91	±	0.26	0.92	±	0.25	0.72	±	0.13	0.906	**0.017**	**0.012**
GSH	1.31	±	0.31	1.22	±	0.24	1.41	±	0.28	0.355	0.295	0.054
TAU	1.93	±	0.54	2.20	±	0.58	2.32	±	0.40	0.142	0.034	0.496
ASP	2.53	±	1.38	3.22	±	1.76	3.38	±	1.93	0.273	0.180	0.786
MYO	7.18	±	0.76	6.41	±	1.21	7.44	±	0.94	**0.014**	0.447	**0.004**
SCY	0.37	±	0.07	0.35	±	0.07	0.39	±	0.05	0.235	0.422	0.052
ASC	0.94	±	0.66	0.73	±	0.51	1.16	±	0.49	0.289	0.259	0.033
TCH	2.18	±	0.16	2.19	±	0.16	2.16	±	0.22	0.892	0.764	0.665
TCR	6.52	±	0.81	6.41	±	0.86	6.45	±	0.79	0.702	0.795	0.907
TNAA	11.07	±	0.86	10.95	±	0.97	10.84	±	0.87	0.722	0.465	0.703

HC – healthy controls; MDD- major depressive disorder; SZ – schizophrenia
GLU – glutamate; GLN – glutamine; GLY – glycine; GSH – glutathione; TAU – taurine; ASP – aspartate; MYO – *myo*-inositol; SCY – *scyllo*-inositol; ASC – ascorbate; TCH – total choline; TCR – total creatine; TNAA – total NAA.
p(HC-MDD) – HC vs MDD, alpha=0.05/3 (Bonferroni corrected), two-tailed. Bolded values indicate significance
p(HC-SZ) – HC vs SZ, alpha=0.05/3 (Bonferroni corrected), two-tailed. Bolded values indicate significance
p(MDD-SZ) – MDD vs SZ, alpha=0.05/3 (Bonferroni corrected), two-tailed. Bolded values indicate significance

hypofunction, which would cause increases in the glutamine synthetase activity and would lead to increased GLN[30].

The lack of findings in GLN and GLU concentrations in the ACC and in GLU concentrations in the thalamus did not agree with the originally stated hypothesis. The absence of an observed significant increase in GLN in the ACC could be due to the duration of illness of the sample of SZ subjects, as it has also been shown that although SZ subjects have an initial increase at the onset of the illness, they also decrease their GLN concentrations faster than healthy controls. With the average duration of illness being 29.50 ± 17.50 months, it is possible a significant decrease had already begun. It is also possible that more subjects are necessary to observe any significant differences.

There were no significant differences in either GLU or GLN in the SZ group compared to the MDD psychiatric control group, although a non-significant (trend-level) increase in GLN in the thalamus was observed ($p=0.072$). It is likely that with more participants a significant difference would be observed, but it is also possible that GLN changes relative to healthy controls are easier to observe in SZ participants compared to MDD participants due to the greater severity of negative and cognitive symptoms in SZ compared to MDD.

The MDD group also did not significantly differ from the healthy control GLU and GLN concentrations. It has previously been shown that decreased GLU (often observed as GLX (GLU+GLN)) is a common finding in MDD compared to healthy controls[13,31], but this was not observed in this study.

3.4.2 GLY as a potential therapeutic target

Studies have examined the serum and plasma of people with SZ to examine GLY concentrations, among other neurotransmitters[32,33], but no studies have examined GLY concentrations in SZ using ^{1}H-MRS. This is partly due to the difficulty in examining GLY *in vivo*. At lower field strengths, the GLY peak overlaps strongly with the MYO peak. As magnetic field strength increases so does their peak separation. In this study,

the use of a 7 T MRI provided adequate peak separation and signal to quantify GLY separately from MYO. Recent techniques, however, have demonstrated reliable GLY concentration changes can be detected following regular oral administration of GLY for two weeks using a 4 T MRI and a TE-averaged PRESS sequence[34].

The reduction in GLY observed in the thalamus of the SZ group corresponds very well with the observed increases in GLN. GLY is a co-agonist of the GLU NMDA receptor. Without an adequate supply of GLY, GLU neurotransmission, via the NMDA receptor, will be impeded. The synaptic supply of GLY is normally maintained below the level of saturation[9], so any decrease in GLY could directly reduce NMDA activity, increasing glutamine synthetase activity[30] and potentially explaining the observed increases in the GLN concentrations.

Many strategies towards altering glutamatergic activity via pharmacological interventions have been explored but have presented with various challenges. GLU itself does not cross the blood-brain barrier well[35] and extracellular concentrations need to be controlled to prevent GLU excitotoxicity[7]. Other strategies have targeted GLY or GLY transporters. GLY is rapidly metabolized and does not cross the blood-brain barrier well either[9], but oral administrations have led to detectable changes in the brain[34]. The GLY activity is modulated by GLY transporter proteins, GLYt2 and GLYt1[5]. GLYt2 is involved in the inhibitory function of GLY and GLYt1 regulates the concentrations of GLY in the synaptic cleft[9]. New drug therapies are selectively targeting this GLYt1 transporter protein to increase the synaptic supply of GLY in hopes of saturating the NMDA receptor GLY subunit to increase its activity[36,37]. A potential future study could use high-field ^{1}H-MRS to detect GLY and GLN concentrations in the thalamus before and after medication. Decreased GLN from the baseline value would potentially indicate increased NMDA receptor activation causing reduced glutamine synthetase activity and less GLN present. One study found that GLY concentrations increased in the plasma of subjects with SZ after receiving clozapine treatment[32] and another found that serum levels were significantly lower in patients taking clozapine[33]. It is now possible to monitor the effects of clozapine on brain levels of both GLY and GLN concentrations with reasonable precision using ^{1}H-MRS.

3.4.3 Inositol in MDD

The main finding in the MDD group was the reduced MYO observed in the ACC and TH and reduced SCY observed in the ACC. MYO has many functions, including being an important osmolyte, a structural component of eukaryotic cells and a precursor for second messengers involved in neurotransmission[38]. Although MYO is consumed regularly in the average diet, it can be created *de novo* in the brain from glucose and it is readily lost from brain tissue when cell integrity is compromised[38]. It has commonly been described as a marker of glial cell integrity, but this has been brought into question as many neurons contain just as much or more MYO than glial cells[38]. There is a possibility that reduced MYO is due to the significant gender differences between the MDD group and the other groups ($p=0.018$), but it is unlikely given that reduced MYO has previously been reported in MDD patients frontal lobes[13,14,39] in post-mortem brain tissue[15] and in cerebrospinal fluid[40]. Other studies have shown a normalization or an increase in MYO in recovered MDD patients[14,41] and it is believed that drugs that reduce mania in bipolar disorder act by reducing MYO content[42]. MYO oral supplementation has been investigated as a treatment for MDD. Taylor et al[43] examined the results of four studies consisting of unipolar and/or bipolar subjects taking daily inositol and found no significant effect. However, a more recent meta-analyses by Mukai et el[44] examined seven studies of mixed MDD, bipolar, and premenstrual dysphoric disorder patients and suggests that inositol may have some therapeutic effect for people with depression. Although the MANOVA was not significant, it is interesting that SCY, an isomer of MYO that typically has a concentration of 5-12% that of MYO in the human brain[38], had significantly reduced concentrations when looking at the pairwise comparisons of the remaining metabolites. It is becoming increasing evident that there may be a role for inositol in the regulation of mood. More studies are necessary to further elucidate the exact role played and whether MYO (or even SCY) could be a potential target of pharmacological intervention in MDD.

3.4.4 Future studies

There are a number of avenues to explore based on these results. For the SZ group, a confirmation study finding reduced GLY in the thalamus could be performed, followed by a study investigating GLY concentrations as influenced by administration of oral GLY supplementation. It would also be interesting to see how GLY concentrations in SZ patients taking clozapine compare to those taking first or second generation antipsychotics. Similarly, in the MDD group, a ^{1}H-MRS study investigating before and after effects of MYO supplementation in the diet should be explored.

3.4.5 Conclusions

As far as the authors are aware, this is the first ^{1}H-MRS study of SZ or MDD using a 7 T MRI and the first ^{1}H-MRS study looking at GLY in SZ. No GLU differences were observed in either the ACC or the thalamus, but decreased GLY was observed in the thalamus along with increased GLN in the SZ group relative to healthy controls, supporting the notion of NMDA receptor hypofunction in SZ. Decreased MYO was observed in the MDD group relative to both the healthy control group and the SZ group in both the ACC and the thalamus. Metabolic effects of drug interventions should be explored next.

3.5 References:

1. Miyamoto, S., Miyake, N., Jarskog, L. F., Fleischhacker, W. W. & Lieberman, J. a. Pharmacological treatment of schizophrenia: a critical review of the pharmacology and clinical effects of current and future therapeutic agents. *Mol. Psychiatry* **17,** 1206–1227 (2012).

2. Poels, E. M. P. *et al.* Imaging glutamate in schizophrenia: review of findings and implications for drug discovery. *Mol. Psychiatry* **19,** 20–9 (2014).

3. Coyle, J. T. & Tsai, G. The NMDA receptor glycine modulatory site: a therapeutic target for improving cognition and reducing negative symptoms in schizophrenia. *Psychopharmacology (Berl).* **174,** 32–38 (2004).

4. Stone, J. M. Glutamatergic antipsychotic drugs: a new dawn in the treatment of schizophrenia? *Ther. Adv. Psychopharmacol.* **1,** 5–18 (2011).

5. Gilbert-Rahola, J. & Villena-Rodriguez, A. Glutamatergic drugs for schizophrenia treatment. *Actas españolas Psiquiatr.* **42,** 234–241 (2014).

6. Javitt, D. C., Zukin, S. R., Heresco-Levy, U. & Umbricht, D. Has an angel shown the way? Etiological and therapeutic implications of the PCP/NMDA model of schizophrenia. *Schizophr. Bull.* **38,** 958–966 (2012).

7. Mark, L. P. *et al.* Pictorial review of glutamate excitotoxicity: Fundamental concepts for neuroimaging. *Am. J. Neuroradiol.* **22,** 1813–1824 (2001).

8. Marsman, A. *et al.* Glutamate in schizophrenia: A focused review and meta-analysis of 1H-MRS studies. *Schizophr. Bull.* **39,** 120–129 (2013).

9. Harvey, R. J. & Yee, B. K. Glycine transporters as novel therapeutic targets in schizophrenia, alcohol dependence and pain. *Nat. Rev. Drug Discov.* **12,** 866–85 (2013).

10. Williamson, P. Are anticorrelated networks in the brain relevant to schizophrenia? *Schizophr. Bull.* **33,** 994–1003 (2007).

11. Théberge, J. *et al.* Glutamate and glutamine measured with 4.0 T proton MRS in never-treated patients with schizophrenia and healthy volunteers. *Am. J. Psychiatry* **159,** 1944–1946 (2002).

12. Boksman, K. *et al.* A 4.0-T fMRI study of brain connectivity during word fluency in first-episode schizophrenia. *Schizophr. Res.* **75,** 247–263 (2005).

13. Yildiz-Yesiloglu, A. & Ankerst, D. P. Review of 1H magnetic resonance spectroscopy findings in major depressive disorder: A meta-analysis. *Psychiatry Res. - Neuroimaging* **147,** 1–25 (2006).

14. Chen, L. P., Dai, H. Y., Dai, Z. Z., Xu, C. T. & Wu, R. H. Anterior cingulate cortex and cerebellar hemisphere neurometabolite changes in depression treatment: A 1H magnetic resonance spectroscopy study. *Psychiatry Clin. Neurosci.* **68,** 357–364 (2014).

15. Coupland, N. J. *et al.* Decreased prefrontal myo-inositol in major depressive disorder. *Biol. Psychiatry* **57,** 1526–1534 (2005).

16. First, M., Spitzer, R., Gibbon, M. & Williams, J. *Structured Clinical Interview (SCID) for DSM-IV Axis 1 Disorders*. (American Psychiatric Press Inc, 1997).

17. Andreasen, N. C. *Scale for the Assessment of Positive Symptoms (SAPS)*. (The University of Iowa, 1984).

18. Andreasen, N. C. *Scale for the Assessment of Negative Symptoms (SANS)*. (The University of Iowa, 1984).

19. Montgomery, S. A. & Asberg, M. Scale Designed to be Sensitive to Change. *Br. J. Psychiatry* **134,** 382–9 (1979).

20. Young, R. C., Biggs, J. T., Ziegler, V. E. & Meyer, D. A. A rating scale for mania : reliability , validity and sensitivity A Rating Scale for Mania : Reliability , Validity and Sensitivity. *Br. J. Psychiatry* **133,** 429–435 (2011).

21. Aoyama, N. *et al.* Grey matter and social functioning correlates of glutamatergic metabolite loss in schizophrenia. *Br. J. Psychiatry* **198,** 448–456 (2011).

22. Gilbert, K. M., Curtis, A. T., Gati, J. S., Klassen, L. M. & Menon, R. S. A radiofrequency coil to facilitate B 1 + shimming and parallel imaging acceleration in three dimensions at 7 T. *NMR Biomed.* **24,** 815–823 (2011).

23. Curtis, A. T., Gilbert, K. M., Klassen, L. M., Gati, J. S. & Menon, R. S. Slice-by-slice B1+ shimming at 7 T. *Magn. Reson. Med.* **68,** 1109–16 (2012).

24. Klassen, L. M. & Menon, R. S. Robust Automated Shimming Technique Using Arbitrary Mapping Acquisition Parameters (RASTAMAP). *Magn. Reson. Med.* **51,** 881–887 (2004).

25. Tkáć, I. & Gruetter, R. Methodology of 1 H NMR Spectroscopy of the Human Brain at Very High Magnetic Fields. *Appl. Magn. Reson.* **29,** 139–157 (2005).

26. Penner, J. & Bartha, R. Semi-LASER 1H MR spectroscopy at 7 Tesla in human brain: Metabolite quantification incorporating subject-specific macromolecule removal. *Magn. Reson. Med.* **00,** 1–9 (2014).

27. Brown, M. A. Time-domain combination of MR spectroscopy data acquired using phased-array coils. *Magn. Reson. Med.* **52,** 1207–1213 (2004).

28. Bartha, R., Drost, D. J., Menon, R. S. & Williamson, P. C. Spectroscopic lineshape correction by QUECC: Combined QUALITY deconvolution and eddy current correction. *Magn. Reson. Med.* **44,** 641–645 (2000).

29. Bartha, R., Drost, D. J. & Williamson, P. C. Factors affecting the quantification of short echo in-vivo 1 H MR spectra : prior knowledge, peak elimination, and filtering. *NMR Biomed.* **12,** 205–216 (1999).

30. Rodrigo, R. & Felipo, V. Control of brain glutamine synthesis by NMDA receptors. *Front. Biosci.* **12,** 883–890 (2007).

31. Jun, C. *et al.* Disturbance of the glutamatergic system in mood disorders. *Exp. Neurobiol.* **23,** 28–35 (2014).

32. Yamamori, H. *et al.* Changes in plasma d-serine, l-serine, and glycine levels in treatment-resistant schizophrenia before and after clozapine treatment. *Neurosci. Lett.* **582,** 93–98 (2014).

33. Hons, J., Vasatova, M., Cermakova, E., Doubek, P. & Libiger, J. Different serine and glycine metabolism in patients with schizophrenia receiving clozapine. *J. Psychiatr. Res.* **46,** 811–818 (2012).

34. Kaufman, M. J. *et al.* Oral glycine administration increases brain glycine/creatine ratios in men: A proton magnetic resonance spectroscopy study. *Psychiatry Res. - Neuroimaging* **173,** 143–149 (2009).

35. Hawkins, R. A. The blood-brain barrier and glutamate 1–4. *Am. J. Clin. Nutr.* **90,** 867–874 (2009).

36. Umbricht, D. *et al.* Effect of Bitopertin, a Glycine Reuptake Inhibitor, on Negative Symptoms of Schizophrenia: A Randomized, Double-Blind, Proof-of-Concept Study. *JAMA psychiatry* **71,** 637–46 (2014).

37. Tsai, C. H. *et al.* Activation of N-methyl-D-aspartate receptor glycine site temporally ameliorates neuropsychiatric symptoms of Parkinson's disease with dementia. *Psychiatry Clin. Neurosci.* 692–700 (2014). doi:10.1111/pcn.12175

38. Fisher, S. K., Novak, J. E. & Agranoff, B. W. Inositol and higher inositol phosphates in neural tissues: Homeostasis, metabolism and functional significance. *J. Neurochem.* **82,** 736–754 (2002).

39. Järnum, H. *et al.* Longitudinal MRI study of cortical thickness, perfusion, and metabolite levels in major depressive disorder. *Acta Psychiatr. Scand.* **124,** 435–446 (2011).

40. Barkai, A., Dunner, D., Gross, H., Mayo, P. & Fieve, R. Reduced myo-inositol levels in cerebrospinal fluid from patients with affective disorder. *Biol. Psychiatry* **13,** 65–72 (1978).

41. Taylor, M. J., Selvaraj, S., Norbury, R., Jezzard, P. & Cowen, P. J. Normal glutamate but elevated myo-inositol in anterior cingulate cortex in recovered depressed patients. *J. Affect. Disord.* **119,** 186–189 (2009).

42. Kofman, O. & Belmaker, R. H. Ziskind-Somerfeld Research Award 1993. Biochemical, behavioral, and clinical studies of the role of inositol in lithium treatment and depression. *Biol. Psychiatry* **34,** 839–852 (1993).

43. Taylor, M. J., Wilder, H., Bhagwagar, Z. & Geddes, J. Inositol for depressive disorders. *Cochrane Database Syst. Rev.* CD004049 (2004). doi:10.1002/14651858.CD004049.pub2

44. Mukai, T., Kishi, T., Matsuda, Y. & Iwata, N. A meta-analysis of inositol for depression and anxiety disorders. *Hum. Psychopharmacol.* **29,** 55–63 (2014).

Chapter 4

4 Increased glutamate levels observed upon functional activation in the anterior cingulate cortex using the Stroop Task and functional spectroscopy.

The study presented in this chapter was performed to demonstrate that it is possible to detect changes in the main excitatory neurotransmitter, glutamate, upon functional activation using a cognitive functional paradigm using a 7 T MRI and functional magnetic resonance spectroscopy in a group of healthy controls. A cognitive task would be desirable for this technique because it could then be used to examine psychiatric disorders that have cognitive deficiencies. A version of this chapter has been published in NeuroReport (2015; 26:107-112). No permission letters are needed to reproduce this article in this dissertation.

4.1 Introduction

Proton magnetic resonance spectroscopy (^{1}H-MRS) is a useful tool for the noninvasive study of the brain's chemistry. ^{1}H-MRS has an inherently low signal-to-noise ratio (SNR); thus, traditional studies have assumed constant metabolite concentrations during the long scan durations required to acquire a spectrum with sufficient SNR for accurate quantification. Advances in MRI technology such as higher magnetic field strengths, improvements in radiofrequency head coils, pre-amplification, and signal detection systems have considerably increased the available SNR for ^{1}H-MRS. This has made it feasible to examine the brain in a dynamic state using functional ^{1}H-MRS (^{1}H-fMRS). It has been shown previously with ^{1}H-fMRS that alterations in the local neurochemistry occur when a particular area of the brain becomes engaged in task transaction[1–10]. One metabolite of interest is glutamate (GLU), the main excitatory neurotransmitter in the

brain, which has been shown to be related directly to the brain's consumption of glucose for the production of energy[11] and has been implicated in the pathophysiology of psychiatric disorders, such as schizophrenia[12,13].

Few studies have used ^{1}H-fMRS to date. Three studies have shown small (2–4%) but significant increases in the GLU concentration in the occipital cortex upon functional activation with a visual stimulus, such as a flickering checkerboard[1,2,6]. Recent results showed a 2% increase in the motor cortex upon functional activation with a finger-tapping paradigm [3]. Two other studies have used pain as a stimulus and have identified 9.3 and 18.1% increases in the mean GLU concentration in the anterior cingulate cortex (ACC) and the anterior insular cortex, respectively, when the participants are exposed to the pain[4,5]. Finally, two studies have examined GLU changes in the lateral occipital cortex using a repetition suppression task and have found GLU increases of 11%[9] and 12%[10].

Cognitive tasks are generally less sensitive for detection when assessed through standard BOLD fMRI than visual (flickering checkerboard) or motor (finger tapping) tasks[14]. To the best of our knowledge, there has been only one study to date that has used fMRS to examine metabolite changes using a cognitive task as the activation paradigm[8]. This study did not find any changes in GLX [GLU +glutamine (GLN)], but they did find that GABA increased in concentration upon functional stimulation of the left dorsolateral prefrontal cortex and then decreased in subsequent runs of the task. Although GLX, in this case, combines GLU with GLN, it would be ideal to use a cognitive task to examine the response of GLU independent of GLN as both are crucial to brain function. As GLU abnormalities have been found in neuropsychiatric disorders in the ACC[12,13], a cognitive task that robustly activates the ACC is desirable for the investigation of abnormalities in the dynamic regulation of GLU levels in this area.

In addition to influencing our perception of pain, the ACC is implicated in many other cognitive functions, including selective encoding of stimulus properties[15], general attention[16], and organization of conflicting stimuli[17]. The aim of this exploratory study is to show that with ^{1}H-fMRS of the ACC, it is feasible to detect GLU concentration

changes using a cognitive task as the activation paradigm. The color-word Stroop Task is a common psychological task that involves differentiating potentially conflicting word and color stimuli under congruent (i.e. the word 'RED' written in red ink) and incongruent (i.e. the word 'BLUE' written in red ink) conditions[18]. The Stroop Task was chosen for this study because it activates the ACC and has been implicated previously in schizophrenia[17], a potential application of this technique.

It has been proposed that GLU concentrations will increase upon functional activation of the ACC with a cognitive task because of the increase in the cycling rate of neuronal GLU with GLN with an approximate 1 : 1 stoichiometry to the neuronal glucose oxidation rate, which is directly related to functional MRI signal changes upon stimulation[11]. No other specific hypotheses have been made in terms of other metabolites.

4.2 Methods

Seven healthy control individuals (age 39.8 ± 3.8 years) provided informed written consent according to the guidelines of the Review Board for Health Sciences Research Involving Human Subjects at Western University. The participants included five men and two women.

In this study, the Stroop Task involved four conditions, incongruent, congruent, word only (the name of the color written in white), and color only (written as 'XXXX'), with each condition represented in 25% of the trials. Four colors were chosen for the task: red, green, blue, and yellow. The participants were asked to respond as quickly and accurately as possible on a four-button keypad. They were allotted 2 s to respond, and stimuli were separated by 1 s of cross fixation. The task was explained to each participant and rehearsed outside of the scanner until it could be performed consistently with 80% accuracy or greater. An angled mirror attached to the head coil allowed the participants to visualize the words of the Stroop Task projected on the screen in the scanner synchronously with the ^{1}H-fMRS acquisition. Participants were initially positioned in the scanner with the button press keypad in their hands ready to perform the task. This

minimized additional movement at the onset of the Stroop Task. The fMRS acquisition began with a 4-min resting period in which the participants were asked to fixate on a cross in the center of the projection screen. The final 3 s of the resting period were used to prompt the participant that the Stroop Task was about to start with the word 'Ready' projected onto the screen. The Stroop paradigm then lasted for 4 min and was followed by a 4-min recovery period. The procedure was written using PsychoPy[19]. The accuracy and response times were recorded to ensure participants' compliance.

All measurements were acquired on a 7.0 T Agilent/ Magnex head-only MRI (Agilent, Inc, Walnut Creek, California, USA) with a Siemens AC84 head gradient coil (Siemens, Erlangen, Germany), located at the Center for Functional and Metabolic Mapping at Western University. A transmit-only receive-only (TORO) head coil with 15 transmitters and 23 receivers[20] was used for all scans. A map of the transmit field for each transmitter was acquired at the beginning of the session to facilitate optimized homogeneity correction of the transmit field for each scan using a B1-shimming approach developed in-house[21]. The magnetic field uniformity (B0-shim) was adjusted automatically over the field of view with first-order and second-order shims using RASTAMAP[22] before all acquisitions.

The MRS voxels were 2.0 × 2.0 × 2.0 cm (8 cm3) in size. In every individual, a voxel was centered medially and encompassed the bilateral ACC using two fast low-angle shot 2D anatomical imaging sequences in the sagittal [45 slices, repetition time (TR) = 950 ms, echo time (TE)=5.23 ms, flip-angle (α)= 30°, gap between slices=1 mm, thickness= 2 mm, field of view (FOV) 220 × 220 mm, and matrix size of 220 × 200] and axial (20 slices, TR = 500 ms, TE =5.23 ms, α =30°, gap between slices=1 mm, thickness= 2 mm, FOV =220 × 220 mm, and matrix size 220 × 220) directions, both using lipid saturation. Voxel positions were prescribed by the scanner operator (R.T.) using anatomical landmarks as trained by a neuroanatomist (N.R.) to ensure consistent voxel placement (Fig. 4-1).

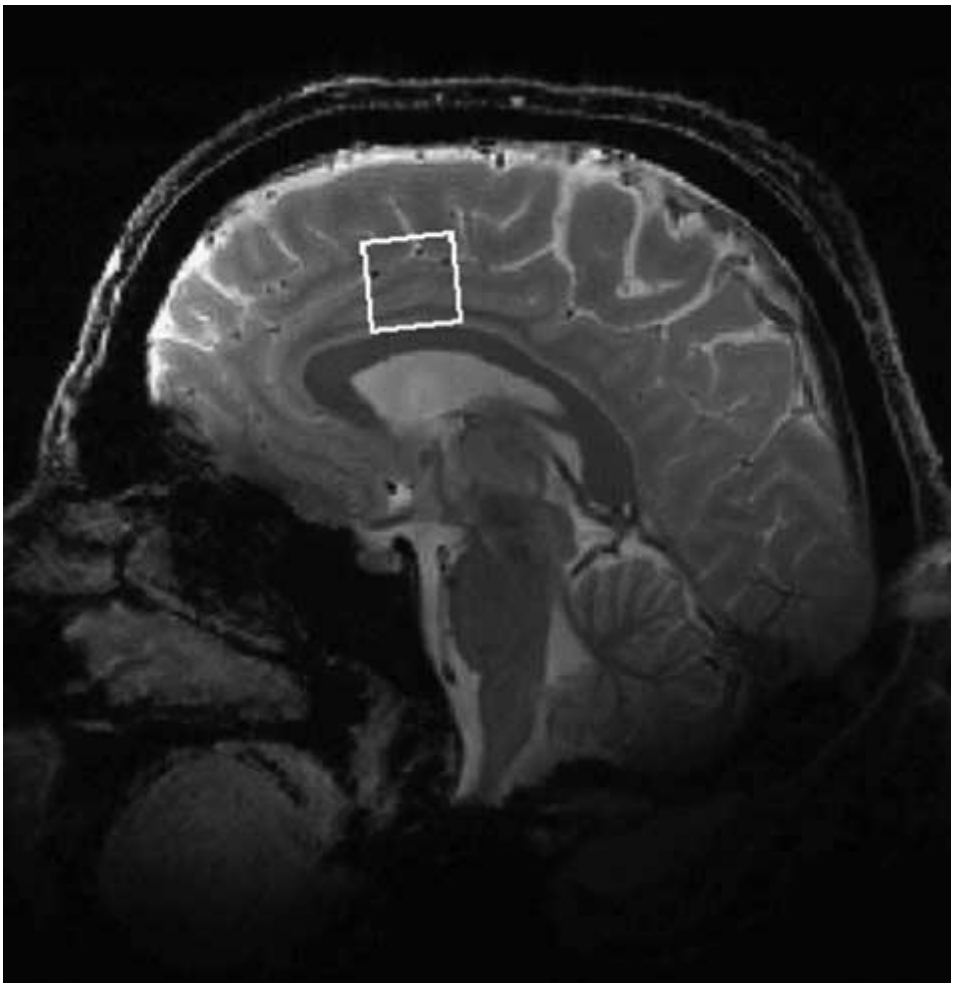

Figure 4-1. A sagittal cross-section of the brain with the MRS voxel placed in the anterior cingulate cortex. MRS = magnetic resonance spectroscopy

MRS spectra were acquired individually during the performance of the Stroop paradigm using an ultra-short echo time stimulated echo acquisition mode sequence with outer volume suppression[23] [TR =3 s, TE = 10 ms, mixing time (TM) = 32 ms, 4000 complex pairs, four steady state scans, 1 s acquisition time, eight-step phase cycle] with 16 water unsuppressed spectra and 240 water suppressed spectra, 80 spectra for each 4 min section of the Stroop paradigm (Rest, Stroop, Recovery). An eight-pulse VAPOR preparation sequence, with an additional water suppression pulse during the TM period[23], provided efficient water suppression. A separate metabolite suppressed spectrum was acquired to assess the macromolecule content[24]. Each acquisition outputted 23 spectra, one for each receiver, which required channel combination before use[25]. After the channels had been combined, each spectrum was frequency and phase corrected before being averaged

together. Quality Eddy Current Correction (QUECC)[26] reduced linewidth distortions before spectral fitting. Spectra were quantified using fitMAN, a time-domain fitting algorithm[27]. All spectra were inspected visually for quality.

Because of our directional hypotheses for GLU concentrations, a three-level repeated-measures analysis of variance (rmANOVA) design using the metabolite concentrations at each 4 min (80 spectral averages) section of the functional paradigm was examined using SPSS v.20 (IBM Corp, Armonk, New York, USA) to determine significant variations over time for GLU (α= 0.025, one tailed with Bonferroni correction). Because of the exploratory nature of this paper, the remaining metabolites were also tested for significance using a repeated measures multivariate analysis of variance (rmMANOVA) (α =0.025, two tailed with Bonferroni correction). Only metabolites with Cramer–Rao lower bounds less than 20% were included in the analysis.

4.3 Results

The average linewidths of the unsuppressed water signal were 12.8 ± 2.0 Hz after first-order and second-order shim adjustments. The average metabolite linewidth in the resting condition was 8.6 ± 0.8 Hz and no significant narrowing of the linewidths was observed in the activated condition compared with the resting condition. The water signal was suppressed sufficiently as the residual water signal was less than the height of the NAA peak in every spectrum.

A total of 15 metabolites were quantified consistently with Cramer–Rao lower bounds less than 20% for each of the resting, activated, and recovery spectra (Table 4-1). The time course of group-averaged GLU activation in 1 min increments is shown in Fig. 4-2 (all stats were performed on the 4 min, 80 averaged spectra). The concentration increases upon onset of the Stroop Task, plateau, and then decrease over 2 min toward the baseline. When the GLU concentrations between the resting, Stroop, and recovery periods were compared, there was a significant 2.6 ± 1.0% (0.24 ± 0.09 µmol/g) increase in the activated state relative to the initial resting period (P= 0.02, one tailed), followed by a

non-significant −2.4 ± 1.2% (− 0.23 ± 0.13 μmol/g) trend for the GLU signal to return to baseline after the activation period had ended (P =0.06, one tailed). However, when GLU concentrations were normalized to their baseline value in the resting period, the relative decrease in the recovery period became significant before Bonferroni corrections (0.025 < P < 0.05). Six of the seven participants showed this increase in GLU upon activation (1.0, 1.3, 5.3, −0.4, 6.0, 0.3, and 5.0%) and six of the seven participants showed the subsequent decrease (1.2, − 2.0, −8.8, − 1.5, −1.1, − 2.9, and – 1.6%).

Table 4-1. Quantified metabolites with their resting concentrations (μmol/g) and relative changes (%) during the task completion and the recovery period presented as means ± SE

		Concentration Change (Task – Rest)		Concentration Change (Recovery – Task)	
	Resting Concentration (μmol/g)	(%)	*p*	(%)	*p*
GLN	2.4 ± 0.3	-0.2 ± 5.6	0.738	6.8 ± 4.7	0.179
GLU	8.9 ± 0.3	2.6 ± 1.0	*0.021	-2.4± 1.2	0.046
TAU	2.4 ± 0.3	5.1± 7.3	0.509	-1.4 ± 5.6	0.539
ASP	2.5 ± 0.6	0.3 ± 5.9	0.853	-1.7 ± 3.5	0.404
NAAG	1.1 ± 0.3	2.6 ± 7.2	0.730	-4.6 ± 7.6	0.505
MYO	7.9 ± 0.5	0.9 ± 1.5	0.567	1.7 ± 1.4	0.261
SER	2.0 ± 0.3	7.5 ± 6.7	0.237	-2.4 ± 6.3	0.482
GLC	0.8 ± 0.2	-6.4 ± 10.2	0.955	14.9 ± 5.3	0.061
NAA	7.9 ± 0.3	2.6 ± 1.8	0.199	-1.1 ± 0.5	0.309
LAC	0.5 ± 0.1	22.9 ± 20.3	0.351	35.4 ± 13.1	0.155
GLY	0.7 ± 0.1	2.1 ± 1.5	0.200	-12.2 ± 7.0	0.130
SCY	0.4 ± 0.0	3.3 ± 2.8	0.279	1.5 ± 3.7	0.663
ASC	1.0 ± 0.1	-11.5 ± 11.6	0.764	33.1 ± 17.5	0.030
TCHO	2.1 ± 0.1	2.2 ± 1.2	0.111	-0.6 ± 0.6	0.399
TCR	7.7 ± 0.3	2.2 ± 1.2	0.122	-0.0 ± 0.6	0.920
GLX	11.3 ± 0.5	2.0 ± 1.7	0.302	-1.1 ± 1.1	0.324

ASC, ascorbate; ASP, aspartate; GLC, glucose; GLN, glutamine; GLU, glutamate; GLY, glycine; GLX, glutamate + glutamine; LAC, lactate; MYO, myo-inositol; NAA, N-acetylaspartate; NAAG, N-acetylaspartylglutamate; SCY, scyllo-inositol; SER, serine; TAU, taurine; TCHO (cho + PC + GPC), total choline; TCR (CR + PCR), total creatine.
*$p < 0.025$ significance (Bonferroni adjusted) for a two-tailed comparison, with the exception of Glu, which is one-tailed due to it being a planned directional comparison

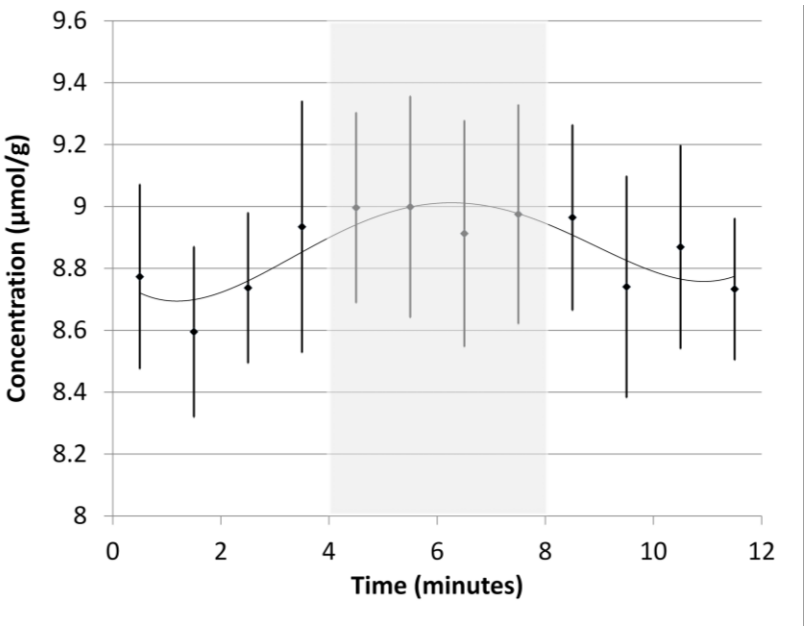

Figure 4-2. A time-course of the average glutamatergic response to the Stroop Task Each data point represents the temporal average of 20 spectra (1 min) per participant combined and quantified and subsequently averaged over all participants (n=7). Error bars indicate the inter-individual SEM at each point. The trend line is a fourth-order polynomial fit to the data. The shaded area indicates the 4 min of Stroop activation.

Other than GLU, the remaining metabolites were not significant in the rmMANOVA. It should be noted, though, that in the univariate pair-wise comparisons, ascorbate (Asc) increased 33.1 ± 17.5% (0.20 ± 0.06 µmol/ g) during the 4-min recovery period relative to the activation period (P= 0.03, two tailed). However, this is only a trend because of the Bonferroni correction.

All participants recorded at least 90% correct responses. Group-averaged response times were 725 ± 278 ms for the congruent condition, 976 ± 261 ms for the incongruent condition, 750 ± 270 ms for the word-only condition, and 721 ± 230 ms for the color-only condition. Only correct responses were considered.

4.4 Discussion

Using a Stroop Task as the functional paradigm for an ^{1}H-fMRS examination of the dynamic metabolic response to activation in the ACC, an observed significant increase of 2.6 ± 1.0% was found in GLU upon onset of the task, followed by a non-significant trend to return to the baseline in a small sample size of healthy controls (n=7). The high percentage of correct responses shows that there was high compliance with the Stroop Task among the participants.

The increase in GLU is comparable with recent ^{1}H-fMRS studies of the occipital cortex[1,2,6] and the motor cortex[3], which found GLU increases from 2 to 4% over the course of minutes, with a subsequent decrease upon cessation of the stimuli. Figure 4-2 indicates that the concentration increased to its new steady state within the first minute of activation. This is relatively faster than that in the above studies, which show that it takes 1–2 min before the concentration reaches its new state. One possible explanation is that because of the involvement of ACC in attention networks[16], and, specifically, selective encoding of stimulus properties[15] the ACC had already been in a state of minor activation. This is consistent with the final data point of the first resting condition in Fig. 4-2 that is seemingly already ascending toward the peak concentration. The resting GLU concentration is slightly lower than what was observed in other ^{1}H-fMRS studies at 7 T[1–3,6]; however, different scanners, techniques, and brain areas studied led to natural variation in the observed values between studies.

One departure from previous ^{1}H-fMRS studies at 7 T[1–3,6] is that a significant difference in lactate or glucose was not observed. These are difficult metabolites to quantify reliably; thus, perhaps more participants would be needed to observe significant differences. It is also possible that the lactate response was specific to certain tasks or brain areas.

It is conceivable that the ACC accumulates GLU faster than other brain regions upon stimulation as can be extrapolated from a study of the ACC using a painful stimulus[4]. Mullins and colleagues used ^{1}H-fMRS at 3 T to detect a 9.3% increase in GLU and an 11.4% increase in GLX (GLU+ GLN). The GLU increases observed by Mullins et al.[4]

are markedly higher than the response detected in the present study. This could be because of the nature of the experimental stimuli (pain versus cognitive task) such that the brain may have adapted a separate GLU response to painful stimuli as a similar increase in GLU was observed with a painful stimuli in the anterior insula cortex[5]. Two studies have used event-related ^{1}H-fMRS to detect >10% increases in the lateral occipital cortex[9,10]. It is possible that with an event-related Stroop Task, larger similar increases in GLU in the ACC could be observed. However, with the current block design, the magnitude of GLU changes agrees more with the previous work in the visual cortex[1,2,6] and the motor cortex[3].

One study at 3 T presented GABA changes with a working memory task in the dorsolateral prefrontal cortex, but did not detect any changes in GLX (GLU + GLN)[8]. The study used a dedicated pulse sequence to detect GABA specifically, which can otherwise be a difficult metabolite to quantify as it was not consistently quantified reliably in this study. They observed an initial increase in GABA concentrations, but subsequent decreases with repeated runs of the task. In a future study, it would be interesting to observe how GLU would respond to repeated runs of the Stroop Task.

Another study that was carried out at 3 T has used an ^{1}H-fMRS technique to study the ACC using visually evoked sexual arousal[7] and found significant 10–20% increases in GLX with activation. At lower field strength, it is often necessary to measure a combination of GLU and surrounding metabolites that can include GLN, glutathione, GABA, and sometimes macromolecules together as GLX. It is not clear which metabolites were included in their GLX definition, making it harder to compare these results. A common definition of GLX is simply GLU plus its precursor GLN, as was used in the pain study[4] and the working memory study[8] mentioned above. Using this definition, GLX was examined in this study, but no significant differences were observed.

The increase in Asc in the recovery period, although not significant after Bonferroni correction or at the multivariate level, is intriguing. It has been reported previously by Wilson et al.[28] that GLU triggers the release of Asc from astrocytes and increases the

extracellular concentration of Asc. Asc is an antioxidant. This is important because GLU neurotransmission leads to increased mitochondrial activity and as a result increased free radicals[29]. Wilson et al.[28] showed that this effect takes some time to observe; thus, it is possible that the increase in GLU during the activated phase led to the delayed increase in Asc concentration that was observed in the recovery phase.

GLU is the main excitatory neurotransmitter in the brain. It is synthesized from glucose in the mitochondria, released into the synaptic cleft through exocytosis, and then binds with the postsynaptic membrane to induce neurotransmission[30]. It is then taken up into the adjacent glial cell, where it is converted into GLN before being transferred back into the neuron and converted back into GLU[30]. There is an increase in glucose consumption during functional activation that specifically supports the increased turnover rate of the GLU/GLN cycle [11]. Therefore, an increase in oxidative metabolism could lead to the increased number of GLU molecules flowing within the GLU/GLN cycle during the functional activation of the ACC with the Stroop Task leading to the increased GLU observed in bulk brain tissue using MRS. The lack of change in GLN concentrations may indicate that the conversion of GLN back into GLU in the neuron is not a rate-limiting step in the GLU/GLN cycle.

This proof-of-concept study shows that the Stroop Task is a robust task that can be used for ^{1}H-fMRS studies in the ACC. This introduces a new method to study the abnormalities of GLU modulation in brain disorders. Schizophrenia research may particularly benefit from this method as it is a population that has been shown to have abnormal resting levels of glutamatergic metabolites in the ACC compared with healthy controls[12,13] and impaired ACC activation during performance of the Stroop Task[17]. Dysfunction of glutamatergic metabolism may manifest itself as an inability to dynamically upregulate GLU cycling or excessive upregulation of GLU, or even GLN, concentrations during performance of the Stroop Task. The limitations of the study include its small sample size and the possibility that the GLU changes observed are because of movement-induced phase shifts from the participant responding to the task, although it is unlikely that a phase shift would induce consistent increases in GLU rather

than decreases. Future studies should have a larger sample size and focus on ^{1}H-fMRS in neuropsychiatric disorders.

4.5 Acknowledgements

This work was supported by a New Investigator Fellowship grant (J.T.) from the Ontario Mental Health Foundation (OMHF). Salary support for R.T., B.S., and M.D., was funded in part by operating funds from the Canadian Institute of Health Research (P.C.W., MT-12078).

4.6 Conflicts of Interest

There are no conflicts of interest.

4.7 References

1. Mangia, S. *et al.* Sustained neuronal activation raises oxidative metabolism to a new steady-state level: evidence from 1H NMR spectroscopy in the human visual cortex. *J. Cereb. Blood Flow Metab.* **27,** 1055–1063 (2007).

2. Schaller, B., Mekle, R., Xin, L., Kunz, N. & Gruetter, R. Net increase of lactate and glutamate concentration in activated human visual cortex detected with magnetic resonance spectroscopy at 7 tesla. *J. Neurosci. Res.* **91,** 1076–1083 (2013).

3. Schaller, B., Xin, L., O'Brien, K., Magill, A. W. & Gruetter, R. Are glutamate and lactate increases ubiquitous to physiological activation? A 1H functional MR spectroscopy study during motor activation in human brain at 7Tesla. *Neuroimage* **93,** 138–145 (2014).

4. Mullins, P. G., Rowland, L. M., Jung, R. E. & Sibbitt, W. L. A novel technique to study the brain's response to pain: Proton magnetic resonance spectroscopy. *Neuroimage* **26,** 642–646 (2005).

5. Gussew, A. *et al.* Time-resolved functional 1H MR spectroscopic detection of glutamate concentration changes in the brain during acute heat pain stimulation. *Neuroimage* **49,** 1895–1902 (2010).

6. Lin, Y., Stephenson, M. C., Xin, L., Napolitano, A. & Morris, P. G. Investigating the metabolic changes due to visual stimulation using functional proton magnetic resonance spectroscopy at 7 T. *J. Cereb. Blood Flow Metab.* **32,** 1484–1495 (2012).

7. Kim, T. H., Kang, H. K. & Jeong, G. W. Assessment of Brain Metabolites Change during Visual Sexual Stimulation in Healthy Women Using Functional MR Spectroscopy. *J. Sex. Med.* **10,** 1001–1011 (2013).

8. Michels, L. *et al.* Frontal gaba levels change during working memory. *PLoS One* **7,** e31933 (2012).

9. Lally, N. *et al.* Glutamatergic correlates of gamma-band oscillatory activity during cognition: A concurrent ER-MRS and EEG study. *Neuroimage* **85,** 823–833 (2014).

10. Apsvalka, D., Gadie, A. & Mullins, P. G. Event-related dynamics of glutamate and BOLD signal at 3 T in a repetition suppression paradigm. *ISMRM Proc.* **22,** 3796 (2014).

11. Rothman, D. L., Behar, K. L., Hyder, F. & Shulman, R. G. In vivo NMR studies of the glutamate neurotransmitter flux and neuroenergetics: implications for brain function. *Annu. Rev. Physiol.* **65,** 401–427 (2003).

12. Poels, E. M. P. *et al.* Imaging glutamate in schizophrenia: review of findings and implications for drug discovery. *Mol. Psychiatry* **19,** 20–9 (2014).

13. Théberge, J. *et al.* Glutamate and glutamine measured with 4.0 T proton MRS in never-treated patients with schizophrenia and healthy volunteers. *Am. J. Psychiatry* **159,** 1944–1946 (2002).

14. Drobyshevsky, A., Baumann, S. B. & Schneider, W. A rapid fMRI task battery for mapping of visual, motor, cognitive, and emotional function. *Neuroimage* **31,** 732–744 (2006).

15. Neufeld, R. W. J., Boksman, K., Vollick, D., George, L. & Carter, J. R. Stochastic dynamics of stimulus encoding in schizophrenia: Theory, testing, and application. *J. Math. Psychol.* **54,** 90–108 (2010).

16. Posner, M. I. & Petersen, S. E. The Attention System of the Human Brain. 31 (1989). doi:10.1146/annurev.ne.13.030190.000325

17. Ungar, L., Nestor, P. G., Niznikiewicz, M. A., Wible, C. G. & Kubicki, M. Color Stroop and negative priming in schizophrenia: An fMRI study. *Psychiatry Res. - Neuroimaging* **181,** 24–29 (2010).

18. Eidels, A., Townsend, J. T. & Algom, D. Comparing perception of Stroop stimuli in focused versus divided attention paradigms: Evidence for dramatic processing differences. *Cognition* **114,** 129–150 (2010).

19. Peirce, J. W. PsychoPy-Psychophysics software in Python. *J. Neurosci. Methods* **162,** 8–13 (2007).

20. Gilbert, K. M., Curtis, A. T., Gati, J. S., Klassen, L. M. & Menon, R. S. A radiofrequency coil to facilitate B 1 + shimming and parallel imaging acceleration in three dimensions at 7 T. *NMR Biomed.* **24,** 815–823 (2011).

21. Curtis, A. T., Gilbert, K. M., Klassen, L. M., Gati, J. S. & Menon, R. S. Slice-by-slice B1+ shimming at 7 T. *Magn. Reson. Med.* **68,** 1109–16 (2012).

22. Klassen, L. M. & Menon, R. S. Robust Automated Shimming Technique Using Arbitrary Mapping Acquisition Parameters (RASTAMAP). *Magn. Reson. Med.* **51,** 881–887 (2004).

23. Tkáć, I. & Gruetter, R. Methodology of 1 H NMR Spectroscopy of the Human Brain at Very High Magnetic Fields. *Appl. Magn. Reson.* **29,** 139–157 (2005).

24. Penner, J. & Bartha, R. Semi-LASER 1H MR spectroscopy at 7 Tesla in human brain: Metabolite quantification incorporating subject-specific macromolecule removal. *Magn. Reson. Med.* **00,** 1–9 (2014).

25. Brown, M. A. Time-domain combination of MR spectroscopy data acquired using phased-array coils. *Magn. Reson. Med.* **52,** 1207–1213 (2004).

26. Bartha, R., Drost, D. J., Menon, R. S. & Williamson, P. C. Spectroscopic lineshape correction by QUECC: Combined QUALITY deconvolution and eddy current correction. *Magn. Reson. Med.* **44,** 641–645 (2000).

27. Bartha, R., Drost, D. J. & Williamson, P. C. Factors affecting the quantification of short echo in-vivo 1 H MR spectra : prior knowledge, peak elimination, and filtering. *NMR Biomed.* **12,** 205–216 (1999).

28. Wilson, J. X., Peters, C. E., Sitar, S. M., Daoust, P. & Gelb, A. W. Glutamate stimulates ascorbate transport by astrocytes. *Brain Res.* **858,** 61–66 (2000).

29. Patel, M., Day, B. J., Crapo, J. D., Fridovich, I. & McNamara, J. O. Requirement for superoxide in excitotoxic cell death. *Neuron* **16,** 345–355 (1996).

30. Hertz, L., Dringen, R., Schousboe, A. & Robinson, S. R. Astrocytes: Glutamate producers for neurons. *J. Neurosci. Res.* **57,** 417–428 (1999).

Chapter 5

5 Functional magnetic resonance spectroscopy of glutamate in schizophrenia and major depressive disorder: Anterior cingulate activity during a color-word Stroop task.

The study presented in this chapter aimed to utilize functional magnetic resonance spectroscopy with a cognitive functional paradigm to obtain dynamic measurements of glutamate and glutamine in a psychiatric group for the first time. A version of this work is currently in press to be published in npj Schizophrenia (Nature Partner Journals Schizophrenia; NPJSCHZ#00068).

5.1 Introduction

Schizophrenia (SZ) has been suggested to be associated with dysfunction in brain areas that utilize glutamate (GLU) for neurotransmission[1]. It has been postulated that GLU N-methyl-D-aspartate (NMDA) receptor hypofunction may contribute to symptoms of SZ[2–4] and this body of literature has been recently reviewed[5,6]. This, and other lines of evidence has led to the notion that GLU abnormalities can explain a wider range of symptoms of SZ than dopamine abnormalities alone, thus characterization of GLU abnormalities in SZ is sorely needed in light of potential GLU-modulating treatment strategies[6].

Proton magnetic resonance spectroscopy (^{1}H-MRS) has demonstrated abnormal brain GLU concentrations, with its metabolic precursor/by-product, glutamine (GLN), in individuals with SZ[7,8]. However, findings may not be specific to this illness. Both major depressive disorder (MDD) and bipolar disorder have demonstrated abnormalities of GLU in multiple brain areas using ^{1}H-MRS[9–11]. While MDD has been consistently reported to have lower glutamatergic metabolites (GLU, GLN, or GLX (GLU+GLN)), bipolar disorder has demonstrated inconsistent results, with a tendency to be elevated[9–11].

The consistency of studies of GLU in MDD makes it a preferable choice for a psychiatric control group.

An increasing number of studies demonstrate the utility of functional ^{1}H-MRS (^{1}H-fMRS) in dynamic measures of metabolic content[12–24]. Much like its parent technique, ^{1}H-MRS, ^{1}H-fMRS assesses concentrations of brain metabolites that are orders of magnitude smaller than the water content. Essentially, ^{1}H-fMRS is a time course of ^{1}H-MRS spectra that typically measures slow metabolic responses to prolonged stimuli in a small volume of tissue within the brain[13–16,18–20].

Increases in concentrations of glutamatergic metabolites have been demonstrated in ^{1}H-fMRS studies of healthy controls in the occipital lobe using visual stimuli[14,16,17,19], the lateral occipital cortex using a repetition suppression task[23,24], the motor cortex using a finger tapping paradigm[18] and the anterior cingulate cortex (ACC) using pain paradigms[21,22], a sexual arousal paradigm[13], and the color-word Stroop task[20]. Increases in glutamatergic metabolites upon stimulation is not surprising given the tight coupling of GLU and GLN cycling to neural response[25]. ^{1}H-fMRS with controlled rest and activation periods could provide unique information about the dynamic nature of glutamatergic abnormalities in SZ.

In the simplest of tasks, stimuli received by the brain must be organized and encoded for further use by brain centers involved in cognition. It is postulated that deficits of stimulus encoding are central to cognitive deficits in schizophrenia[26,27]. Previous literature using the Stroop task in healthy controls and in SZ has shown that this is a task that both participant groups conduct to the same level of proficiency (rate of correct answers) and robustly activates the ACC, although with some hypofunction in SZ[28,29].

The purpose of this study is to measure ACC glutamatergic concentrations dynamically during the performance of a color-word Stroop task in SZ compared to healthy controls and psychiatric controls with MDD using a ^{1}H-fMRS technique. It is hypothesized that there will be smaller GLU responses along with slower response times in the SZ group compared to both the healthy controls and MDD group due to the increased number of encoding subprocesses (constituent cognitive operations), indicating involvement of more

brain areas as well as diversion of activity away from the ACC[26,30]. Within groups, it is hypothesized that there will be an increase in GLU concentrations during activation of the ACC, with a subsequent return to baseline after the task. Because neuronal GLU levels have been shown to be related to cognition[31], it is expected that concentrations of the glutamatergic metabolites will negatively correlate with the response times.

5.2 Methods

5.2.1 Participants

There were 16 participants in each of the healthy, MDD, and SZ groups who gave informed written consent according to the guidelines of the Review Board for Health Sciences Research Involving Human Subjects at the University of Western Ontario. The number of participants was chosen based on previous ^{1}H-fMRS studies that have observed GLU changes of 2-4%[14,16–20]. Volunteers with neurological or major medical illnesses, clinically significant head injury, other psychiatric disorders, MRI contra-indications, or substance abuse within the previous year were excluded from the study. Any healthy volunteer with a known family history of psychiatric disorder in a first or second degree relative was also excluded.

A consensus diagnosis was established on all participants by a psychiatrist and trained assistant with the Structured Clinical Interview for DSM-IV[32]. SZ subjects were rated with the Scale for Assessment of Negative Symptoms and the Scale for the Assessment of Positive Symptoms[33,34] and MDD patients were assessed with the Montgomery Asberg Depression Scale[35] and the Young Mania Rating Scale[36]. Fourteen SZ patients were receiving atypical neuroleptics with Chlorpromazine Equivalent 409 ± 293mg (3 taking olanzapine; quetiapine/venlafaxine; 2 taking risperidone; quetiapine/paliperidone/ escitalopram; 4 taking paliperidone; clozapine; risperidone/escitalopram; quetiapine/ escitalopram) and 2 patients were not medicated. Ten of the 16 MDD patients were receiving antidepressant medications at the time of the scan (bupropion/citalopram/ methylphenidate; venlafaxine; lamotrigine; desvenlafaxine; bupropion/citalopram; escitalopram; citalopram; sertraline; citalopram/mirtazapine/quetiapine; levothyroxine/

melatonin). Demographic information including age, handedness, education, parental education, clinical rating scores, and length of illness were collected according to our previous study[37] and are shown in Table 5-1.

Table 5-1. Participant demographics

Group	Controls	MDD	SZ
Age	23.9 ± 4.7	21.7 ± 3.3	22.7 ± 2.9
M/F	11/5	6/10	13/3
R/L	14/2	14/2	15/1
Educ	3.1 ± 0.9	2.6 ± 0.6	2.2 ± 0.8
PEduc	3.1 ± 0.9	3.0 ± 0.6	3.3 ± 0.8
H Anx		12.7 ± 10.9	
H Dep		12.4 ± 9.1	
Mania		5.4 ± 6.8	
Montg		17.4 ± 10.4	
CPZ (mg)			358 ± 307
SANS			9.7 ± 7.7
SAPS			7.6 ± 10.4

M/F - male/female

R/L - right/left

Educ - education rating of the participant (1= in high school, 2=completed high school, 3=some college, 4= completed college)

PEduc - education rating of the participant's parent (1= in high school, 2=completed high school, 3=some college, 4= completed college)

H Anx - Hamilton Anxiety Scale

H Dep - Hamilton Depression Scale

Mania - mania rating from the Montgomery Asperg Depression Scale

Montg - result of the Montgomery Asperg Depression Scale

CPZ - chlorapromazine equivalent

SANS - Scale for Assessment of Negative Symptoms

SAPS - Scale for Assessment of Positive Symptoms

5.2.2 Anterior cingulate activation paradigm

We have previously described details of the color-word Stroop Task chosen for the functional paradigm[20]. Briefly, it was a four-condition (congruent, incongruent, word-only, color-only) by four-color (red, green, blue, yellow) design. The subjects were asked

to respond as quickly and accurately as possible on a four-button keypad with the color of the ink as the correct answer for all but the word-only conditions within which the answer was the color-word. Stimuli were presented for two seconds followed by one second of cross fixation. In the scanner, subjects first engage in cross-fixation for four minutes prior to a four-minute block of activation (Stroop1), which is then followed by four minutes of recovery (Recovery1). In contrast to the previous study by Taylor et al[20], an additional four minutes of Stroop activation (Stroop2) was acquired after Recovery1, which was then followed by another four-minute recovery period (Recovery2). This additional block of activation will help assess the glutamatergic response to repeated, prolonged Stroop stimuli in the ACC. The procedure was written and presented using PsychoPy[38], which also recorded accuracy and response times. A confirmatory fMRI was acquired post-^{1}H-fMRS to ensure activation within the fMRS voxel. The fMRI lasted nine minutes and was divided into one-minute blocks cycling between resting (cross-fixation) and Stroop activation, for a total of four minutes of Stroop activation. Image preprocessing and statistical analysis were conducted using Statistical Parametric Mappping (SPM8; Wellcome Department of Neurology, London, UK) within Matlab 7.1 (The Mathworks Inc., MA).

5.2.3 ^{1}H-fMRS Data Collection and Analysis

All measurements were acquired on a 7.0 T Agilent/Magnex head-only MRI (Agilent, Inc, Walnut Creek, California, USA) with a Siemens AC84 head gradient coil (Siemens, Erlangen, Germany), located at the Center for Functional and Metabolic Mapping at Western's Robarts Research Institute. A transmit-only receive-only (TORO) head coil with 15 transmitters and 23 receivers[39] was used for all scans with a B1-shimming approach to facilitate optimized homogeneity correction of the transmit field for each scan[40]. The magnetic field uniformity (B0-shim) was adjusted automatically over the field of view with first-order and second-order shims using RASTAMAP[41].

The ^{1}H-MRS voxels were 2.0 × 2.0 × 2.0 cm (8 cm^{3}) in size. In every individual, a voxel was centered medially and encompassed the bilateral ACC (Fig. 5-1) using two fast low-

angle shot 2D anatomical imaging sequences in the sagittal (45 slices, repetition time (TR)=950 ms, echo time (TE)=5.23ms, flip-angle (α)=30°, gap between slices=1 mm, thickness=2 mm, field of view (FOV)=220 × 220 mm, matrix size=220 × 200) and axial (20 slices, TR=500ms, TE=5.23ms, α=30°, gap=1mm, thickness=2mm, FOV=220 × 220mm, matrix size=220 × 220) directions, both with lipid saturation. The voxels were placed in the areas of the ACC where activation was expected based on previous fMRI studies that used a color-word Stroop task[42,43].

^{1}H-MRS spectra were acquired individually throughout the Stroop paradigm using an ultra-short TE stimulated echo acquisition mode sequence with outer volume suppression[44] (TR=3s, TE=10ms, mixing time (TM)=32ms, 4000 complex pairs, 4 steady state scans, 1s acquisition time, 8 step phase cycle) with 16 water unsuppressed spectra and 400 water suppressed spectra, 80 spectra for each 4 min section of the Stroop paradigm (Resting, Stroop1, Recovery1, Stroop2, Recovery2). An eight-pulse VAPOR preparation sequence, with an additional water suppression pulse during the TM period[44], provided efficient water suppression. A separate metabolite-suppressed spectrum was acquired to assess the macromolecular content[45] for each individual. This metabolite-suppressed spectrum was modelled using a Hankel-Lanczos singular value decomposition (HLSVD)[46,47] routine and included in the fitting template. Each acquisition produced 23 spectra, one for each receiver, which required channel combination before use[48]. Spectra were frequency and phase corrected before being averaged together. QUality Eddy Current Correction (QUECC)[49] reduced linewidth distortions before spectral fitting with fitMAN, a time-domain fitting algorithm[50]. Metabolite concentrations were calculated with corrections for gray and white matter content, as previously described in Stanley et al[51]. All spectra were inspected visually for quality. To ensure reliable quantification, only metabolites with Cramer-Rao lower bounds (CRLB) less than 10% were included in the analysis.

To illustrate the dynamic response of GLU throughout the acquisition, spectra were subdivided and averaged into 20 spectra (one-minute intervals). These were fit for each person, then combined via a moving average for each group.

A 5x3 repeated-measures analysis of variance (rmANOVA) design using the metabolite concentrations at each 4 min (80 spectral averages) section of the functional paradigm was examined using SPSS v.20 (IBM Corp, Armonk, New York, USA) to determine significant variations over time and across groups. One-tailed tests were employed for GLU due to the directional hypotheses of concentration increases with activation by the Stroop Task followed by decreases during the recovery. GLN and GLX were similarly explored; GLX, with one-tailed tests as GLU is the main contributor to GLX concentration, and GLN with two-tailed tests. For pairwise comparison, the blocks of the Stroop paradigm were compared to both the previous block and the sequential block. Metabolite changes will similarly be explored with concentrations that are normalized to their resting values. To accommodate multiple comparisons, alpha was divided by four ($p<0.05/4$). Kolmogorov-Smirnov tests were used to ensure the assumption of normality.

5.3 Results:

Significant Family-Wise Error (FWE) corrected ($p<0.05$) activation of the ACC was observed in the confirmatory fMRI (Fig.5-1c). The activation observed was within the location of voxel placement in the ACC.

Unsuppressed water spectra were acquired with average linewidths of 10.79±1.08 Hz after shimming and the water peak was effectively suppressed in the metabolite spectra (Fig. 5-2). GLU and GLN concentrations were estimated from the fit (Fig. 5-1) with CRLB less than 1% and 10%, respectively, indicating high quality fits of the data. A moving average of fluctuations in GLU levels throughout the activation paradigm is presented in Fig. 5-3 for each participant group.

The rmANOVA (alpha=0.05) yielded a significant main effect of time for GLU ($p<0.001$) and GLX ($p<0.001$) but not GLN ($p=0.132$). Strongly significant increases occurred for GLU ($p=0.002$) and GLX ($p=0.001$) in Stroop1 over all groups. There were no significant time by group interactions (GLU, $p=0.377$; GLN, $p=0.317$; GLX, $p=0.616$) and there were no main effects of group (GLU, $p=0.797$; GLN, $p=0.137$; GLX, $p=0.700$).

The planned pairwise comparisons (alpha=0.05/4) of adjacent periods of the Stroop Task yielded significantly increased GLU (p=0.006) concentrations in the healthy controls during Stroop1 (Table 5-2). GLU then decreased towards the resting value in Recovery1 (p=0.007). In the SZ group, GLX concentrations had a trend to increase Stroop1 (p=0.016). The SZ group was the only group to show significant GLN changes, going from 1.21±0.52 mmol/kg_{ww} at rest to 1.44±0.50 mmol/kg_{ww} (p=0.004, two-tailed) in Stroop1, then returning to 1.18±0.48 mmol/kg_{ww} in Recovery1 (p=0.001, two-tailed). The MDD group did not show any significant changes in glutamatergic concentrations during Stroop1.

Stroop2 yielded unexpected decreases in GLU and GLX concentrations relative to Recovery1. Using two-tailed tests (as the assumptions for one-tailed tests were no longer valid), the MDD group showed significantly decreased GLU and GLX (p=0.003, p=0.006, respectively) and the SZ group showed a near-significant decrease for GLU (p=0.024).

Combining all groups yielded significant decreases in GLU (p=0.003) and GLX (p=0.008). Statistical comparisons using concentrations normalized to resting values yielded highly similar results (Table 5-3). A post-hoc test (alpha=0.05) comparing the GLU concentrations during the two Stroop conditions indicated lower concentrations in Stroop2 for the MDD group (p=0.001) and the SZ group (p=0.026) but not the healthy control group (p=0.053). GLU concentrations in Stroop2 were found to be lower in every group when the concentrations were normalized to the resting values (p=0.009, p=0.002, p=0.034 for control, MDD, and SZ groups, respectively).

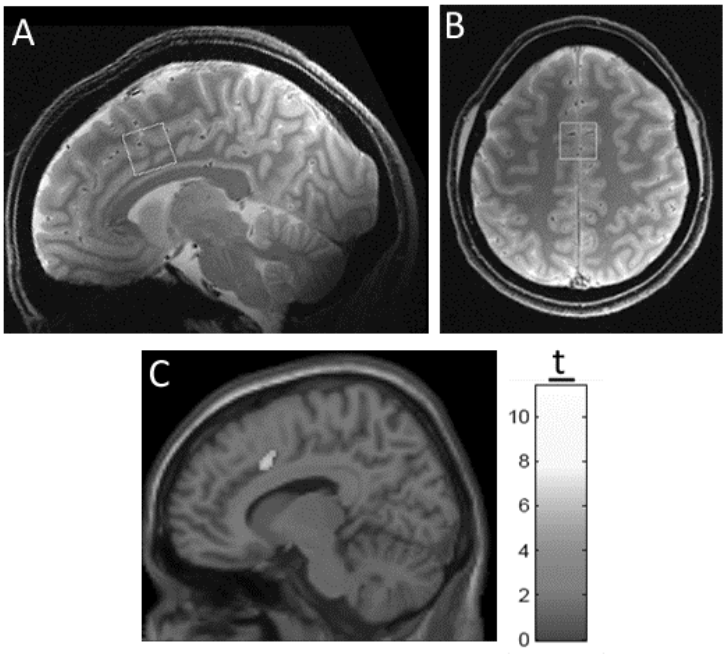

Figure 5-1. (A) Sagittal and (B) transverse cross-sections depicting the position of the ^{1}H-fMRS voxel located in the bilateral ACC of one participant.
The voxel was centered on the junction of the right cingulate sulcus with the paracentral sulcus, angled to the AP line and placed superior to the first fold of grey matter above the corpus callosum in the sagittal cross-sections and centered on the interhemispheric fissure in the transverse cross-sections. (C) The Family-Wise Error (FWE) corrected ($p<0.05$) confirmatory fMRI on a normalized average brain for all groups showing significant activation within the ACC in the right hemisphere of all participant groups and Stroop conditions combined.

Table 5-2. Pairwise comparisons for adjacent blocks of the 1H-fMRS paradigm for GLU, GLN, and GLX concentrations

Group		Resting	Stroop1	*p(S1-B)*	Recovery1	*p(R1-S1)*	Stroop2	*p(S2-R1)*	Recovery2	*p(R2-S2)*
HC	[GLU]	8.79 ± 0.85	9.07 ± 0.91	**0.004**	8.85 ± 0.85	**0.016**	8.69 ± 1.08	0.261	8.95 ± 1.11	0.072
	[GLN]	1.37 ± 0.52	1.41 ± 0.56	0.533	1.46 ± 0.50	0.564	1.40 ± 0.56	0.443	1.43 ± 0.52	0.775
	[GLX]	9.98 ± 1.02	10.31 ± 0.97	**0.012**	10.13 ± 1.02	0.074	9.92 ± 1.38	0.224	10.2 ± 1.24	0.12
MDD	[GLU]	9.24 ± 1.4	9.38 ± 1.47	0.079	9.27 ± 1.53	0.121	8.91 ± 1.52	**0.018**	8.95 ± 1.4	0.788
	[GLN]	1.75 ± 0.84	1.84 ± 0.97	0.275	1.85 ± 1.00	0.858	1.86 ± 1.07	0.876	1.76 ± 0.81	0.285
	[GLX]	10.63 ± 2.16	10.86 ± 2.36	0.049	10.75 ± 2.45	0.184	10.31 ± 2.5	**0.016**	10.35 ± 2.16	0.823
SZ	[GLU]	9.11 ± 1.33	9.24 ± 1.23	0.105	9.20 ± 1.21	0.367	8.94 ± 1.49	0.076	8.91 ± 1.41	0.804
	[GLN]	1.29 ± 0.51	1.52 ± 0.48	**0.005**	1.24 ± 0.49	**0.002**	1.26 ± 0.38	0.811	1.30 ± 0.43	0.737
	[GLX]	10.16 ± 1.78	10.47 ± 1.72	**0.015**	10.21 ± 1.58	**0.020**	9.97 ± 1.87	0.173	9.96 ± 1.75	0.963
All	[GLU]	9.05 ± 1.21	9.23 ± 1.21	**0.001**	9.11 ± 1.21	**0.018**	8.85 ± 1.35	**0.003**	8.94 ± 1.29	0.288
	[GLN]	1.46 ± 0.65	1.58 ± 0.69	**0.009**	1.51 ± 0.71	0.142	1.50 ± 0.74	0.844	1.48 ± 0.61	0.769
	[GLX]	10.26 ± 1.71	10.55 ± 1.75	**0.001**	10.37 ± 1.77	0.065	10.07 ± 1.93	**0.005**	10.17 ± 1.73	0.314

p(S1-B) = Stroop1 vs resting, (alpha=0.05/4 (Bonferroni corrected); one-tailed (GLU, GLX), and two-tailed (GLN)), bolded values indicate statistical significance
p(R1-S1) = Recovery1 vs Stroop1, (alpha=0.05/4 (Bonferroni corrected); one-tailed (GLU, GLX), and two-tailed (GLN)), bolded values indicate statistical significance
p(S2-R1) = Stroop2 vs Recovery1, (alpha=0.05/4 (Bonferroni corrected); two-tailed (GLU, GLN, GLX)), bolded values indicate statistical significance
p(R2-S2) = Recovery2 vs Stroop2, (alpha=0.05/4 (Bonferroni corrected); two-tailed (GLU, GLN, GLX)), bolded values indicate statistical significance
HC = Healthy controls
MDD = Major Depressive Disorder
SZ = Schizophrenia
All = the combination of all participants across groups
[GLU] = The concentration of glutamate (mmol/kg_{ww})
[GLN] = The concentration of glutamine (mmol/kg_{ww})
[GLX] = The concentration of GLX (glutamate + glutamine; mmol/kg_{ww})

Table 5-3. Pairwise comparisons for adjacent blocks of the 1H-fMRS paradigm, normalized to the resting concentration for GLU, GLN, and GLX

Group		Resting	Stroop1	*p(S1-B)*	Recovery1	*p(R1-S1)*	Stroop2	*p(S2-R1)*	Recovery2	*p(R2-S2)*
HC	GLU_N	1.000 ± 0.000	1.032 ± 0.055	**0.005**	1.004 ± 0.059	**0.006**	1.001 ± 0.052	0.808	1.012 ± 0.075	0.340
	GLN_N	1.000 ± 0.000	1.044 ± 0.214	0.598	1.041 ± 0.282	0.968	0.982 ± 0.180	0.491	1.002 ± 0.157	0.715
	GLX_N	1.000 ± 0.000	1.033 ± 0.060	**0.013**	1.012 ± 0.062	0.027	1.003 ± 0.043	0.602	1.015 ± 0.075	0.363
MDD	GLU_N	1.000 ± 0.000	1.016 ± 0.049	0.082	1.003 ± 0.059	0.101	0.963 ± 0.055	0.005	0.969 ± 0.035	0.634
	GLN_N	1.000 ± 0.000	1.048 ± 0.249	0.547	1.068 ± 0.275	0.766	1.005 ± 0.290	0.451	0.954 ± 0.276	0.333
	GLX_N	1.000 ± 0.000	1.022 ± 0.060	0.066	1.009 ± 0.069	0.135	0.967 ± 0.084	**0.011**	0.974 ± 0.043	0.598
SZ	GLU_N	1.000 ± 0.000	1.016 ± 0.031	0.081	1.014 ± 0.061	0.420	0.981 ± 0.071	0.017	0.979 ± 0.076	0.892
	GLN_N	1.000 ± 0.000	1.264 ± 0.386	**0.001**	1.048 ± 0.381	**0.002**	1.071 ± 0.313	0.778	1.087 ± 0.326	0.757
	GLX_N	1.000 ± 0.000	1.034 ± 0.049	**0.011**	1.013 ± 0.08	0.027	0.982 ± 0.081	0.065	0.985 ± 0.087	0.840
All	GLU_N	1.000 ± 0.000	1.021 ± 0.045	**0.002**	1.007 ± 0.058	**0.010**	0.981 ± 0.061	**0.002**	0.986 ± 0.066	0.449
	GLN_N	1.000 ± 0.000	1.124 ± 0.309	0.014	1.053 ± 0.311	0.088	1.021 ± 0.267	0.490	1.016 ± 0.266	0.865
	GLX_N	1.000 ± 0.000	1.030 ± 0.056	**0.001**	1.011 ± 0.069	**0.003**	0.984 ± 0.074	**0.006**	0.991 ± 0.071	0.341

p(S1-B) = Stroop1 vs resting, (alpha=0.05/4 (Bonferroni corrected); one-tailed (GLU, GLX), and two-tailed (GLN)), bolded values indicate statistical significance
p(R1-S1) = Recovery1 vs Stroop1, (alpha=0.05/4 (Bonferroni corrected); one-tailed (GLU, GLX), and two-tailed (GLN)), bolded values indicate statistical significance
p(S2-R1) = Stroop2 vs Recovery1, (alpha=0.05/4 (Bonferroni corrected); two-tailed (GLU, GLN, GLX)), bolded values indicate statistical significance
p(R2-S2) = Recovery2 vs Stroop2, (alpha=0.05/4 (Bonferroni corrected); two-tailed (GLU, GLN, GLX)), bolded values indicate statistical significance
HC = Healthy controls
MDD = Major Depressive Disorder
SZ = Schizophrenia
All = the combination of all participants across groups
GLU_N = The concentration of Glutamate normalized to the resting period
GLN_N = The concentration of glutamine normalized to the resting period
GLX_N = The concentration of GLX (glutamate + glutamine) normalized to the resting period

Table 5-4. Behavioural response times (correct-only) to the incongruent Stroop condition and correlation to glutamate and glutamine concentrations and percent changes during those trials

Trial	Subject Group	Response Time (s)	Correlations							
			GLU	*p*	ΔGLU	*p*	GLN	*p*	ΔGLN	*p*
Stroop1	HC	0.92 ± 0.16	-0.42	0.077	0.04	0.446	-0.45	0.081	-0.34	0.151
	MDD	0.95 ± 0.12	-0.37	0.08	-0.30	0.126	-0.41	0.063	-0.67	**0.003**
	SZ	1.03 ± 0.08	-0.35	0.099	-0.23	0.207	-0.50	0.033	-0.65	**0.006**
	All	0.97 ± 0.13	-0.32	0.017	-0.15	0.166	-0.40	**0.005**	-0.33	0.019
Stroop2	HC	0.84 ± 0.15	-0.39	0.107	0.28	0.178	-0.60	0.026	-0.58	0.031
	MDD	0.89 ± 0.13	-0.30	0.133	-0.28	0.144	-0.20	0.249	-0.45	0.055
	SZ	0.93 ± 0.13	0.38	0.083	0.14	0.309	-0.17	0.287	-0.20	0.244
	All	0.89 ± 0.14	-0.08	0.313	0.04	0.387	-0.28	0.040	-0.28	0.045

GLU = glutamate correlation coefficient (Pearson r) with response times
ΔGLU = The normalized glutamate concentration change
GLN = glutamine correlation coefficient (Pearson r) with response times
ΔGLN = The normalized glutamine concentration change correlation coefficient (Pearson r) with response times
p = probability that the correlation is due to chance (alpha=0.05/4 (Bonferroni corrected), one-tailed), bolded values indicate statistical significance
HC= healthy controls
MDD = major depressive disorder
SZ = Schizophrenia
All = the combination of all participants across groups

Table 5-5. Correlation values between behavioural response times for each Stroop condition and GLU and GLN concentrations during Stroop1

		Stroop1					Stroop2				
Group	Metabolite	Congruent	Incongruent	Word Only	Color Only	All	Congruent	Incongruent	Word Only	Color Only	All
HC	GLU	-0.394	-0.419	-0.152	-0.614	-0.471	-0.551	-0.454	-0.085	-0.558	-0.494
	ΔGLU	0.232	0.042	-0.070	0.034	0.074	0.173	0.253	0.190	0.443	0.255
	GLN	-0.559	-0.453	-0.296	-0.552	-0.546	-0.424	-0.643	-0.468	-0.301	-0.540
	ΔGLN	-0.131	-0.343	-0.245	-0.084	-0.242	0.000	-0.216	-0.386	-0.176	-0.209
MDD	GLU	-0.009	-0.368	-0.390	-0.276	-0.304	0.076	-0.270	-0.181	0.013	-0.123
	ΔGLU	-0.344	-0.304	-0.081	-0.348	-0.310	-0.212	-0.137	-0.298	-0.074	-0.203
	GLN	-0.291	-0.443	0.029	0.105	-0.220	0.010	-0.250	-0.305	-0.229	-0.215
	ΔGLN	0.319	-0.525	0.217	0.432	0.172	-0.181	-0.583	-0.200	-0.472	-0.436
SZ	GLU	0.091	-0.352	0.192	0.129	0.028	0.115	0.334	0.002	0.454	0.302
	ΔGLU	-0.088	-0.228	0.166	0.121	0.003	-0.062	-0.429	0.128	-0.238	-0.147
	GLN	-0.077	-0.439	-0.296	-0.132	-0.267	-0.345	-0.290	-0.157	-0.259	-0.324
	ΔGLN	-0.089	-0.676	-0.383	-0.366	-0.427	-0.024	-0.239	-0.019	-0.016	-0.094
All	GLU	-0.055	-0.321	-0.140	-0.214	-0.222	-0.035	-0.097	-0.069	0.069	-0.041
	ΔGLU	-0.092	-0.149	-0.017	-0.131	-0.115	-0.021	-0.092	0.033	-0.113	-0.063
	GLN	-0.207	-0.404	-0.301	-0.214	-0.331	-0.163	-0.310	-0.259	-0.237	-0.284
	ΔGLN	-0.003	-0.330	-0.150	-0.024	-0.154	0.017	-0.213	-0.068	-0.010	-0.092

GLU = glutamate correlation coefficient (Pearson r) with response times
ΔGLU = The normalized glutamate concentration change
GLN = glutamine correlation coefficient (Pearson r) with response times
ΔGLN = The normalized glutamine concentration change correlation coefficient (Pearson r) with response times
HC= healthy controls
MDD = major depressive disorder
SZ = Schizophrenia
All = the combination of all participants across groups

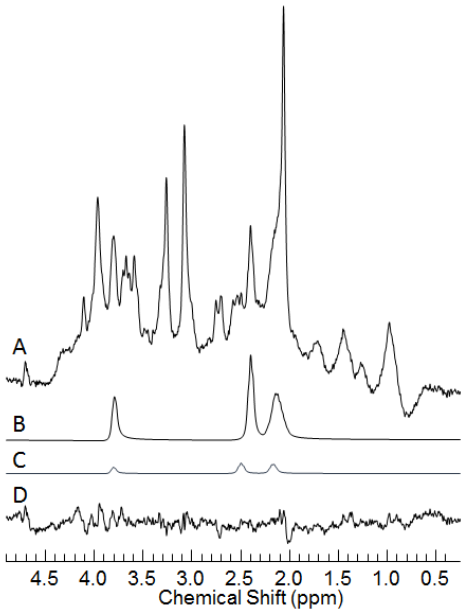

Figure 5-2. (A) An example resting 80 average water suppressed spectrum. This is taken from the ACC of a volunteer with SZ. A 2Hz Lorentzian line broadening has been applied. (B) Resultant estimates of the glutamate and (C) glutamine spectral fits. (D) The residual (spectrum minus the fit of all metabolites) of the spectrum

Every group was able to respond to the stimuli correctly with at least 90% accuracy. Mathematical modeling of Stroop performance confirmed an increased number of subprocesses (constituent cognitive operations) among the SZ group[26,27,52,53]. The response times to the incongruent condition during Stroop1 significantly correlated with GLN concentrations when averaged together over all groups ($p=0.005$; Table 5-4), whereas GLU concentrations only presented with a trend ($p=0.017$). The MDD and SZ groups responses significantly correlated with the normalized GLN responses ($p=0.003$, $p=0.006$, respectively), and no group's response times were significantly correlated with the normalized GLU responses. No significant correlations were observed in Stroop2. The full table of correlations between GLU and GLN concentrations and response times for each of the four Stroop conditions can be found in Table 5-5.

5.4 Discussion:

The GLU response in the ACC of healthy controls (3.2%) compares well with the 2.6% reported previously using the Stroop Task[20] and with the 2-4% reported previously in other brain areas[14,16–19]. A main effect of time was observed for all groups in Stroop1 compared to Resting, nevertheless, planned contrasts were significant for the healthy controls only. GLU and GLN cycling correlates with neuronal glucose consumption in activated conditions[25] and hypofunction of the ACC with color-word Stroop Tasks has been demonstrated in SZ with fMRI[28,29]. In SZ, it seems that the number of processing steps involved in stimulus encoding is increased[26,27,52,53]. The increased processing steps may involve more brain areas than in controls and cause a blunted activation state of the ACC, which could explain the relatively smaller increase in GLU.

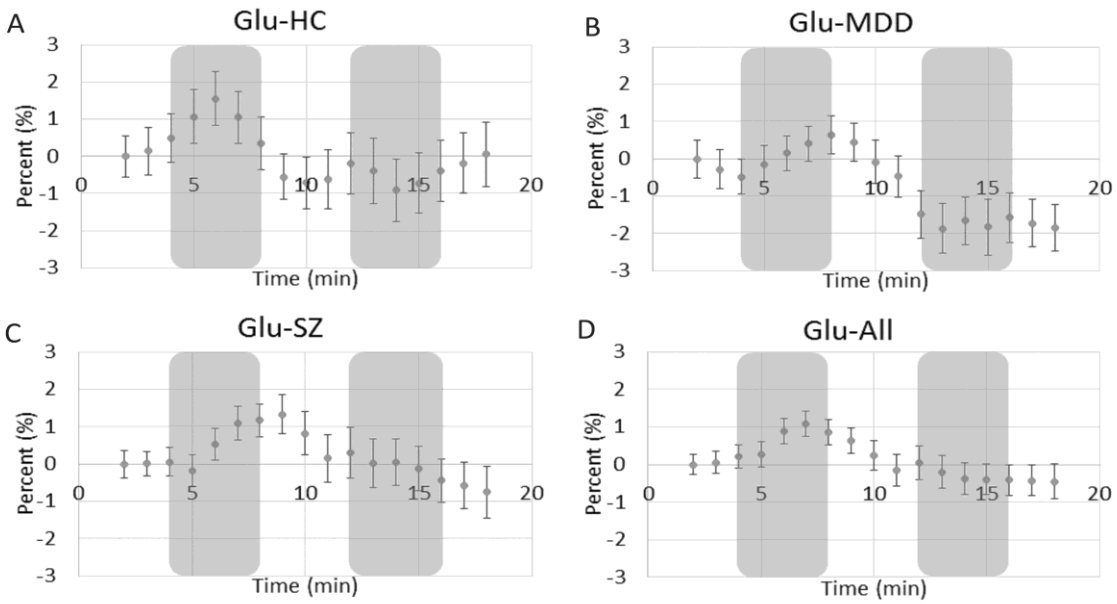

Figure 5-3. Four-minute moving average time courses of glutamate concentrations. Each point represents the percent change from resting concentration (averaged over four minutes) for (A) healthy, (B) Major Depressive Disorder, (C) Schizophrenia groups, and (D) all groups combined. Shaded areas indicate that the Stroop task is being performed during that time. Error bars represent inter-individual standard error of the mean

The observed decreases in GLU and GLX during Stroop2 relative to Stroop1 and Recovery1, particularly in the patient groups, were unexpected. Learning effects on GLU as the task progresses are a possible explanation owing to the increased amount of practice participants have received by the time of the second task. The observed decrease in response times during Stroop2 relative to Stroop1 does indicate that the task became easier. This study is now the second to report a decrease in a neurotransmitter using a cognitive task with ^{1}H-fMRS, as a similar result has been observed in prefrontal cortex GABA concentrations during a working memory task, which initially showed an increase in GABA concentrations followed by three subsequent runs with decreases[15]. This finding is not observed in the visual or motor tasks[14,16–19], so it is not likely that the reduced GLU is due to an inadequate duration of Recovery1. Future fMRS studies using cognitive stimuli should observe a longer recovery time between functional runs to further explore this finding.

The behavioural response times for the incongruent condition during Stroop1 negatively correlated with the GLN concentrations. More GLN readily available could mean quicker responses are possible because less time is required to create GLU for neurotransmission. The normalized changes in GLN during the task were much stronger predictors than GLU, which seemingly had no correlation, indicating the role of GLN in neurotransmission may have substantial influence on cognitive capabilities.

No between-group comparisons yielded significant results but there are still some points worth noting for possible future testing. First, the resting GLU levels were slightly higher in the MDD and SZ groups than the healthy controls. Elevated GLU concentrations can lead to excitotoxicity[54,55] so levels are carefully controlled by re-uptake transporters. It is possible that resting GLU in MDD and SZ groups are closer to a GLU ceiling making GLU upregulation more difficult. It should also be noted that GLU and GLN are involved in many other brain functions, including metabolism, which is likely also in a dynamic state.

Secondly, the SZ group appeared to have a slower GLU response and recovery to Stroop1 when compared to controls and MDD subjects yet showed significant differences in the GLN concentrations during Stroop1 and Recovery1. When GLU is released from the receptor on the post-synaptic membrane it is taken up into the adjacent glial cell[55] and converted to GLN via glutamine synthetase so that it can be transferred back into the neuron[55] where the GLN is converted back into GLU via the phosphate-activated enzyme glutaminase (PAG)[56]. Insufficient PAG would slow the conversion of GLN to GLU, resulting in a slower GLU-GLN cycle and a prolonged recovery from a neurotransmission event. However, no significant difference was observed in the expression of PAG in the ACC in one post-mortem study[57] and increased expression was found in the thalamus in another[58]. Another possible explanation comes from studies that have demonstrated that NMDA hypofunction causes increased glutamine synthetase activity resulting in increased GLN[59]. Consistent with this observation, another study has shown that increased ketamine administration in healthy controls leads to increased GLN concentrations in the ACC[60]. It is possible, that the increased GLN observed in the SZ group arose from NMDA hypofunction when the ACC was challenged.

There is evidence to support a possible glutamatergic dysfunction in MDD as well[9]. While the exact mechanism is yet to be understood, some lines of evidence suggest astrocytic dysfunction may contribute to the pathophysiology of MDD[9,61,62]. Astrocytes are pivotal elements in the GLU-GLN cycle and it is possible that any disruption to the efficiency of their operations in MDD could have contributed to the lack of a significant increase during Stroop1, or to the significant decrease in Stroop2. Previous studies have demonstrated decreased ACC GLU in the MDD[9–11], which was not observed in this study. This could be due to the different placement of voxels within the relatively large ACC or possibly a result of treatment effects. It could also be due to the significant difference in gender in the subject population. In this study, the MDD group had a larger incidence of females than the healthy controls. This is another confound that is difficult to avoid, as women have a higher prevalence of MDD than males at a ratio of 1.64:1 in Canada[63]. This must be considered when interpreting the results as gender has previously been shown to influence GLU[64] and GLN[65] concentrations.

A limitation of the study is the possible influence of the medications, which have been shown to affect glutamatergic concentration levels[66,67]. Antipsychotic and antidepressant medications are often unavoidable confounds of studies involving SZ and MDD patients. Although the subjects in this study were in relatively early stages of the illness (30 ± 16 months and 29 ± 14 months for the SZ and MDD groups, respectively), medications have been shown to influence the GLU concentration of medicated SZ patients in as early as 4 weeks[67]. This could have influenced the baseline levels of GLU and, possibly, the GLU responses to functional activation.

Although the confirmatory fMRI suggests correct voxel placement, another limitation of this study is that there was no fMRI guidance prior to the ^{1}H-fMRS acquisition. The confirmatory fMRI was acquired post-fMRS to decrease the impact of task learning effects to elicit the strongest ACC response, to which the reduction in response times and GLU changes observed during Stroop2 do suggest that considerable learning effects occur.

Detailed analyses of the confirmatory fMRI and mathematical modeling of the behavioural response times are beyond the scope of this work and will be presented in other venues[52].

5.5 Conclusion:

GLU concentrations measured with ^{1}H-fMRS were demonstrated to significantly increase in a healthy control group upon functional activation of the ACC using a color-word Stroop task but not in a MDD or SZ group. This is the first study to perform ^{1}H-fMRS in the ACC at 7 T in a psychiatric population. Use of a psychiatric control group (MDD) demonstrated that the increases in GLN were specific to SZ, but the blunted GLU response during Stroop1 was not. Observed response times of the MDD group were slower than the healthy controls, but were not as slow as the SZ group, indicating a stronger deterioration of function in SZ. Future studies should try to include psychiatric control groups to assess the specificity of the results. Future studies should examine

other cognitive tasks that activate the ACC, perhaps with varying levels of complexity to get a better understanding of the GLU and GLN response in SZ, with longer response times and varying stimulus encoding loads to study the GLU recovery process in greater detail.

Supplementary information is available at npj Schizophrenia's website.

5.5.1 Acknowledgements:

The authors would like to thank Joe Gati for assistance with the MRI imaging protocol.

5.5.2 Competing Interests: None to disclose

5.5.3 Funding:

This work was supported by a New Investigator Fellowship grant (J.T.) from the Ontario Mental Health Foundation (OMHF). Salary support for R.T. and B.S., was funded in part by operating funds from the Canadian Institute of Health Research (P.C.W., MT-12078).

5.5.4 Contributions:

RT with PCW, RWJN, NR, and JT designed the study protocol. BS recruited study participants and performed the SCID. EAO helped with MDD subject recruitment. RT acquired the data and post-processed spectra. MD analyzed all fMRI work. RT wrote the first draft of the paper. RWJN, EAO, BS, MD, NR, PCW, and JT all reviewed and approved the manuscript.

5.6 References:

1. Gruber, O., Santuccione, A. C. & Aach, H. Magnetic resonance imaging in studying schizophrenia, negative symptoms, and the glutamate system. *Front. Psychiatry* **5,** 1–11 (2014).

2. Javitt, D. C. & Zukin, S. R. Recent advances in the phencyclidine model of schizophrenia. *Am. J. Psychiat.* **148,** 1301–1308 (1991).

3. Coyle, J. T. & Tsai, G. The NMDA receptor glycine modulatory site: a therapeutic target for improving cognition and reducing negative symptoms in schizophrenia. *Psychopharmacology (Berl).* **174,** 32–38 (2004).

4. Tamminga, C. A., Holcomb, H. H., Gao, X. M. & Lahti, A. C. Glutamate pharmacology and the treatment of schizophrenia: current status and future directions. *International clinical psychopharmacology* **10 Suppl 3,** 29–37 (1995).

5. Gilbert-Rahola, J. & Villena-Rodriguez, A. Glutamatergic drugs for schizophrenia treatment. *Actas españolas Psiquiatr.* **42,** 234–241 (2014).

6. Stone, J. M. Glutamatergic antipsychotic drugs: a new dawn in the treatment of schizophrenia? *Ther. Adv. Psychopharmacol.* **1,** 5–18 (2011).

7. Poels, E. M. P. *et al.* Imaging glutamate in schizophrenia: review of findings and implications for drug discovery. *Mol. Psychiatry* **19,** 20–9 (2014).

8. Marsman, A. *et al.* Glutamate in schizophrenia: A focused review and meta-analysis of 1H-MRS studies. *Schizophr. Bull.* **39,** 120–129 (2013).

9. Jun, C. *et al.* Disturbance of the glutamatergic system in mood disorders. *Exp. Neurobiol.* **23,** 28–35 (2014).

10. Yüksel, C. & Öngür, D. Magnetic resonance spectroscopy studies of glutamate-related abnormalities in mood disorders. *Biol. Psychiatry* **68,** 785–794 (2010).

11. Yildiz-Yesiloglu, A. & Ankerst, D. P. Review of 1H magnetic resonance spectroscopy findings in major depressive disorder: A meta-analysis. *Psychiatry Res. - Neuroimaging* **147,** 1–25 (2006).

12. Gussew, A. *et al.* Time-resolved functional 1H MR spectroscopic detection of glutamate concentration changes in the brain during acute heat pain stimulation. *Neuroimage* **49,** 1895–1902 (2010).

13. Kim, T. H., Kang, H. K. & Jeong, G. W. Assessment of Brain Metabolites Change during Visual Sexual Stimulation in Healthy Women Using Functional MR Spectroscopy. *J. Sex. Med.* **10,** 1001–1011 (2013).

14. Lin, Y., Stephenson, M. C., Xin, L., Napolitano, A. & Morris, P. G. Investigating the metabolic changes due to visual stimulation using functional proton magnetic resonance spectroscopy at 7 T. *J. Cereb. Blood Flow Metab.* **32,** 1484–1495 (2012).

15. Michels, L. *et al.* Frontal gaba levels change during working memory. *PLoS One* **7,** e31933 (2012).

16. Mangia, S. *et al.* Sustained neuronal activation raises oxidative metabolism to a new steady-state level: evidence from 1H NMR spectroscopy in the human visual cortex. *J. Cereb. Blood Flow Metab.* **27,** 1055–1063 (2007).

17. Bednařík, P. *et al.* Neurochemical and BOLD responses during neuronal activation measured in the human visual cortex at 7 Tesla. *J. Cereb. Blood Flow Metab.* 1–10 (2015). doi:10.1038/jcbfm.2014.233

18. Schaller, B., Xin, L., O'Brien, K., Magill, A. W. & Gruetter, R. Are glutamate and lactate increases ubiquitous to physiological activation? A 1H functional MR spectroscopy study during motor activation in human brain at 7Tesla. *Neuroimage* **93,** 138–145 (2014).

19. Schaller, B., Mekle, R., Xin, L., Kunz, N. & Gruetter, R. Net increase of lactate and glutamate concentration in activated human visual cortex detected with magnetic resonance spectroscopy at 7 tesla. *J. Neurosci. Res.* **91,** 1076–1083 (2013).

20. Taylor, R. *et al.* Increased glutamate levels observed upon functional activation in the anterior cingulate cortex using the Stroop Task and functional spectroscopy. *Neuroreport* **26,** 107–112 (2015).

21. Mullins, P. G., Rowland, L. M., Jung, R. E. & Sibbitt, W. L. A novel technique to study the brain's response to pain: Proton magnetic resonance spectroscopy. *Neuroimage* **26,** 642–646 (2005).

22. Cleve, M., Gussew, A. & Reichenbach, J. R. In vivo detection of acute pain-induced changes of GABA+ and Glx in the human brain by using functional 1H MEGA-PRESS MR spectroscopy. *Neuroimage* **105,** 67–75 (2015).

23. Lally, N. *et al.* Glutamatergic correlates of gamma-band oscillatory activity during cognition: A concurrent ER-MRS and EEG study. *Neuroimage* **85,** 823–833 (2014).

24. Apsvalka, D., Gadie, A. & Mullins, P. G. Event-related dynamics of glutamate and BOLD signal at 3 T in a repetition suppression paradigm. *ISMRM Proc.* **22,** 3796 (2014).

25. Rothman, D. L., Behar, K. L., Hyder, F. & Shulman, R. G. In vivo NMR studies of the glutamate neurotransmitter flux and neuroenergetics: implications for brain function. *Annu. Rev. Physiol.* **65,** 401–427 (2003).

26. Neufeld, R. W. J. On the centrality and significance of stimulus-encoding deficit in schizophrenia. *Schizophr. Bull.* **33,** 982–993 (2007).

27. Neufeld, R. W. J., Boksman, K., Vollick, D., George, L. & Carter, J. R. Stochastic dynamics of stimulus encoding in schizophrenia: Theory, testing, and application. *J. Math. Psychol.* **54,** 90–108 (2010).

28. Minzenberg, M. J., Laird, A. R., Thelen, S., Carter, C. S. & Glahn, D. C. Meta-analysis of 41 functional neuroimaging studies of executive function in schizophrenia . PubMed Commons. *Arch. Gen. Psychiatry* **66,** 1–2 (2014).

29. Ungar, L., Nestor, P. G., Niznikiewicz, M. A., Wible, C. G. & Kubicki, M. Color Stroop and negative priming in schizophrenia: An fMRI study. *Psychiatry Res. - Neuroimaging* **181,** 24–29 (2010).

30. Boksman, K. *et al.* A 4.0-T fMRI study of brain connectivity during word fluency in first-episode schizophrenia. *Schizophr. Res.* **75,** 247–263 (2005).

31. Falkenberg, L. E., Westerhausen, R., Specht, K. & Hugdahl, K. Resting-state glutamate level in the anterior cingulate predicts blood-oxygen level-dependent response to cognitive control. *Proc. Natl. Acad. Sci.* **109,** 5069–5073 (2012).

32. First, M., Spitzer, R., Gibbon, M. & Williams, J. *Structured Clinical Interview (SCID) for DSM-IV Axis 1 Disorders*. (American Psychiatric Press Inc, 1997).

33. Andreasen, N. C. *Scale for the Assessment of Positive Symptoms (SAPS)*. (The University of Iowa, 1984).

34. Andreasen, N. C. *Scale for the Assessment of Negative Symptoms (SANS)*. (The University of Iowa, 1984).

35. Montgomery, S. A. & Asberg, M. Scale Designed to be Sensitive to Change. *Br. J. Psychiatry* **134,** 382–9 (1979).

36. Young, R. C., Biggs, J. T., Ziegler, V. E. & Meyer, D. A. A rating scale for mania : reliability , validity and sensitivity A Rating Scale for Mania : Reliability , Validity and Sensitivity. *Br. J. Psychiatry* **133,** 429–435 (2011).

37. Aoyama, N. *et al.* Grey matter and social functioning correlates of glutamatergic metabolite loss in schizophrenia. *Br. J. Psychiatry* **198,** 448–456 (2011).

38. Peirce, J. W. PsychoPy-Psychophysics software in Python. *J. Neurosci. Methods* **162,** 8–13 (2007).

39. Gilbert, K. M., Curtis, A. T., Gati, J. S., Klassen, L. M. & Menon, R. S. A radiofrequency coil to facilitate B 1 + shimming and parallel imaging acceleration in three dimensions at 7 T. *NMR Biomed.* **24,** 815–823 (2011).

40. Curtis, A. T., Gilbert, K. M., Klassen, L. M., Gati, J. S. & Menon, R. S. Slice-by-slice B1+ shimming at 7 T. *Magn. Reson. Med.* **68,** 1109–16 (2012).

41. Klassen, L. M. & Menon, R. S. Robust Automated Shimming Technique Using Arbitrary Mapping Acquisition Parameters (RASTAMAP). *Magn. Reson. Med.* **51,** 881–887 (2004).

42. Laird, A. R. *et al.* A comparison of label-based review and ALE meta-analysis in the stroop task. *Hum. Brain Mapp.* **25,** 6–21 (2005).

43. Reid, M. A. *et al.* Assessments of function and biochemistry of the anterior cingulate cortex in schizophrenia. *Biol. Psychiatry* **68,** 625–633 (2010).

44. Tkáć, I. & Gruetter, R. Methodology of 1 H NMR Spectroscopy of the Human Brain at Very High Magnetic Fields. *Appl. Magn. Reson.* **29,** 139–157 (2005).

45. Penner, J. & Bartha, R. Semi-LASER 1H MR spectroscopy at 7 Tesla in human brain: Metabolite quantification incorporating subject-specific macromolecule removal. *Magn. Reson. Med.* **00,** 1–9 (2014).

46. De Beer, R. & Van Ormondt, D. Analysis of NMR Data Using Time Domain Fitting Procedures. *NMR Basic Princ. Prog.* **26,** 201–248 (1992).

47. Van den Boogaart, a, Ala-Korpela, M., Jokisaari, J. & Griffiths, J. R. Time and frequency domain analysis of NMR data compared: an application to 1D 1H spectra of lipoproteins. *Magn. Reson. Med.* **31,** 347–358 (1994).

48. Brown, M. A. Time-domain combination of MR spectroscopy data acquired using phased-array coils. *Magn. Reson. Med.* **52,** 1207–1213 (2004).

49. Bartha, R., Drost, D. J., Menon, R. S. & Williamson, P. C. Spectroscopic lineshape correction by QUECC: Combined QUALITY deconvolution and eddy current correction. *Magn. Reson. Med.* **44,** 641–645 (2000).

50. Bartha, R., Drost, D. J. & Williamson, P. C. Factors affecting the quantification of short echo in-vivo 1 H MR spectra : prior knowledge, peak elimination, and filtering. *NMR Biomed.* **12,** 205–216 (1999).

51. Stanley, J. A., Drost, D. J., Williamson, P. C. & Thompson, R. T. The use of a priori knowledge to quantify short echo in vivo 1H MR spectra. *Magn. Reson. Med.* **34,** 17–24 (1995).

52. Taylor, R., Théberge, J., Williamson, P. C. & Neufeld, R. W. J. Model-Driven fMRI of Deviations in Stroop Perofrmance in Schizophrenia. *J. Math. Psychol.*

53. Taylor, R., Théberge, J., Williamson, P. C., Densmore, M. & Neufeld, R. W. J. Using Systems factorial Technology to Elucidate the 'f' of Clinical fMRS (functional Magnetic Resonance Spectroscopy). *Syst. factorial Technol. A theory driven Methodol. Identif. Percept. Cogn. Mech.*

54. Plitman, E. *et al.* Glutamate-mediated excitotoxicity in schizophrenia: A review. *Eur. Neuropsychopharmacol.* **24,** 1591–1605 (2014).

55. Mark, L. P. *et al.* Pictorial review of glutamate excitotoxicity: Fundamental concepts for neuroimaging. *Am. J. Neuroradiol.* **22,** 1813–1824 (2001).

56. Marx, M.-C., Billups, D. & Billups, B. Maintaining the presynaptic glutamate supply for excitatory neurotransmission. *J. Neurosci. Res.* **00,** n/a–n/a (2015).

57. Katsel, P. *et al.* Astrocyte and glutamate markers in the superficial, deep, and white matter layers of the anterior cingulate gyrus in schizophrenia. *Neuropsychopharmacology* **36,** 1171–1177 (2011).

58. Bruneau, E. G., McCullumsmith, R. E., Haroutunian, V., Davis, K. L. & Meador-Woodruff, J. H. Increased expression of glutaminase and glutamine synthetase mRNA in the thalamus in schizophrenia. *Schizophr. Res.* **75,** 27–34 (2005).

59. Rodrigo, R. & Felipo, V. Control of brain glutamine synthesis by NMDA receptors. *Front. Biosci.* **12,** 883–890 (2007).

60. Rowland, L. M. *et al.* Effects of ketamine on anterior cingulate glutamate metabolism in healthy humans: A 4-T proton MRS study. *Am. J. Psychiatry* **162,** 394–396 (2005).

61. Sanacora, G. & Banasr, M. From pathophysiology to novel antidepressant drugs: Glial contributions to the pathology and treatment of mood disorders. *Biol. Psychiatry* **73,** 1172–1179 (2013).

62. Rajkowska, G. & Stockmeier, C. a. Astrocyte pathology in major depressive disorder: insights from human postmortem brain tissue. *Curr. Drug Targets* **14,** 1225–36 (2013).

63. Romans, S. E., Tyas, J., Cohen, M. M. & Silverstone, T. Gender differences in the symptoms of major depressive disorder. *J. Nerv. Ment. Dis.* **195,** 905–911 (2007).

64. Marsman, A. *et al.* GABA and glutamate in schizophrenia: A 7 T 1H-MRS study. *NeuroImage Clin.* **6,** 398–407 (2014).

65. Tayoshi, S. *et al.* Metabolite changes and gender differences in schizophrenia using 3-Tesla proton magnetic resonance spectroscopy (1H-MRS). *Schizophr. Res.* **108,** 69–77 (2009).

66. Kegeles, L. S. *et al.* Elevated Prefrontal Cortex -Aminobutyric Acid and Glutamate-Glutamine Levels in Schizophrenia Measured In Vivo With Proton Magnetic Resonance Spectroscopy. *Arch. Gen. Psychiatry* **69,** 449–459 (2012).

67. De la Fuente-Sandoval, C. *et al.* Glutamate levels in the associative striatum before and after 4 weeks of antipsychotic treatment in first-episode psychosis: a longitudinal proton magnetic resonance spectroscopy study. *JAMA psychiatry* **70,** 1057–66 (2013).

Chapter 6

6 Summary, Future Work, and Conclusions

This section will begin with a discussion of each paper to put into perspective how they all fit together to complete a story. There will then be suggestions for possible future avenues of research based on the results of this thesis, with some recommendations for ways in which the methodologies can be improved. This will be followed by a brief conclusion.

6.1 Summary of chapters

6.1.1 Simulations

Simulations were designed to isolate common sources of variation in metabolite quantification precision (i.e. how consistent the measurements are), accuracy (i.e. how close the measured concentrations are to the correct values) and correlations between metabolite concentration estimates (i.e. how do the concentration estimates interact with each other) using simulated human brain spectra of four commonly used B_0, 1.5 T, 3.0T, 4.0T, and 7.0T. Three SNR were assumed for each B_0, one with 64 spectral averages, another with 256 spectral averages, and one with a theoretical SNR of 1024 (practically unachievable in water suppressed human brain spectra). The precision and the completeness of the initial estimate of the metabolite fitting template were also assessed. The focus of the study was on J-coupled metabolites, such as GLU and GLN, but all metabolites were evaluated.

With the exception of the fitting templates with omitted metabolites, the accuracy of metabolite concentration estimates was generally unaffected for all conditions studied. It was found that the precision generally improved as B_0 increased, with the largest improvements in quantification precision coming from J-coupled metabolites. J-coupled metabolites also had the strongest reductions in correlations between metabolite concentration estimates when B_0 increased, meaning they can be quantified more

independently. Precision also improved when SNR increased as a consequence of increasing B_0. An important observation that was independent of B_0 is that the precision of the initial estimate of the spectral fitting template did affect quantification precision, so care is needed in providing a reasonable initial estimate.

This study has confirmed the hypothesis that there are significant benefits to using higher B_0 for ^{1}H-MRS studies aiming to reliably quantify GLU and GLN. The increase in SNR reduces the number of averages necessary to acquire quality spectra, which is important for any application of ^{1}H-fMRS. A stronger B_0 will also help in quantifying lower concentration and heavily overlapped metabolites, such as GLY. Therefore, a 7 T MRI and ultra-short echo time STEAM sequence were employed for all the ^{1}H-MRS and ^{1}H-fMRS work included in this thesis.

6.1.2 Single-voxel ^{1}H-MRS

The aim of this study was to examine concentrations of GLU, GLN, and GLY in the ACC and thalamus of SZ compared to healthy controls and MDD using the aforementioned benefits in metabolite quantification that is possible with a 7 T MRI. The key findings of the study were increased GLN and decreased GLY in the thalamus of people with SZ compared to the healthy control group, and decreased MYO in both the ACC and thalamus of the MDD group compared to the healthy control group and SZ groups. No differences in GLU were found in any group. It was the first study to examine GLY concentrations in the brains of a schizophrenic population *in vivo* using ^{1}H-MRS.

The increased GLN and decreased GLY in the SZ group fit well with the NMDA hypofunction model of SZ and agree with the hypotheses of increased GLN and abnormal GLY concentrations in SZ. As demonstrated in Fig 1-3, GLY availability is critical to GLU neurotransmission via the NMDA receptor. Therefore, insufficient concentrations of GLY in the synaptic cleft could lead to a deficiency in NMDA function. The increased GLN fits into this model as well. NMDA hypofunction increases the activity of glutamine synthetase, which then increases the concentrations of

GLN[1]. The thalamus is involved in the transmission of most sensory input and is a central hub of the BGTHC circuits that mediate communications between motivation and action. It is a critical location for communication to areas involved in both the positive symptoms of SZ via the substantia nigra and nucleus accumbens, and the negative symptoms of SZ via the prefrontal cortex and the ACC. There were no glutamatergic changes in the ACC of the SZ group relative to either healthy control or MDD groups. This was unexpected based on previous studies in the literature[2], including previous results from this lab[3,4], and contradicted that part of the hypothesis. This could be due to the time gap between diagnoses to the time of the scan, which was on average 30 months for this subject group. It has previously been shown that the concentration of GLN is initially higher in the ACC of people with SZ, and this concentration gradually decreases over time[2,5]. It is possible that there initially was an increase in GLN, but, due to the length of illness, the concentration decreased and was no longer significant.

It was also expected that the MDD group would present with GLU abnormalities relative to the SZ and control groups. There is growing evidence that excitatory synapses and NMDA receptors play a role in MDD symptomatology[6]. Ketamine, the NMDA antagonist known to induce SZ-like behavior in healthy controls[7], when administered in low doses has anti-depressant properties in people with MDD[6]. A dysfunction in the NMDA receptors in MDD could explain the lack of observed significant differences in GLN between the SZ group and the MDD group.

It should be noted that the SZ and MDD groups in this study were no longer drug-naïve. It has previously been demonstrated that medications can influence GLU concentrations in a short time frame[8,9] and that GLU concentrations vary throughout the disease progression[2,5]. It is, therefore, a possibility that medications and/or disease duration had some influence on the results. Obtaining data from unmedicated patients early in their illness is, of course, challenging. SZ is only prevalent in about 1% of the population with the typical disease onset during adolescence. A drug-naïve first-episode study would rely on an influx of young adolescents experiencing psychiatric symptoms that agree to volunteer for an MRI and often require their parents' permission. With this study in particular, due to technical challenges associated with implementing the ^{1}H-MRS

protocol on the 7 T scanner (planned decommissioning within 2 years of the start of the study), the available time-window only permitted the scanning of young patients with SZ, still early in their illness (30 ± 15 months), but not drug-naïve. It is possible that this could have influenced GLU concentrations in the ACC and thalamus. Future studies should explore a longitudinal design starting at the first-episode, never-treated time point.

Another confound of this study is that as many as 60% of people with SZ are smokers[10], and smoking has been shown to affect GLU levels in the thalamus[11]. The prevalence of smokers in SZ is believed to be partially due to the increased dopamine activity from smoking[10]. Cigarette smoking was not an exclusion criteria for this study, so it needs to be considered when interpreting the results.

Reduced MYO concentrations were observed in the thalamus and the ACC of the MDD group relative to the healthy control and SZ groups. MYO is an osmolyte in the brain and is a precursor to many phosphorylated derivatives and second messengers that have various important functions[12]. It has also traditionally been a marker for glial cell integrity although some have questioned this claim[12]. However, if the assumption is made that MYO concentrations are reflective of glial cell integrity, then these results do support the theory of a reduction in glial cell density in MDD. The glia are actively involved in the GLU-GLN cycle, so disruption of these processes could directly influence GLU neurotransmission and impede healthy brain function. With MYO being involved in so many brain functions, it is difficult to interpret what exactly is causing this decrease in MYO. It is curious, though, that treatments of mania often reduce MYO concentrations[12] and that increased MYO concentrations have been reported in recovered MDD subjects[13]. Although this is speculative, it seems likely that the MYO concentrations somehow influence (or are influenced by) mood. Inositol has been examined as a possible treatment for MDD previously. The results are mixed, but one meta-analyses determined that there may be a clinical benefit to inositol as a treatment[14]. The number of studies, however, are still small[12,13,14], so more are necessary to confirm this finding.

It is important to note that there was a significant difference in the number of females to males in the MDD group compared to the SZ and healthy control groups. This is difficult to avoid due to the increased prevalence of MDD in females compared to males (1.64:1 in Canada). There have yet to be any studies that have demonstrated differences in MYO concentrations between males and females, but still an important point to consider.

This study found interesting significant differences in metabolite concentrations between SZ, MDD, and healthy control subjects. However, this study was conducted in a resting state with one static measurement as hundreds of other studies of SZ with ^{1}H-MRS have done. As the very definition of SZ is entirely based on behavioural abnormalities, one may wonder why an entire literature was formed around MRS measurements of resting individuals with SZ. Although good rationales and hypotheses have been developed to explain abnormalities in resting levels of glutamate in SZ, it is reasonable to think that NMDA hypofunction may affect the ability to dynamically modify GLU concentrations to transact functional activation. It may be possible to visualize manifestations of NMDA hypofunction by acquiring dynamic measurements of metabolite concentrations using ^{1}H-fMRS of glutamate. GLU changes occurring during performance of a behavioural task had never been demonstrated using ^{1}H-fMRS at 7 T in healthy humans. Before we could begin a study using this technique in individuals with SZ, the technique needed to be developed and demonstrated in healthy controls.

6.1.3 ^{1}H-fMRS in healthy controls

The purpose of this paper was to first demonstrate that ^{1}H-fMRS with a cognitive behavioural task can induce detectable GLU changes using an ultra-high field 7 T MRI in healthy controls. Prior to this study, the only ^{1}H-fMRS studies that had successfully demonstrated GLU changes upon functional activation were conducted in the visual cortex using a visual paradigm[17–19], the motor cortex using a finger tapping paradigm[20], the lateral occipital cortex using a repetition suppression task[21,22], the anterior insula using a pain paradigm[23], the dorsal anterior cingulate using a pain paradigm[24], and the pregenual anterior cingulate using a pain paradigm[25] and a sexual arousal paradigm[26].

None of these past ^{1}H-fMRS studies had used a cognitive paradigm. Impairments in cognition have been well studied in SZ and there exists a number of well-established paradigms to study these impairments. After much debate over which cognitive task would provide the most robust activation of the ACC while allowing performance of the task in a prolonged manner and comparable performance accuracy between patients and controls, the color-word Stroop task was used as the cognitive task for this study, but certain implementation challenges remained and are discussed below.

First, the location of the ^{1}H-fMRS voxel has typically been placed in the area that elicits the strongest blood-oxygen level dependent (i.e. BOLD) response in fMRI to a specific task because of the assumption that the BOLD response is indicative of increased functional activation. Cognitive and behavioural tasks elicit weaker BOLD responses relative to the visual and motor tasks[27], so it may be expected that a difference in GLU may be harder to detect. The Stroop task was chosen as the cognitive task to maximize the possibility of detecting GLU, as it still induces a relatively robust fMRI activation in the ACC (although not as prominent as visual and motor tasks in their respective brain regions).

Cognitive tasks typically require some kind of motion to respond to the stimuli, usually via a button press or verbal communication. This creates the possibility of increased motion artifacts in the spectra. Although it is possible to have the subjects perform the cognitive stimuli silently in their minds, it would then not be possible to confirm the subject was attentive and performing the task with the presumed accuracy demonstrated during practice. This would also ignore a considerable amount of valuable data in the processing of the responses (i.e. mean response times, variances, percent correct, etc) between subject groups. Therefore, care was taken to setup the subject in the MRI in a position such that they are ready to respond in an attempt to minimize any movement when responding on the four-button keypad provided.

An additional obstacle in using a cognitive task is that the neural response is more complex, such that different mechanisms become involved as the task is performed. The subject learns to perform the task more efficiently, which may blunt the response. Visual

and motor responses activate specific areas of the brain and can be activated repeatedly, so these ^{1}H-fMRS studies have utilized fMRI guidance to locate the voxel. With cognitive tasks, performing the fMRI guidance would mean that the subjects would have increased exposure to the task, which may reduce activation in the area of interest during the ^{1}H-fMRS acquisition and make GLU changes harder to detect. By locating a consistent site of activation, it is possible to use anatomical landmarks to avoid this problem.

One final challenge is that some people will find certain cognitive tasks harder than other people. Prior to the ^{1}H-fMRS acquisition, it is important to ensure all participants can perform the task to the same level of proficiency by giving them some practice and meeting a specific criterion. For this study, all subjects had to achieve 80% correct responses on a desktop computer outside of the scanner prior to being examined.

A significant detectable increase in GLU concentrations in the ACC was observed in a small sample (n=7) of healthy controls after functional activation with the color-word Stroop task agreeing with the originally stated hypothesis. The magnitude of the GLU response was consistent with the visual and motor cortex ^{1}H-fMRS studies that also used prolonged stimulation periods (i.e. on the order of minutes)[17–20] but had a smaller response than event-related ^{1}H-fMRS of the ACC using pain stimuli[23–25]. It is possible that there is a separate, rapid, GLU response to event-related stimuli, in particular, pain. Pain is one the bodies most ancient and evolved responses, so it is possible that it has adapted a separate GLU response for faster reactions, perhaps utilizing the rapid synaptic currents produced by the AMPA GLU receptors[28].

A limitation of this study is the small sample size of participants. Although the sample size was low, 6 of the 7 participants showed increases in GLU in the first run of the task and 6 of the 7 showed decreases in the recovery period. This demonstrates that the Stoop task is a robust cognitive paradigm to detect GLU changes with functional activation in the ACC.

With the Stroop ^{1}H-fMRS paradigm able to successfully detect GLU increases in healthy controls, the next step was to examine GLU dynamically in psychiatric populations.

6.1.4 ^{1}H-fMRS in schizophrenia and major depressive disorder

The objective of this study was to gain insight into the health of GLU neurotransmission and the GLU-GLN cycle in SZ using a dynamic ^{1}H-MRS protocol. This was accomplished using a ^{1}H-fMRS technique similar to the one developed in the previous chapter was applied to the ACC of SZ, MDD, and healthy control groups using a color-word Stroop paradigm and a 7 T MRI. Each participant underwent a twenty-minute Stroop paradigm consisting of five, four-minute blocks that cycled between resting and stimulated conditions (i.e. rest, Stroop, recovery, Stroop, recovery), in which eighty spectral averages were acquired during each block. Prior to entering the MRI, each participant needed to perform the Stroop task with >80% accuracy to ensure comparable levels of proficiency between participants. Metabolite concentrations were extracted from the fits of the spectra from each block and tracked temporally. The healthy controls were the only group to significantly increase the concentrations of GLU during the first run of the task, which was then followed by a significant decrease in the recovery period. Neither the SZ nor MDD group presented with significant GLU concentration increases during the first run of the Stroop task, but the SZ group did present with significant increases in GLN concentrations. The GLU concentrations in the MDD group decreased significantly during the second run of the task, and there was a significant decrease over all groups. In addition, there was an overall significant negative correlation between the GLN concentrations and the response times, suggesting that the GLN levels are important to efficient cognitive functioning. This was the first study to examine GLU concentrations using ^{1}H-fMRS in a psychiatric population.

The increase in GLU concentrations in the healthy control group is consistent with the Stroop ^{1}H-fMRS from chapter 4 and is again comparable to the visual and motor ^{1}H-fMRS studies[17–20]. Both the MDD group and the SZ group did increase their GLU concentrations in the first run of the task, but not significantly. This blunted or aberrant response may suggest an inefficiency in the functioning of GLU within the ACC as NMDA receptors and excitatory synapses are implicated in both disorders[6,29,30]. If the NMDA receptors are not functioning optimally then the GLU-GLN cycle will be directly

affected, which could explain the smaller increase (below statistical significance threshold) in GLU concentrations in the SZ group. Specifically in the SZ group, the increase in the GLN concentration could suggest hypofunction of NMDA receptors when the region is stimulated, as NMDA hypofunction leads to increased GLN concentrations[1].

The decrease in the GLU concentrations during the second run of the Stroop was an unexpected result, based on what has previously been reported in ^{1}H-fMRS studies that have repeated visual or motor stimuli. This suggests two possible explanations. First, it is possible that the ACC is no longer required to the same magnitude due to processes involved in learning and improving the task, such that, with practice, different brain areas begin to contribute; Second, the GLU response observed is on the order of minutes, so it may be that four minutes was not enough for all the mechanisms involved to fully recover.

An important outcome of this study is that the mental state of the participant needs to be controlled for in "resting" ^{1}H-MRS studies examining GLU or GLN to avoid confounding the results. Instructions should be provided to the participant not unlike the instructions that would be given prior to a resting state fMRI scan: relax, close their eyes, try not to sleep and try to let their mind wander. Alternatively, a cross-fixation could be applied to control the mental state. This has not been a common procedure in past ^{1}H-MRS studies, which could have had some influence on the results. Going forward, a method for controlling the resting state should be a component of every ^{1}H-MRS protocol examining GLU or GLN.

There are similar limitations present in this study as the study mentioned in chapter 3. There was significantly more females in the MDD group than in the SZ and healthy control groups, the subjects were not drug-naïve, and smoking was not controlled for in the subject recruitment. The effects of these limitations have already been discussed in detail in chapter 6.1.2.

One limitation of studying cognitive tasks in psychiatric populations is that avolition is one of the key negative symptom of SZ, so the differences observed in the fMRI or ^{1}H-fMRS data could be due to a lack of effort. This is a difficult confound to control, but a

task that is challenging and engaging should help. In our Stroop task, we controlled performance based on the number of correct answers and we showed that participants with SZ were able to conduct the task with similar levels of proficiency (>90%). It may be debatable whether control for performance accuracy is equivalent to controlling for motivational/effort level.

6.2 Future Work

The results of these studies advance the literature and provide avenues for further exploration with more questions yet to be answered. There are many possible directions to move forward, some of which are briefly discussed below.

6.2.1 Simulations

This manuscript has received comments from reviewers after it was submitted for publication to Magnetic Resonance in Medicine and is currently in revisions in preparation to resubmit. The discussion below pertains to the comments and issues mentioned by the reviewers along with some suggestions for future work.

This simulation study demonstrated that with higher B_0 it is possible to improve metabolite quantification when using the time-domain fitting algorithm, fitMAN[31]. Whether these results are transmittable to other fitting algorithms has been brought into question. Many fitting algorithms share a common theme of reducing residuals between the data and the fit using *a priori* information. It has previously been demonstrated that the frequency-domain fitting algorithm LCModel[32] and the time-domain fitting algorithm AMARES[33] produce very similar concentrations in a study utilizing metabolite phantoms. The challenges relating to metabolite quantification including SNR, metabolite signature overlap and J-dephasing are not specific to fitMAN and would be challenges in other fitting algorithms as well. Similarly, all minimization routines need to have an initial estimate to minimize. It is expected that identical results would be obtained using

other common fitting algorithms like LCModel or AMARES. A similar simulation study utilizing multiple fitting algorithms could be performed to confirm.

Many ^{1}H-MRS studies utilize Cramer-Rao Lower Bounds (CRLB) to report the quality of the spectral fits. The CRLB are useful because they provide information on the minimum variance to be expected from the fitting parameters from a single fit. The advantage of examining the coefficient of variation (CV) is that all sources of variation are considered, including the variation from the fitting parameters, and provides a more realistic expectation of variation one would expect from a spectral acquisition. Still, due to the prevalence of CRLB in the research community, it would be wise to examine the same quantification relationships using the CRLB as well as the CV. This would provide information towards the minimum variance coming from the fitting of the parameters, and the difference would give an estimate on the variation that arises from other sources as well. In general, simulations are a good way to examine sources of quantification variation, mainly because the sources can be isolated, and the simulations can be repeated in a Monte Carlo format to achieve a desired power.

There are a number of ways in which the simulation study could be further explored. First, it should implement even more metabolites that are present in very low concentrations. There are still many more metabolites that contribute to the spectral area in ^{1}H-MRS that cannot typically be quantified reliably. The increase in SNR obtained by working at 7 T pushes some lower concentration metabolites not typically part of human brain ^{1}H-MRS quantification template above the detectability threshold. Addition of candidate metabolites to the simulation would be useful to get an idea of whether the spectral area from these metabolites are currently being consistently absorbed into the fit of any other specific metabolites when they are omitted from the fitting templates, which would lead to inaccuracies in measured metabolite concentrations.

Another way to extend the simulation study would be to isolate the effects of each of the constrained parameters on quantification. That is, to use inexact seeding for a single parameter, while using exact seeding for the remaining parameters. This would characterize which parameters, when seeded poorly, reduce quantification performance

the most (i.e. chemical shift, amplitude, linewidth, or phase). This would be an easy study to perform that can be run similarly with Monte Carlo simulations, all performed with a batch script on a computer. A study like this would help to further our understanding of which parameters affect quantification precision and accuracy the most. Practical knowledge suggests, for example, that small errors in initial chemical shift have greater impact than smaller errors in initial amplitude or phase. However, the sensitivity of parameter seeding has not been formally studied (beyond what one can deduct from analytical formulations of CRLB and Fisher information matrices).

6.2.2 Single-voxel ^{1}H-MRS in SZ and MDD

The ^{1}H-MRS study of the ACC and the thalamus in people with SZ and MDD produced some interesting results that should certainly be explored further. Ideally, a similar study would be conducted to confirm the findings, specifically for the reduced GLY in the thalamus as the standard CRLB limit for this study was increased for GLY measurements from 20% to 30%. It would be a more conclusive result if the CRLB limit for GLY could be reduced to the more commonly accepted 20% limit. One way this could be done is by increasing the SNR via longer scans with more averages (i.e. from 64 averages to 256 averages). Increased SNR can also be accomplished by increasing the size of the voxel, but this has its own drawbacks in that the voxel would be include brain areas beyond the thalamus.

The spin-echo full-intensity acquired localized spectroscopy (SPECIAL) sequence[34] is a relatively new ^{1}H-MRS pulse sequence that is capable of getting the short TE that is possible with STEAM, while still getting the SNR that is possible with PRESS, and has been previously utilized at 7 T[19,20]. Implementation and optimization of a new pulse sequence is a significant endeavor. However, using a SPECIAL sequence with 256 averages in the same region in the thalamus would, theoretically, improve the spectral SNR by a factor of 4 compared to the STEAM sequence with 64 averages that was used in this study. Given that the SPECIAL sequence would not compromise the metabolite spectral lineshapes, a significant improvement in the precision of metabolite

concentration estimates would be expected. A SPECIAL pulse sequence should be implemented and optimized for future ^{1}H-MRS studies.

One group used an echo time-averaged (TEAV) sequence[35] that utilizes the f1=0 component of a PRESS-2D J-resolved acquisition[36,37] to reliably detect GLY concentrations *in vivo* using ^{1}H-MRS at 3 T before and after ingestion of GLY supplementation in healthy controls[38]. They were able to quantify GLY as a ratio to creatine measurements with CRLB of 20 ± 2.9% and 17 ± 5.1% for their before and after scans, respectively, although one subject's CRLB exceeded 40% and was removed. It is likely that the achieved CRLB would have been improved to below the standard CRLB limit of 20% using a 7 T scanner.

Using the improved quantification precision that would be attainable with these techniques, a study that examines the concentrations of GLY before and after oral administration in a SZ group compared to healthy controls and a placebo group would be valuable. This would be especially useful if the target SZ group was first-episode and drug naïve at the start of the GLY administration and then were followed longitudinally over time. If a detectable increase in GLY concentrations after oral administration is found in the thalamus of people with SZ, then a correlation between SANS and SAPS scores, or any changes in them, would be especially interesting.

The same can be said for the MDD group and the observed reduced MYO concentrations. A study that tracks MYO levels before and after its ingestion over a period of time and similarly tracked the levels of depression would be valuable. Using the SPECIAL pulse sequence would not really be necessary to measure MYO concentrations as it is not usually a difficult metabolite to quantify reliably, but would add to quantification precision nonetheless.

Unfortunately, ^{1}H-MRS voxels tend to be larger than what is ideal to study a brain area of interest due to the inherent SNR limitation in ^{1}H-MRS. At higher B_0, the voxels can afford to be smaller so that the results will have increased specificity for a particular brain area. Although the technology may not be there yet, it would, one day, be interesting to study the individual thalamic nuclei that compose the thalamus using high B_0 and small

voxels. In a typical MRI image (T1 or T2 weighted), thalamic nuclei are not readily resolvable. However, using a segmentation algorithm called Thalamus Optimzed Multi-Atlas Segmentation (THOMAS)[39], it may be possible to localize a specific thalamic nucleus to place a small ^{1}H-MRS voxel. There are a couple of limitations to this approach. First, it would likely require longer acquisition times to account for the reduced SNR in a small voxel. Second, the probability of significant subject motion displacing the voxel from the nucleus of interest is greatly increased both due to the size of the voxel and, as a consequence of the smaller voxel, the increased acquisition times. Still, a study like this could one day aid in the understanding of glutamatergic abnormalities in SZ.

Clozapine is the only accepted pharmaceutical to treat the negative symptoms of SZ, and it is believed to influence GLY in some way[40–42]. A ^{1}H-MRS study comparing the GLY concentrations of people with SZ taking clozapine to people with SZ not taking clozapine and healthy controls would be of interest. A similar study has been performed examining the serum concentrations of people with SZ taking clozapine compared to those not taking it and found lower GLY levels in the people taking clozapine[40]. Another study examined plasma levels of people with treatment-resistant SZ before and after taking clozapine and found an increase in GLY levels after clozapine treatment[42]. The benefit of ^{1}H-MRS compared to plasma and serum studies is the localization of the voxels to specific brain regions, while plasma and serum studies are not specific to any brain region.

6.2.3 ^{1}H-fMRS

This ^{1}H-fMRS study of the SZ and MDD groups is likely the first study of many that will utilize ^{1}H-fMRS with a behavioural task to study a neurological condition. As this was the first study of its kind, it certainly raises follow-up questions for future work. Some suggestions for future studies and ways in which the current studies could be improved are mentioned below.

The GLU concentration reduction in the second run of the task needs to be further understood. This is not the first study to demonstrate a reduction in a neurotransmitter following a ^{1}H-fMRS behavioural task. Michels et al[43] similarly found an initial increase in GABA concentrations followed by multiple reductions in each subsequent run of a working memory task. A ^{1}H-fMRS study with a Stroop paradigm should examine metabolite concentrations in multiple groups of healthy controls, each with a different recovery time between blocks of activation, to characterize the reduced GLU response. An additional third block of Stroop stimuli could be added as well to see if GLU concentrations would continue the same pattern of successive reductions in concentration with each block of activation.

It may be useful to know when GLU levels start to decrease after the start of the Stroop stimuli block. If it is during the Stroop stimuli block, this would reduce the average GLU level observed. The rate and timing of GLU increases and decreases can similarly provide valuable information towards to the health of GLU dynamics in SZ. In addition, if the reduction in GLU concentrations is due to insufficient recovery times between blocks, then it may be feasible to perform fMRI guidance of the fMRS voxel with a sufficiently long recovery time between the sequences. It is possible that some people activate the ACC in a slightly different location than others when performing the Stroop. fMRI guidance would address this limitation of the results.

As mentioned for the static metabolite measurements from the ACC and thalamus, the ^{1}H-fMRS study would benefit from the additional SNR from the SPECIAL sequence. The improved SNR may lead to improved temporal resolution to track the GLU concentrations while the subjects are performing the tasks.

Of course, more cognitive tasks should also be explored using ^{1}H-fMRS in the ACC and in other regions as well. It would be of interest to utilize a cognitive task that can vary in level of difficulty, such as the Sternberg Memory Task[44], and see if GLU concentration changes correlate with the level of difficulty. The Stroop Task and/or the Sternberg Memory Task should be tested using an event-related ^{1}H-MRS design to assess any immediate GLU changes that occur when the area is stimulated. In addition, future

studies should aim to correlate the BOLD fMRI response to the behavioural response times and to the GLU changes. This would require identical BOLD fMRI and GLU fMRS paradigms.

It would also be of great interest to perform the ^{1}H-fMRS study after administration of an NMDA antagonist, such as ketamine. This would help to further clarify whether these results are indicative of NMDA hypofunction in SZ.

6.3 Closing remarks

Each of the chapters in this thesis contributes to the overall agenda to study the health of GLU neurotransmission in SZ. Using the state-of-the-art 7 T MRI, it was possible to acquire high quality ^{1}H-MRS data and then to evolve the existing ^{1}H-MRS methodology into a technique that reliably measures dynamic concentrations of metabolites, ^{1}H-fMRS. The *in vivo* work presented in this thesis include the first study to measure GLY concentrations in the ACC and thalamus using ^{1}H-MRS, the first study to measure GLU changes using a Stroop cognitive ^{1}H-fMRS paradigm, and, finally, the first study to measure GLU changes dynamically in a psychiatric population.

A consistent theme throughout this thesis is NMDA hypofunction in SZ, and the results certainly provide strong support for such a theory. However, simply knowing that there is NMDA hypofunction in SZ will not be enough. The studies in this thesis have laid the ground work for monitoring of GLU dynamics during rest and activation. This tool can be used to examine disease-related abnormalities in GLU dynamics and the effect of GLU-modulating treatments. There is still much work that needs to be done. With each new study, a new building block is laid and our understanding of GLU abnormalities in SZ progresses towards one day having effective treatments for the full range of symptoms of SZ.

6.4 References

1. Brenner, E., Kondziella, D., Håberg, A. & Sonnewald, U. Impaired glutamine metabolism in NMDA receptor hypofunction induced by MK801. *J. Neurochem.* **94,** 1594–1603 (2005).

2. Marsman, A. *et al.* Glutamate in schizophrenia: A focused review and meta-analysis of 1H-MRS studies. *Schizophr. Bull.* **39,** 120–129 (2013).

3. Théberge, J. *et al.* Glutamate and glutamine in the anterior cingulate and thalamus of medicated patients with chronic schizophrenia and healthy comparison subjects measured with 4.0-T proton MRS. *Am. J. Psychiatry* **160,** 2231–2233 (2003).

4. Théberge, J. *et al.* Glutamate and glutamine measured with 4.0 T proton MRS in never-treated patients with schizophrenia and healthy volunteers. *Am. J. Psychiatry* **159,** 1944–1946 (2002).

5. Théberge, J. *et al.* Longitudinal grey-matter and glutamatergic losses in first-episode schizophrenia. *Br. J. Psychiatry* **191,** 325–334 (2007).

6. Thompson, S. M. *et al.* An excitatory synapse hypothesis of depression. *Trends Neurosci.* **38,** 279–294 (2015).

7. Lahti, A. C., Weiler, M. a., Michaelidis, T., Parwani, A. & Tamminga, C. a. Effects of ketamine in normal and schizophrenic volunteers. *Neuropsychopharmacology* **25,** 455–467 (2001).

8. De la Fuente-Sandoval, C. *et al.* Glutamate levels in the associative striatum before and after 4 weeks of antipsychotic treatment in first-episode psychosis: a longitudinal proton magnetic resonance spectroscopy study. *JAMA psychiatry* **70,** 1057–66 (2013).

9. Kegeles, L. S. *et al.* Elevated Prefrontal Cortex -Aminobutyric Acid and Glutamate-Glutamine Levels in Schizophrenia Measured In Vivo With Proton Magnetic Resonance Spectroscopy. *Arch. Gen. Psychiatry* **69,** 449–459 (2012).

10. Šagud, M. *et al.* Smoking and schizophrenia. *Psychiatr. Danub.* **21,** 371–375 (2009).

11. O'Neill, J. *et al.* Thalamic glutamate decreases with cigarette smoking. *Psychopharmacology (Berl).* **231,** 2717–2724 (2014).

12. Fisher, S. K., Novak, J. E. & Agranoff, B. W. Inositol and higher inositol phosphates in neural tissues: Homeostasis, metabolism and functional significance. *J. Neurochem.* **82,** 736–754 (2002).

13. Taylor, M. J., Selvaraj, S., Norbury, R., Jezzard, P. & Cowen, P. J. Normal glutamate but elevated myo-inositol in anterior cingulate cortex in recovered depressed patients. *J. Affect. Disord.* **119,** 186–189 (2009).

14. Mukai, T., Kishi, T., Matsuda, Y. & Iwata, N. A meta-analysis of inositol for depression and anxiety disorders. *Hum. Psychopharmacol.* **29,** 55–63 (2014).

15. Yildiz-Yesiloglu, A. & Ankerst, D. P. Review of 1H magnetic resonance spectroscopy findings in major depressive disorder: A meta-analysis. *Psychiatry Res. - Neuroimaging* **147,** 1–25 (2006).

16. Taylor, M. J., Wilder, H., Bhagwagar, Z. & Geddes, J. Inositol for depressive disorders. *Cochrane Database Syst. Rev.* CD004049 (2004). doi:10.1002/14651858.CD004049.pub2

17. Lin, Y., Stephenson, M. C., Xin, L., Napolitano, A. & Morris, P. G. Investigating the metabolic changes due to visual stimulation using functional proton magnetic resonance spectroscopy at 7 T. *J. Cereb. Blood Flow Metab.* **32,** 1484–1495 (2012).

18. Mangia, S. *et al.* Sustained neuronal activation raises oxidative metabolism to a new steady-state level: evidence from 1H NMR spectroscopy in the human visual cortex. *J. Cereb. Blood Flow Metab.* **27,** 1055–1063 (2007).

19. Schaller, B., Mekle, R., Xin, L., Kunz, N. & Gruetter, R. Net increase of lactate and glutamate concentration in activated human visual cortex detected with magnetic resonance spectroscopy at 7 tesla. *J. Neurosci. Res.* **91,** 1076–1083 (2013).

20. Schaller, B., Xin, L., O'Brien, K., Magill, A. W. & Gruetter, R. Are glutamate and lactate increases ubiquitous to physiological activation? A 1H functional MR spectroscopy study during motor activation in human brain at 7Tesla. *Neuroimage* **93,** 138–145 (2014).

21. Lally, N. *et al.* Glutamatergic correlates of gamma-band oscillatory activity during cognition: A concurrent ER-MRS and EEG study. *Neuroimage* **85,** 823–833 (2014).

22. Apsvalka, D., Gadie, A. & Mullins, P. G. Event-related dynamics of glutamate and BOLD signal at 3 T in a repetition suppression paradigm. *ISMRM Proc.* **22,** 3796 (2014).

23. Gussew, A. *et al.* Time-resolved functional 1H MR spectroscopic detection of glutamate concentration changes in the brain during acute heat pain stimulation. *Neuroimage* **49,** 1895–1902 (2010).

24. Cleve, M., Gussew, A. & Reichenbach, J. R. In vivo detection of acute pain-induced changes of GABA+ and Glx in the human brain by using functional 1H MEGA-PRESS MR spectroscopy. *Neuroimage* **105,** 67–75 (2015).

25. Mullins, P. G., Rowland, L. M., Jung, R. E. & Sibbitt, W. L. A novel technique to study the brain's response to pain: Proton magnetic resonance spectroscopy. *Neuroimage* **26,** 642–646 (2005).

26. Kim, T. H., Kang, H. K. & Jeong, G. W. Assessment of Brain Metabolites Change during Visual Sexual Stimulation in Healthy Women Using Functional MR Spectroscopy. *J. Sex. Med.* **10,** 1001–1011 (2013).

27. Drobyshevsky, A., Baumann, S. B. & Schneider, W. A rapid fMRI task battery for mapping of visual, motor, cognitive, and emotional function. *Neuroimage* **31,** 732–744 (2006).

28. Purves, D. *et al.* in *Neuroscience* (Sinauer Associates, 2001).

29. Williamson, P. C. *Mind, Brain, and Schizophrenia*. (Oxford University Press, 2006).

30. Javitt, D. C. Twenty-five years of glutamate in schizophrenia: Are we there yet? *Schizophr. Bull.* **38,** 911–913 (2012).

31. Bartha, R., Drost, D. J. & Williamson, P. C. Factors affecting the quantification of short echo in-vivo 1 H MR spectra : prior knowledge, peak elimination, and filtering. *NMR Biomed.* **12,** 205–216 (1999).

32. Provencher, S. Estimation of metabolite concentrations from localized in vivo proton NMR spectra. *Magn. Reson. Med.* **30,** 672–679 (1993).

33. Mierisová, Š. *et al.* New approach for quantitation of short echo time in vivo 1H MR spectra of brain using AMARES. *NMR Biomed.* **11,** 32–39 (1998).

34. Mlynárik, V., Gambarota, G., Frenkel, H. & Gruetter, R. Localized short-echo-time proton MR spectroscopy with full signal-intensity acquisition. *Magn. Reson. Med.* **56,** 965–970 (2006).

35. Hurd, R. *et al.* Measurement of Brain Glutamate Using TE-Averaged PRESS at 3T. *Magn. Reson. Med.* **51,** 435–440 (2004).

36. Hurd, R. E., Gurr, D. & Sailasuta, N. Proton spectroscopy without water suppression: the oversampled J-resolved experiment. *Magn. Reson. Med.* **40,** 343–347 (1998).

37. Thomas, M. a, Ryner, L. N., Mehta, M. P., Turski, P. a & Sorenson, J. a. Localized 2D J-resolved 1H MR spectroscopy of human brain tumors in vivo. *J. Magn. Reson. Imaging* **6,** 453–9 (1996).

38. Kaufman, M. J. *et al.* Oral glycine administration increases brain glycine/creatine ratios in men: A proton magnetic resonance spectroscopy study. *Psychiatry Res. - Neuroimaging* **173,** 143–149 (2009).

39. Su, J., Tourdias, T., Saranathan, M. & Rutt, B. THOMAS: Thalamus Optimized Multi-Atlas Segmentation Target Audience: in *Proceedings of the International Society for Magnetic Resonance in Medicine* **23,** 3747 (2015).

40. Hons, J., Vasatova, M., Cermakova, E., Doubek, P. & Libiger, J. Different serine and glycine metabolism in patients with schizophrenia receiving clozapine. *J. Psychiatr. Res.* **46,** 811–818 (2012).

41. Harvey, R. J. & Yee, B. K. Glycine transporters as novel therapeutic targets in schizophrenia, alcohol dependence and pain. *Nat. Rev. Drug Discov.* **12,** 866–85 (2013).

42. Yamamori, H. *et al.* Changes in plasma d-serine, l-serine, and glycine levels in treatment-resistant schizophrenia before and after clozapine treatment. *Neurosci. Lett.* **582,** 93–98 (2014).

43. Michels, L. *et al.* Frontal gaba levels change during working memory. *PLoS One* **7,** e31933 (2012).

44. Sternberg, S. Memory-scanning - Mental processes revealead by reaction-time experiments.pdf. *Am. Sci.* **57,** 421–457 (1969).

Appendices

Appendix A. Ethics approval to acquire ^{1}H-fMRS in schizophrenia at 7 T

Western

Office of Research Ethics

The University of Western Ontario

Website: www.uwo.ca/research/ethics

Use of Human Subjects - Ethics Approval Notice

Principal Investigator: Dr. J. Théberge
Review Number: 15326 **Review Level:** Full Board
Review Date: July 22, 2008
Protocol Title: High Field Functional Magnetic Resonance Spectroscopy of Glutamate in Schizophrenia
Department and Institution: Imaging, St. Joseph's Health Care London
Sponsor:
Ethics Approval Date: October 21, 2008 **Expiry Date:** September 30, 2010
Documents Reviewed and Approved: UWO Protocol, Letter of Information and Consent Form - Patients and Letter of Information and Consent Form - Healthy Volunteers dated Sep 26 2008 and Advertisement
Documents Received for Information:

This is to notify you that The University of Western Ontario Research Ethics Board for Health Sciences Research Involving Human Subjects (HSREB) which is organized and operates according to the Tri-Council Policy Statement: Ethical Conduct of Research Involving Humans and the Health Canada/ICH Good Clinical Practice Practices: Consolidated Guidelines; and the applicable laws and regulations of Ontario has reviewed and granted approval to the above referenced study on the approval date noted above. The membership of this REB also complies with the membership requirements for REB's as defined in Division 5 of the Food and Drug Regulations.

The ethics approval for this study shall remain valid until the expiry date noted above assuming timely and acceptable responses to the HSREB's periodic requests for surveillance and monitoring information. If you require an updated approval notice prior to that time you must request it using the UWO Updated Approval Request Form.

During the course of the research, no deviations from, or changes to, the protocol or consent form may be initiated without prior written approval from the HSREB except when necessary to eliminate immediate hazards to the subject or when the change(s) involve only logistical or administrative aspects of the study (e.g. change of monitor, telephone number). Expedited review of minor change(s) in ongoing studies will be considered. Subjects must receive a copy of the signed information/consent documentation.

Investigators must promptly also report to the HSREB:

a) changes increasing the risk to the participant(s) and/or affecting significantly the conduct of the study;
b) all adverse and unexpected experiences or events that are both serious and unexpected;
c) new information that may adversely affect the safety of the subjects or the conduct of the study.

If these changes/adverse events require a change to the information/consent documentation, and/or recruitment advertisement, the newly revised information/consent documentation, and/or advertisement, must be submitted to this office for approval.

Members of the HSREB who are named as investigators in research studies, or declare a conflict of interest, do not participate in discussion related to, nor vote on, such studies when they are presented to the HSREB.

Chair of HSREB: Dr. Joseph Gilbert

Ethics Officer to Contact for Further Information

This is an official document. Please retain the original in your files.

cc: ORE File
LHRI

Appendix B. Ethics approval for ^{1}H-MRS in schizophrenia at 7 T

Research Western

Use of Human Participants - Ethics Approval Notice

Principal Investigator: Dr. Peter Williamson
File Number:102328
Review Level: Full Board
Approved Local Adult Participants:93
Approved Local Minor Participants:0
Protocol Title: Candidate Neuronal Circuits in Mental Illness (REB# 18828)
Department & Institution: Schulich School of Medicine and Dentistry\Medical Biophysics,Western University
Sponsor: Canadian Institutes of Health Research

Ethics Approval Date: April 25, 2012
Ethics Expiry Date: September 30, 2017

Documents Reviewed & Approved & Documents Received for Information:

Document Name	Comments	Version Date
Western University Protocol	(including instruments noted in section 8.1)	
Letter of Information & Consent	Patients	2012/03/19
Letter of Information & Consent	Healthy Volunteers	2012/03/19
Other	Advertisements	

This is to notify you that the University of Western Ontario Health Sciences Research Ethics Board (HSREB) which is organized and operates according to the Tri-Council Policy Statement: Ethical Conduct of Research Involving Humans and the Health Canada/ICH Good Clinical Practice Practices: Consolidated Guidelines; and the applicable laws and regulations of Ontario has reviewed and granted approval to the above referenced study on the approval date noted above. The membership of this HSREB also complies with the membership requirements for REB's as defined in Division 5 of the Food and Drug Regulations.

The ethics approval for this study shall remain valid until the expiry date noted above assuming timely and acceptable responses to the HSREB's periodic requests for surveillance and monitoring information. If you require an updated approval notice prior to that time you must request it using the University of Western Ontario Updated Approval Request form.

Member of the HSREB that are named as investigators in research studies, or declare a conflict of interest, do not participate in discussions related to, nor vote on, such studies when they are presented to the HSREB.

The Chair of the HSREB is Dr. Joseph Gilbert. The HSREB is registered with the U.S. Department of Health & Human Services under the IRB registration number IRB 00000940.

Signature

Ethics Officer to Contact for Further Information

This is an official document. Please retain the original in your files.

The University *of* Western Ontario
Office of Research Ethics

Appendix C. Curriculum Vitae for Reggie Taylor

Curriculum Vitae

Reggie Taylor 31 Aug 2015

Education

- **The University of Western Ontario**, Ph.D. Program in Medical Biophysics (Reclassified from M.Sc.). Supervisors: Dr. Jean Théberge, Dr. Peter Williamson. Sept. 2008 – Aug. 2015.

- **International Society of Magnetic Resonance in Medicine (ISMRM)** workshop, "Ultra-High Field Systems and Applications: 7 T & Beyond: Progress, Pitfalls, and Potential". Lake Louise, AB, Canada. 20-23 Feb. 2011

- **International Society of Magnetic Resonance in Medicine (ISMRM)** workshop, "MR Spectroscopy as Applied to Neuropsychiatric Disorders". Quebec, Quebec, Canada. 7-10 Nov. 2008

- **The University of Western Ontario**, Bachelor of Medical Sciences: Honours Specialization in Medical Biophysics (Medical Science Concentration). London, ON, Canada. Sept. 2004 - April 2008

Qualifications

- 5 years experience working with an ultra-high field 7 T MRI in its development phase.

- Advanced understanding of MR theory through 4 graduate MR courses at The University of Western Ontario.

- Programming experience with Visual C++, C# and MATLAB. Proficient with Microsoft Office.

- Experience with planning and executing presentations and seminars.

- Strong writing skills demonstrated via journal and conference submissions and an undergraduate thesis.

- Developed strong leadership experience through supervising and managing co-workers and leading various sports teams

Certifications

- **Emergency First Aid – CPR Level C** from Canadian Red Cross. 23 Sept. 2012

- **Siemens IDEA Sequence Programming Course** on the IDEA programming language used in developing pulse sequences for Siemens Magnetic Resonance Imaging systems. 31 Oct. 2008

Publications

- **Paper (in press): R. Taylor**, R. W. J. Neufeld, B. Schaefer, M. Densmore, E.A. Osuch, N. Rajakumar, P.C. Williamson, J. Théberge. "*Functional magnetic resonance spectroscopy of glutamate and glutamine in schizophrenia and major depressive disorder – Anterior cingulate activity during a color-word Stroop task"*. npj Schizophrenia. NPJSCHZ #00068

- **Paper (in preparation): R. Taylor**, B. Schaefer, N. Rajakumar, E.A. Osuch. J. Théberge, P.C. Williamson. "*Neurometabolic abnormalities observed with MR spectroscopy in the anterior cingulate cortex and thalamus of patients with schizophrenia and Major depressive Disorder at 7 T"*. British Journal of Psychiatry.

- **Paper (in preparation as per invitation to resubmit)**: **R. Taylor**, P.C. Williamson, J. Théberge. "*Sources of variability in the quantification of short-echo time human brain 1H-MRS spectra*". Magnetic Resonance in Medicine. Originally submitted 22 Dec 2014. MRM-14-15719.

- **Paper: R. Taylor**, B. Schaefer, M. Densmore, R. Neufeld, N. Rajakumar, P. Williamson, J. Théberge. *"Increased glutamate levels observed upon Functional Activation in the anterior cingulate cortex using the Stroop Task and functional spectroscopy"*. NeuroReport. 2015;26(3):107-112.

- **Abstract: R. Taylor**, B. Schaefer, E. Osuch, M. Densmore, N. Rajakumar, J. Théberge, P. Williamson. *"Neurometabolic changes observed in the anterior cingulate cortex and the thalamus in schizophrenia and in unipolar mood disorder relative to healthy controls at 7 T"*. ISMRM. Toronto, Ontario, Canada. June 2015. Abstract #2011.

- **Abstract: R. Taylor**, B. Schaefer, R. Neufeld, P. Williamson, J. Théberge. "*Glutamatergic changes detected upon functional activation with a Stroop Task in healthy controls and in subjects with Schizophrenia"* ISMRM. Milan, Italy. May 2014. Abstract #3780.

- **Abstract: R. Taylor**, P. Williamson, J. Théberge. "*Functional MRS in the Anterior Cingulate"* ISMRM. Salt Lake City, Utah, United States. May 2013. Abstract #4417.

- **Abstract: R. Taylor**, P. Williamson, J. Théberge. "The influence of template metabolite omissions on 1H-MRS quantification*"* ISMRM. Melbourne, Victoria, Australia. May 2012. Abstract #4399.

- **Abstract: R. Taylor**, P. Williamson, J. Théberge. *"The dependence of metabolite correlations on the external magnetic field strength"* ISMRM. Montreal, QC, Canada. May 2011. Abstract #2535

- **Abstract**: **R. Taylor**, J. Théberge, P. Williamson. **"***Simulating human brain glutamate fMRS at 7.0T to determine minimum SNR requirements*" ISMRM. Stockholm, Sweden May 2010. Abstract #1805

Presentations

- **Oral:** "*Neurometabolic abnormalities observed with MR spectroscopy in the anterior cingulate cortex and thalamus of patients with schizophrenia and major depressive disorder*" Taylor R, Neufeld RWJ, Schaefer B, Densmore M, Rajakumar N, Osuch EA, Théberge J, Williamson PCW. Department of Psychiatry Academic Research Day. London, Ontario, Canada. 25 June 2015.

- **Poster:** "*Neurometabolic changes observed in the anterior cingulate cortex and thalamus in schizophrenia and unipolar mood disorder at 7 T*" Taylor R**,** B. Schaefer, N. Rajakumar, E.A. Osuch, Williamson P, Théberge J. Lawson Health Research Day. London, Ontario, Canada. 1 April 2015

- **Oral:** *"Resting functional network connectivity in schizophrenia and depression: Investigating abnormalities in directed effort and emotional encoding networks"*. Ford K, Taylor R, Schaefer B, Neufeld R, Théberge Osuch E, Williamson P. Department of Psychiatry Academic Research Day. University of Western Ontario. London, ON, Canada. 19 June 2014. Presented by Reggie Taylor.

- **Poster:***"Glutamatergic changes detected upon functional activation with a Stroop Task in healthy controls and in subjects with Schizophrenia"*. Taylor R, Schaefer B, Neufeld R, Williamson P, Théberge J. Psychiatry Research Day. University of Western Ontario. London, ON, Canada. 19 June 2014

- **Oral:** "*Magnetic Resonance Spectroscopy Studies in Schizophrenia"* Taylor R. Medical Biophysics Seminar Series. Lawson Health Research Institute. 24 Oct. 2013.

- **Oral:** *"7 T Magnetic Resonance Spectroscopy Studies: Functional MRS"* Taylor R**.** Neuropsychiatry Seminar Series. University Hospital, London, ON, Canada. 3 May 2013.

- **Oral:** "*Functional magnetic resonance spectroscopy in the anterior cingulate cortex"*. Taylor R. Medical Biophysics Seminar Series. Lawson Health Research Institute. 18 Oct. 2012.

- **Oral:** *"Resting functional network connectivity in schizophrenia and mood disorders: Emerging evidence of abnormalities in directed effort and emotional encoding networks"*. Ford K, Taylor R, Neufeld R, Théberge J, Manchanda R, Osuch E, Williamson P. Department of Psychiatry Academic Research Day. University of Western Ontario. London, ON, Canada. 21 June 2012. Presented by Reggie Taylor.
- **Poster:***"Functional magnetic resonance spectroscopy as a tool for observing dynamic metabolite changes in the anterior cingulate"*. Taylor R, Théberge J, Williamson P. Psychiatry Research Day. University of Western Ontario. London, ON, Canada. 21 June 2012

- **Poster:** "Reproducibility of MRS spectra in the Anterior Cingulate at 7.0 T" Taylor R. Lawson Research Day. London, ON, Canada. 20 March 2012.

- **Oral:** *"Applications of MRI to schizophrenia"* Taylor R. Medical Biophysics Seminar Series. Lawson Health Research Institute. London, Ontario, Canada. 20 Oct 2011

- **Poster:** "*A Desktop Optical-Imaging System for Teaching the Principles of Radiography and Computed Tomograpy"* Battista J, Miller J, Taylor R, Jordan K, MacDonald I. The Western Conference on Science Education. University of Western Ontario. London, Ontario, Canada. 6-8 July 2011

- **Poster:** "*A Desktop Optical-Imaging System for Teaching the Principles of Radiography and Computed Tomograpy"* Taylor R, Battista J, Jordan K, Miller J, MacDonald I. London Imaging Discovery Day. The London Convention Center. London, Ontario, Canada. 23 June 2011

- **Poster:** "*A Desktop Optical-Imaging System for Teaching the Principles of Radiography and Computed Tomograpy"* Taylor R, Battista J, Jordan K, Miller J, MacDonald I. Oncology Research Day. The Lamplighter Inn. London, Ontario, Canada. 17 June 2011.

- **Poster:***"Resting state analysis of the Default Mode Network in schizophrenia and in mood disorders: preliminary results"*. Taylor R, Ford K, Théberge J, Williamson P. Psychiatry Research Day. University of Western Ontario. London, ON, Canada. 16 June 2011

- **Oral:** "*An overview of the applications of magnetic resonance methods in neuropsychiatry research*". Théberge J, Taylor R, Barton L, Gagnon Y. St. Joseph's Hospital. London, Ontario, Canada. 20 May 2011

- **Poster:** "*The dependence of metabolite correlations on the external magnetic field strength*" Taylor R, Williamson P, Théberge J. ISMRM- Montreal QC, Canada. 9 May 2011.

- **Poster:** "*The dependence of metabolite correlations on the external magnetic field strength*" Taylor R**,** Williamson P, Théberge J. Lawson Research Day. London, Ontario, Canada. 22 March 2011

- **Poster:** "*The dependence of metabolite correlations on the external magnetic field strength*" Taylor R**,** Williamson P, Théberge J. Imaging Network of Ontario Symposium 9th Annual Conference. University of Toronto. Toronto, Ontario, Canada. 31 Jan- 1 Feb 2011

- **Poster:** "*A Desktop Optical-Imaging System for Teaching the Principles of Radiography and Computed Tomograpy"* Battista J, Miller J, Taylor R**,** Jordan K, MacDonald I. Imaging Network of Ontario Symposium 9th Annual Conference. University of Toronto. Toronto, Ontario, Canada. 31 Jan- 1 Feb 2011

- **Oral:** *"fMRI Guided fMRS for the detection of glutamate and glutamine in schizophrenia"* Taylor R. Medical Biophysics Seminar Series. University Hospital. London, Ontario, Canada. 20 Jan 2011

- **Oral:** *"Applications of 7 T MRI to Neuropsychiatry"* Taylor R**.** Neuropsychiatry Seminar Series. University Hospital, London, ON, Canada. 14 January 2011

- **Journal Club:** *"High resolution diffusion-weighted imaging using readout segmented echo planar imaging, parallel imaging and a two-dimensional navigator based reacquisition" Porter D. et al. Magnetic Resonance in Medicine 2009*. Taylor R. Robarts Research Institute. London, Ontario, Canada. 20 Oct 2010.

- **Poster:** Taylor R, Théberge J, Williamson PC. "Simulating human brain glutamate fMRS at 7.0T to determine minimum SNR requirements"- *ISMRM*, Stockholm, Sweden, May 2010

- **Poster:** Taylor R, Théberge J, Williamson PC. "Simulating human brain glutamate fMRS at 7.0T to determine minimum SNR requirements"- *London Imaging Discovery*, London, ON, Canada, 2010

- **Oral:** *"fMRI Guided fMRS for the detection of glutamate and glutamine in schizophrenia"* Taylor R. Medical Biophysics Seminar Series. University Hospital. London, Ontario, Canada. 25 March 2010

- **Poster:** "*Glutamate and glutamine interactions during proton spectral quantification*" Taylor R**,** Williamson PC, Théberge J. SSMD WORLDiscoveries Research Showcase. London Convention Centre. London, Ontario, Canada. 5 Feb 2010.
- **Poster:** "*Glutamate and glutamine interactions during proton spectral quantification*" Taylor R**,** Williamson PC, Théberge J. Imaging Network of Ontario Symposium 8th Annual Conference. University of Toronto. Toronto, Ontario, Canada. 1-3 Feb 2010.

- **Oral:** "*Using fMRS to study glutamate and glutamine in Schizophrenia at 7 T*" Taylor R. Medical Biophysics Seminar Series. St. Joseph's Hospital. London, Ontario, Canada. 15 Jan 2010

- **Oral**: "*Dynamic measurements of glutamate and glutamine by proton functional MRS at 7.0 T in the anterior cingulate and thalamus of Schizophrenia patients"*. Taylor R. Medical Biophysics Seminar Series. University Hospital, London, Ontario, Canada. 7 May 2009

- **Journal Club:** *"Spectral Simplification for Resolved Glutamate and Glutamine Measurement Using a Standard STEAM Sequence with Optimized Timing Parameters at 3, 4, 4.7, 7, and 9.4 T" Yang, S et al. Magnetic Resonance in Medicine 2008*. Taylor R. The University of Western Ontario. London, Ontario, Canada. 18 March 2009.

- **Journal Club:** *"Cognitive impairment and in vivo metabolites in first-episode neuroleptic-naive and chronic medicated schizophrenic patients: A proton magnetic resonance study" Ohrmann P., et al. Journal of Psychiatric Research 2006.* Taylor. The University of Western Ontario. London, Ontario, Canada. 13 March 2009

- **Conference:** *"A New Medicine for Physics: Using Medical Imaging as a Tactic for Teaching Physics"*. Poepping T, Chronik B, MacDonald I, Wong E, Cox J, Taylor R, Battista J. Spring Perspectives on Teaching. The University of Western Ontario. London, Ontario, Canada. 14 May 2008

- **Thesis:** "*Optimizing the quality of CT scans of three Egyptian mummies to quantify wood within a mummy*". Taylor R. The University of Western Ontario. London, Ontario, Canada. 28 March 2008

- **Poster**: "*Optical CT as an Educational Tool".* Taylor R, MacDonald I, Battista J. Expanding Scholarship in Radiology Education: First Annual Conference. The University of Western Ontario. London, Ontario, Canada. 24 August, 2007

Relevant Work Experience

- **Empire Landscaping**: Crew foreman responsible for supervising and managing co-workers, conducting any skilled work. This included building steps and setting grades (Summer 2008)

- **Department of Medical Biophysics, The University of Western Ontario:** Designed laboratory protocols for an Optical CT Scanner

for use in the undergraduate teaching laboratory under supervision of Dr. Jerry Battista and Dr. Ian MacDonald (Summer 2007)

- **Artec Landscaping:** Site manager and foreman. Jobs included managing co-workers and performing skilled work (2005 - 2006

Awards & Scholarships

- **Best Oral Presentation by a Trainee- Department of Psychiatry Academic Research Day:** (June 2015)

- **Educational Stipend – International Society for Magnetic Resonance in Medicine (ISMRM)**: US$435, awarded to select trainees with accepted abstracts to help defer the cost of conference registration and travel expenses to ISMRM, a yearly international conference. (May 2014)

- **Educational Stipend – International Society for Magnetic Resonance in Medicine (ISMRM)**: US$590, awarded to select trainees with accepted abstracts to help defer the cost of conference registration and travel expenses to ISMRM, a yearly international conference. (May 2012)

- **Ontario Graduate Scholarship (OGS):** A competitive scholarship among graduate students, $5000 per term for a maximum of three terms and a minimum of two terms in one academic year (May 2011-April 2012)

- **Educational Stipend – International Society for Magnetic Resonance in Medicine (ISMRM)**: US$450, awarded to select trainees with accepted abstracts to help defer the cost of conference registration and travel expenses to ISMRM, a yearly international conference. (May 2011)

- **Ontario Graduate Scholarship of Science and Technology (OGSST):** A competitive scholarship among graduate students, $5000 per term for a maximum of three terms and a minimum of two terms in one academic year (Sept. 2009-August 2010)

- **Schulich Graduate Scholarship (SGS):** Full tuition ($6670/year) awarded for maintaining a minimum 80% average and enrolling in the Medical biophysics graduate program at UWO (Sept. 2009 – Aug. 2013)

- **Schulich Graduate Scholarship (SGS)**: Full tuition ($6670/year) awarded for having a minimum 80% average in the final two years of my undergraduate degree and enrolling in Medical Biophysics graduate program at UWO (Sept. 2008-Aug. 2009)

Volunteer Work

- **Senior Member at Large – Western Outdoors Club** (May 2013-April 2015): Duties include general assistance to the club's executive committee in addition to planning and organizing club trips and events.

- **President - Western Outdoors Club** (Sept. 2012-May 2013): Duties include overseeing club operations, and managing the club's executive members while concurrently planning and organizing club trips and events.

- **Vice-President of Finance for the Western Outdoors Club** (March 2012- Sept. 2012): Duties included managing club finances, organization of club events, general assistance with club event planning.

- **Vice-President of Finance for Autism Western** (Sept. 2008-April 2010): Duties included managing the clubs finances and preparing detailed budgets for events